POLITECNICO DI MILANO

Scuola di Ingegneria Industriale e dell'Informazione Corso di Laurea Magistrale in Ingegneria Biomedica

Synthesis of titanium dioxide nanotubes coated with soy isoflavones extracts to improve osseointegration

Relatori: Prof. Roberto CHIESA

Correlatori: Prof. Matteo SANTIN

Dott.ssa Monica MOSCATELLI

Tesi di Laurea Magistrale di:

Daiana MAZZOLA

Matr. n. 836811

Anno Accademico 2016/2017

Abstract

Titanium and its alloys are one of the most used biomaterials as hard tissues substitutes, thanks to their features as high biocompatibility, mechanical properties and corrosion resistance [1].

The clinical success of oral or orthopaedic implants is related to their early osseointegration. After the implantation, there are two possible responses that may occur in host tissue: an acute inflammatory process that caused the formation of a fibrous tissue capsule which cause early implant failure, or living and functional bone tissue formation [2].

For this reason, several surface modification treatments have been developed to allow the formation of a micro-rough surface that could enhance implant osseontegration. One example of these processes is the anodization treatment: an electrolytic passivation treatment used to improve thickness of the metal oxide layer [3], which improves bone implant integration [4]. Particularly, using a fluoride-containing solution, the anodization treatment allows the production of a self-ordered nanotubular structure, like the one showed in figure 1.

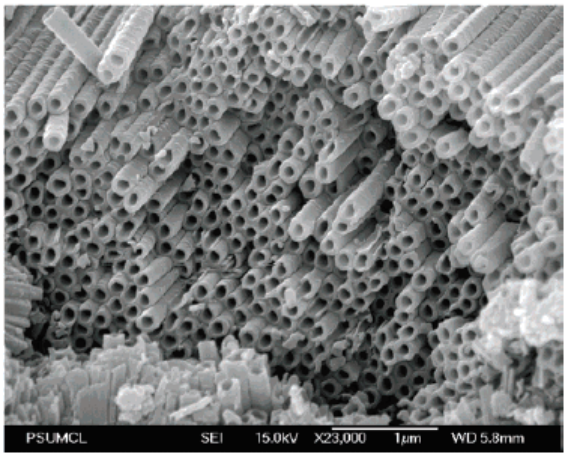

Figure 1: Titanium dioxide nanotubes obtained in an ethylen-glycol solution with an applied voltage of 60 V [5].

The nanotubular structure homogeneity and dimensions could be easily modulated by varying several process parameters [6, 7, 8]. Because titania nanotubes (TiO_2 NTs) could enhance biocompatibility and cells activity [9] and this behaviour is in dependence of diameter size [10, 11], they could be used as coating for titanium implants [12]. Moreover, nanotubes could be loaded with active biomolecules and used as controlled-local drug delivery system, whose trend depends on the nanotubular structure dimensions.

One of the candidates as bioactive molecule that could be loaded on this nano-rough surface is a family of soybean-based biomaterials (Fig. 2), whose properties have been

compared to the ones of other natural biomaterials and revealed the possibility to use them as coatings for tissue regeneration [13].

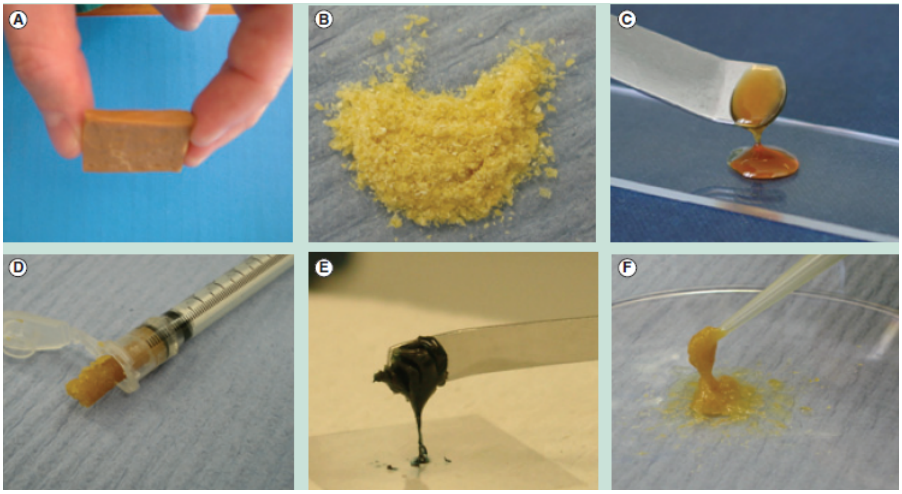

Figure 2: Soybean-based biomaterial formulations: blocks (A), granules (B), hydrogel (C), paste (D), bioglue (E) and injectable paste (F) [13].

The promising features of these soy extracts are due to the presence of isoflavones: a family of molecules with a proved positive effect on bone metabolism. Particularly they contain genistein, that enhances bone matrix production and inhibits cell proliferation, and its glycosilated non-active form genistin [14]. Moreover, genistein could improve osseointegration inhibiting osteoclasts activation [15, 16].
The aim of this projects was to produce a nanotubular structure that could enhance cellular adhesion and be also used to control the release of bioactive molecules that could further increase osteointegration.
Particularly, the point was to define the parameters set that lead to the production of an homogeneous, strong and stable layer of nanotubes, around ten microns thick, with regular diameters, capable to uptake and release a drug. This structure should also have tunable diameters sizes, by varying the applied voltage, to allow the evaluation of how the release of soy isoflavones and osteoblastic cells activity are affected by nanotubes dimensions.

Samples with the three different roughnesses reported in table 1 were treated in two kind of electrolytes (an aqueous-based one and an organic one) and applying different voltages and times to define how the anodization set-up variables affect the nanotubes geometry and regularity. The nanotubular surface hydrophilicity was evaluated through a wettability test.

Sample	Ra [μm]
S1	0.99
S2	0.22
S3	0.12

Table 1: Parameters obtained from the profilometric analysis of samples.

Subsequently, chosen structures with dimensionally different nanotubes were loaded by deep-coating in a solution containing the soy isoflavones. The release trend of genistein and genistin was evaluated in dependence of nanotubes geometry through a spectrophotometric analysis.
Then, samples were biologically characterized: the effect of both nanotubes and isoflavones on Saos-2 cell line morphology and proliferation was evaluated through phalloidin stainings and SEM analysis.

The anodization experiments performed in the aqueous solution showed that a potentiostatic approach is necessary to modulate nanotubes diameter dimensions by varying the applied voltage. Moreover, treating samples in the ethylen-glycole electrolyte allowed the formation of a more regular structure of nanotubes with smooth walls and bigger lengths, as showed in figure 3.

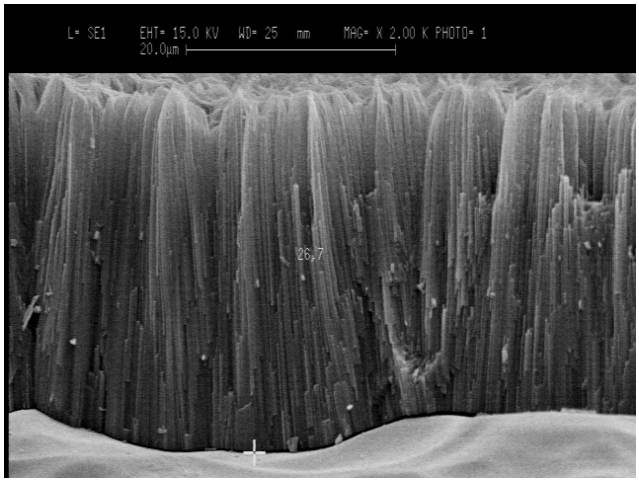

Figure 3: Lateral view of the nanotubular layer of a sample treated in the organic solution.

Based on literature [17, 7], in this kind of electrolyte an overlying irregular and disordered layer, called ”nanograss”, is obtained and its presence could depend on the initial surface roughness of samples. Then, was observed that this disordered layer is more or less compact in dependence of the anodization time. Samples from each kind of sheet were then anodized at 60 V for 6 hours and emerged that the presence of the nanograss layer decrease with an initial better surface quality as showed in figure 4.

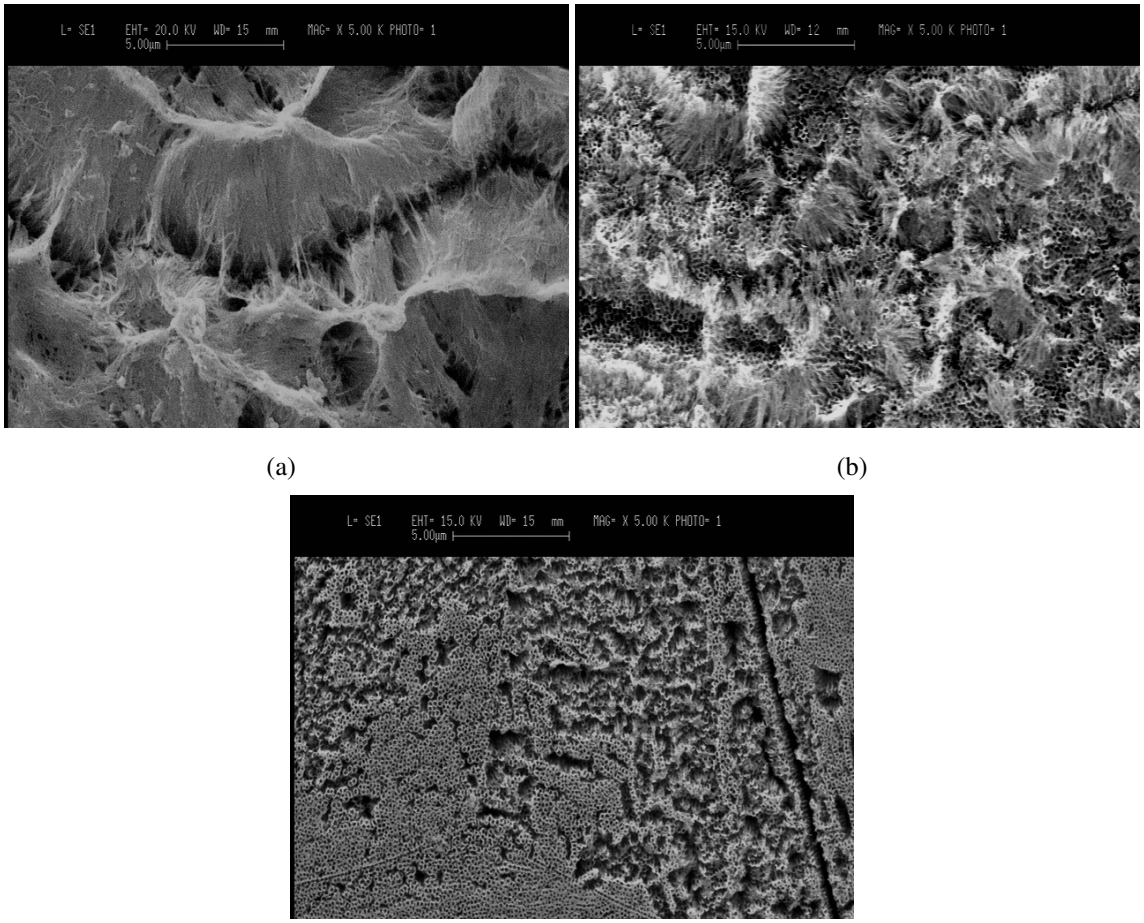

Figure 4: Samples anodized for 6 h at 60 V with different surface roughnesses: (a) 1, (b) 2 e (c) 3.

Specifically, sample with the lowest R_a resulted totally free from the superficial residuals, but the obtained dioxide layer showed a very low adherence to the underlying titanium surface and so samples 2 were chosen for the following experiments.
Then attempts have been made to find a way to remove the nanograss layer after the anodization process. Was proved that a post-treatment in ultrasound for 20 seconds could totally remove the nanograss layer on samples. Furthermore this method resulted effective just if the anodization duration is longer than 2 hours and the applied potential is higher than 50 V.
Concerning nanotubes dimensions, their lengths are bigger with a longer anodization treatment and with an higher applied voltage which also increases diameter size.
Once that the correlation between nanotubes geometry and process parameters was observed, two dimensionally different nanotubular structures, showed in figure 5, were produced. Wettability test performed on those surfaces revealed that their hydrophilicity increases in presence of bigger nanotubes.

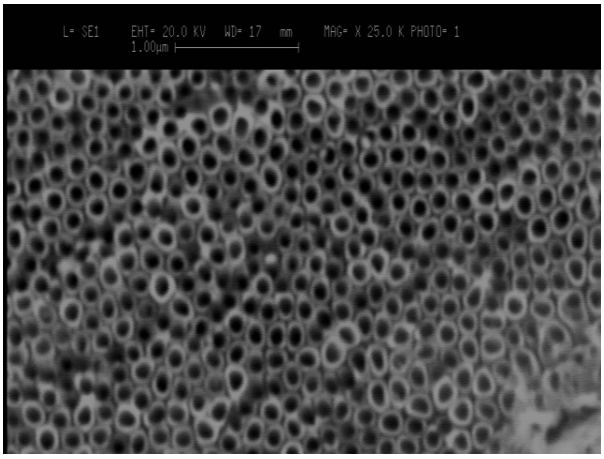

(a)

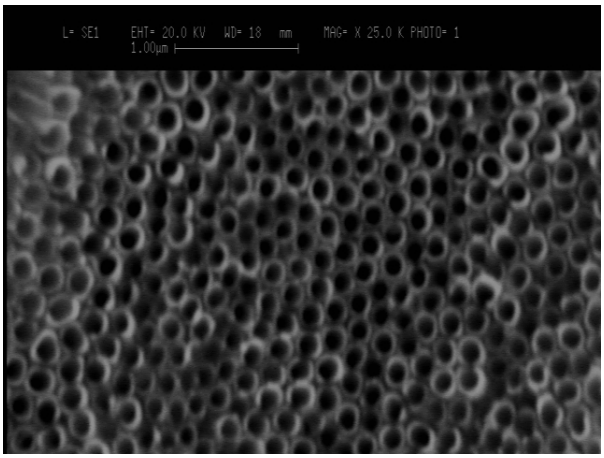

(b)

Figure 5: Example of the obtained natubular structures. Sample anodized in the organic solutions, for 2 h and with and applied voltage equal to (a) 50 V and (b) 70 V.

Considering the drug release, in line with other autors works [18], the trend of genistein and genistin presents an initial high release and then another low release after around 24 hours. The molecules loaded quantity is really bigger on anodized samples and, particularly, this quantity increases on sample with bigger nanotubes.

For what concerns cell morphology and adhesion, was observed that osteoblasts cultured on nanotubes and coated samples for more than 48 hours showed a uniform distribution on all the available area on each kind of substrate. Moreover, Saos-2 appeared flattened, polygonal shaped and interact between each others, specially on the smaller nanotubes. Moreover, cells proliferation increases in presence of titania nanotubes, while it decrease on samples coated with soy isoflavones extracts.

Considering samples coated with soy isoflavones extracts, especially the one anodized at 50 V, from the SEM analysis showed in figure 6 could be observed that respect of the ones on non-coated disks, Saos-2 are more flattened e interacting, especially on sample anodized at 50 V.

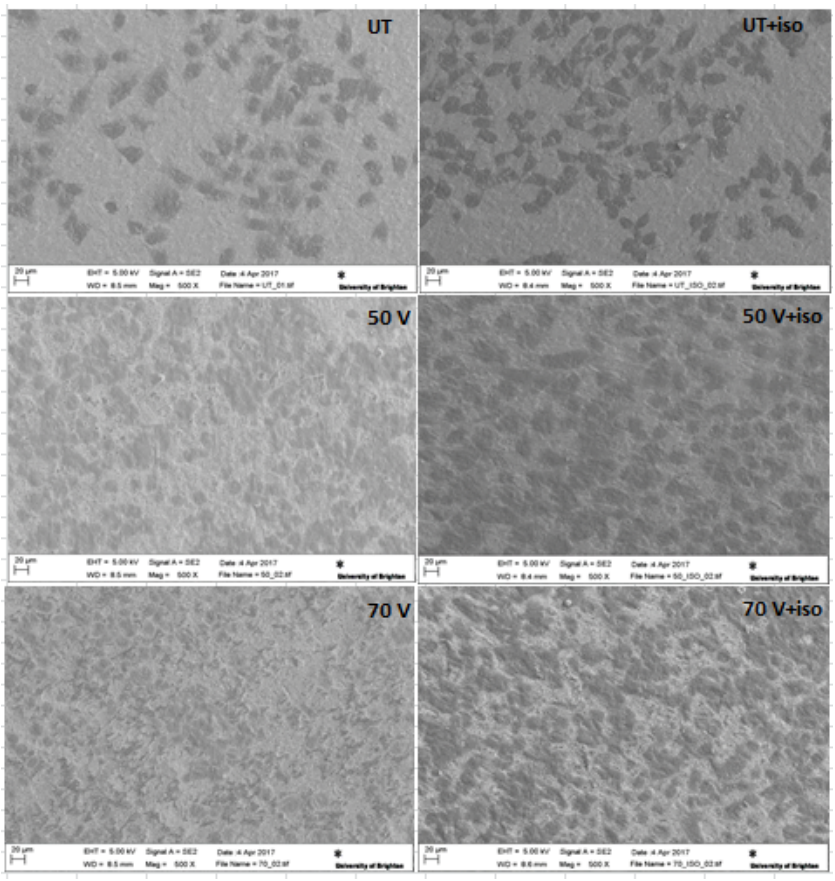

Figure 6: SEM analysis of cells cultured for 65 hours on untreated (UT) and anodized titanium disks uncoated (50 V and 70 V) and coated with soy isoflavones extracts (UT+iso, 50 V+iso and 70 V+iso).

Performed tests led to the production of an opened, regular and homogeneous nanotubular structure with a length of a dozen micron and diameter sizes tunable with the applied voltage value. This nanostructure enhances osteoblastic cells proliferation and could be also used as a local-drug delivery system for the release of molecules that could further increase Saos-2 bioactivity since the first moment after implantation.

Could be interesting, in future, to evaluate if anodizing samples for less than 2 hours could offer the possibility to lower the applied voltage still removing the nanograss layer. This could give the opportunity to produce opened nanotubular structures with smaller diameters and then expand the biological characterization. This could be used also to extend the release experiment and better define the dependence of the drug loaded amount on nanotubes dimensions.

Following tests, like ALP activity analysis on saos-2, could specifically prove that both nanotubes and the soybean-based biomaterial could increase the production of bone matrix and then enhance osteoblast differentiation and implant osseointegration.

Sommario

Il titanio e le sue leghe sono tra i materiali più utilizzati in ambito biomedico come sostituti del tessuto osseo, grazie a caratteristiche come l'elevata biocompatibilità, adeguate proprietà meccaniche e alta resistenza alla corrosione [1].
Sebbene la percentuale di successo di un impianto ortopedico o dentale sia molto elevata [19, 20], il fallimento di questo tipo di device è solitamente improvviso [21, 22]. Le cause che possono determinare il fallimento di un impianto possono essere suddivise in fattori dipendenti dal paziente [23, 24, 25], come l'età, la qualità dell'osso, dalle caratteristiche dell'impianto [26], come le dimensioni o il tipo di finitura superficiale, e dal chirurgo [27], come la durata dell'operazione.
La corretta fissazione di una protesi metallica dipende principalmente dall'osteointegrazione che avviene durante le prime fasi di guarigione. Dopo l'installazione, vi sono due possibili reazioni che possono avvenire all'interfaccia impianto-osso: un processo infiammatorio cronico che porta alla formazione di una capsula fibrotica, che causa il fallimento dell'impianto, o la formazione di tessuto osseo vitale e funzionale [2].
Per questo motivo, sono stati sviluppati diversi trattamenti di modifica superficiale del titanio tramite i quali è possibile ottenere una superficie micro-rugosa che favorisca l'osteointegrazione dell'impianto senza l'interposizione di tessuto connettivo. Un esempio di questo tipo di trattamenti è rappresentato dalla tecnica di anodizzazione: un processo di passivazione elettrolitica usato per aumentare lo spessore dello strato di ossido che ricopre superfici metalliche [3], il quale favorisce l'integrazione tra impianto e osso [4]. In particolare, utilizzando una soluzione contenente ioni fluoro, il trattamento di anodizzazione consente di ottenere una struttura nano-tubolare molto regolare[28] come quella mostrata in figura 7.

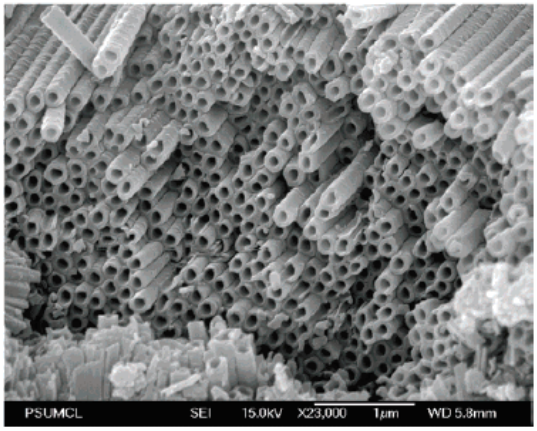

Figura 7: Esempio di nanotubi in ossido di titanio ottenuti con una soluzione a base di etilenglicole applicando un potenziale di 60 V [5].

La regolarità, l'omogeneità e le dimensioni dello strato nanotubolare possono essere modulate variando i diversi parametri di processo come il tipo di elettrolita utilizzato [6, 29], la durata del trattamento [7] o il voltaggio applicato [8].
Negli ultimi anni, data la relativa semplicità con cui possono essere prodotti, i nanotubi in ossido di titanio (TiO_2 NTs) sono stati oggetto di numerosi studi per valutare la loro applicabilità nel campo biomedicale come rivestimento per protesi in titanioi [30, 31, 12]. E' emerso che questa nanostruttura presenta numerosi vantaggi rispetto al titanio puro o superfici micro-rugose, come ad esempio l'incremento della biocompatibilità e dell'attività cellulare [9], le quali dipendono dalle dimensioni dei nanotubi utilizzati [10, 11].
Inoltre, i nanotubi hanno destato grande interesse poichè possono essere caricati con molecole bioattive e usati come device per un rilascio controllato di farmaco localizzato nella sede d'impianto e il cui andamento dipende dalle loro dimensioni.
Tra le sostanze che potrebbero essere caricate in un sistema a rilascio di farmaco con lo scopo di favorire l'osteointegrazione, vi sono dei biomateriali prodotti utilizzando una polvere costituita da estratti di soia i quali sono mostrati in figura 8.

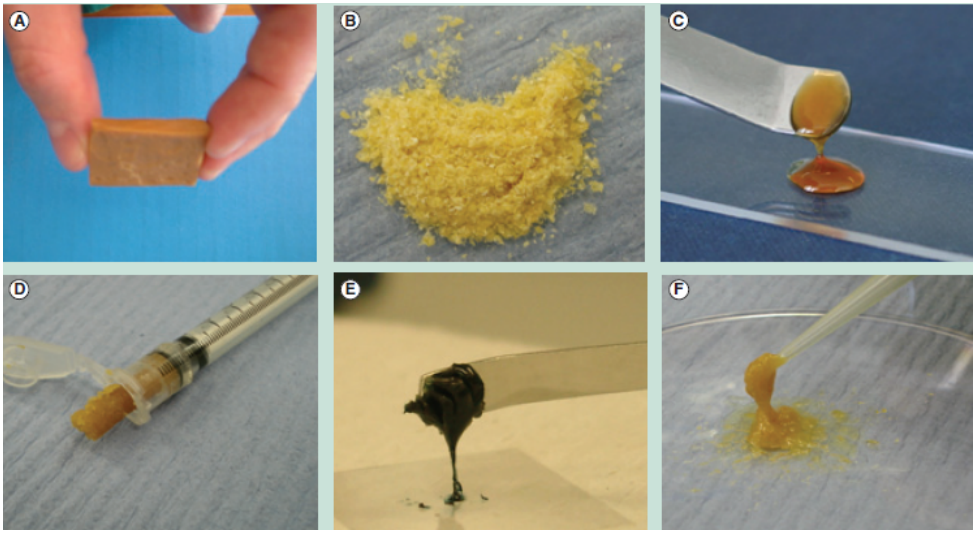

Figura 8: Diverse formulazioni dei biomateriali a base di soia: (A) blocchi, (B) granuli, (C) idrogel, (D) pasta, (E) biocolla, (F) pasta iniettabile [13].

Le proprietà di questi estratti sono state confrontate da altri autori con quelle di altri biomateriali naturali (ad esempio collagene, chitosano o alginato) ed è stata dimostrata la possibilità di poter utilizzare queste sostanze come rivestimenti biodegradabili nell'ambito della rigenerazione dei tessuti [13]. Le promettenti caratteristiche degli estratti di soia sono dovute alla presenza al loro interno degli isoflavoni: una famiglia di molecole con un comprovato effetto positivo sul metabolismo osseo. E' stato dimostrato, infatti, che gli isoflavoni come la genisteina e la daidzeina favoriscono la produzione di matrice ossea in sistemi di coltura cellulare [14]. In particolare, la genisteina ha dimostrato di poter di inibire l'attivazione degli osteoclasti, cellule responsabili del riassorbimento osseo duran-

te il rimodellamento del tessuto, favorendo quindi l'osteointegrazione [15, 16]. Inoltre, è stato anche dimostrato che la genisteina possiede la capacità di bloccare la proliferazione cellulare ed avere effetto antitumorale [13].
Scopo di questo progetto è quindi produrre una struttura nanotubolare che possa incrementare l'adesione cellulare ed essere anche usata per controllare il rilascio di molecole bioattive che potrebbero ulteriormente favorire l'osteointegrazione.
In particolare, l'obiettivo è definire l'insieme di parametri che consenta la formazione di una struttura nanotubolare omogenea, regolare, con uno spessore che garantisca la resistenza meccanica dello strato di nanotubi, i.e. intorno a una decina di micrometri. I nanotubi dovranno anche avere diametri modulabili al variare del potenziale applicato per consentire la valutazione di come il rilascio di isoflavoni e l'attività di cellule osteoblastiche siano influenzati dalle dimensioni dei nanotubi.

Per valutare come le variabili di set-up influissero sulla geometria e la regolarità della struttura nanotubolare, campioni di titanio puro di grado 2, con le diverse rugosità riportate in tabella 2, sono stati trattati in due tipi di soluzione (una a base acquosa ed una organica) e applicando voltaggi e tempi diversi. I vari campioni sono stati osservati tramite analisi SEM e l'idrofilicità delle diverse superfici è stata valutata mediante un test di bagnabilità.

Campione	Ra [μm]
C1	0.99
C2	0.22
C3	0.12

Tabella 2: Parametri ottenuti dall'analisi profilometrica dei campioni

Sono stati quindi selezionati due tipi di strutture con dimensioni dei pori differenti e queste sono state caricate per immersione con un gel contenente gli isoflavoni e l'andamento del rilascio di genisteina nel tempo è stato studiato al variare della geometria dei nanotubi, mediante analisi spettrofometrica dei supernatanti. Inoltre, una cromatografia su strato sottile delle sostanze rilasciate ha consentito di confermare che gli estratti utilizzati contenessero i due isoflavoni principali, genisteina e dadzeina, e le loro forme non-attive.
Quindi, i diversi tipi di campioni sono stati caratterizzati biologicamente: mediante stainings a base di falloidina ed analisi SEM, è stato valutato come la proliferazione e la morfologia di cellule osteoblastiche di linea fossero influenzate dalla presenza dei nanotubi e dell'estratto della soia.

I test di anodizzazione effettuati con la soluzione acquosa hanno mostrato che un approccio di tipo potenziostatico, rispetto a quello galvanostatico, è necessario per avere la possibilità di variare le dimensioni dei diametri dei nanotubi modulando il potenziale applicato.
Inoltre, trattamenti in soluzione a base di etilen-glicole hanno dimostrato che l'utilizzo di un elettrolita organico, rispetto ad una soluzione acquosa, porta alla formazione di una struttura maggiormente ordinata con nanotubi con pareti lisce e lunghezze maggiori, la quale è mostrata in figura 9.

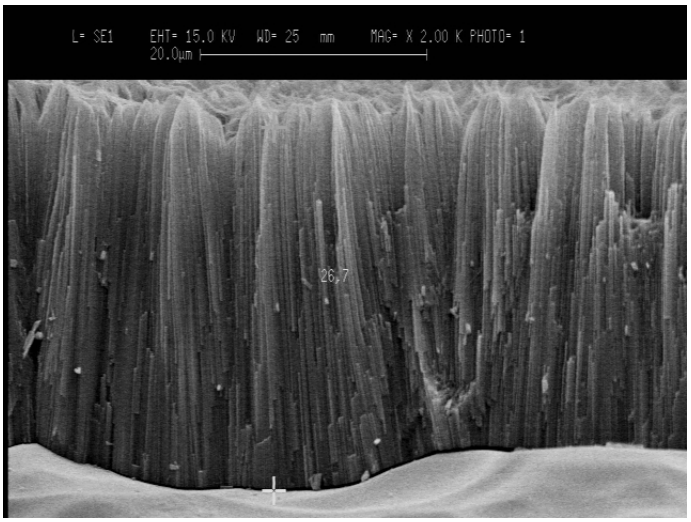

Figura 9: Vista laterale dello strato nanotubolare di un campione anodizzato in soluzione organica.

Si è osservato, tuttavia, che con questo tipo di soluzione si forma superficialmente uno strato irregolare e disordinato, chiamato "nanograss", più o meno compatto a seconda della durata del trattamento. Secondo letteratura [17], la formazione di questa struttura superficiale dipende dalla rugosità della superficie di partenza. Per questo motivo, sono state scelte tre lastre con diverse rugosità: la lastra 2 presentava una lavorazione superficiale più fine della 1, mentre la lastra 3 è stata sottoposta ad un processo di elettrolucidatura. I campioni sono stati quindi trattati alle stesse condizioni, i.e. 60 V per 6 h, e si è visto che la presenza dello strato di nanograss diminuisce all'aumentare della qualità della superficie, come mostrato in figura 10.

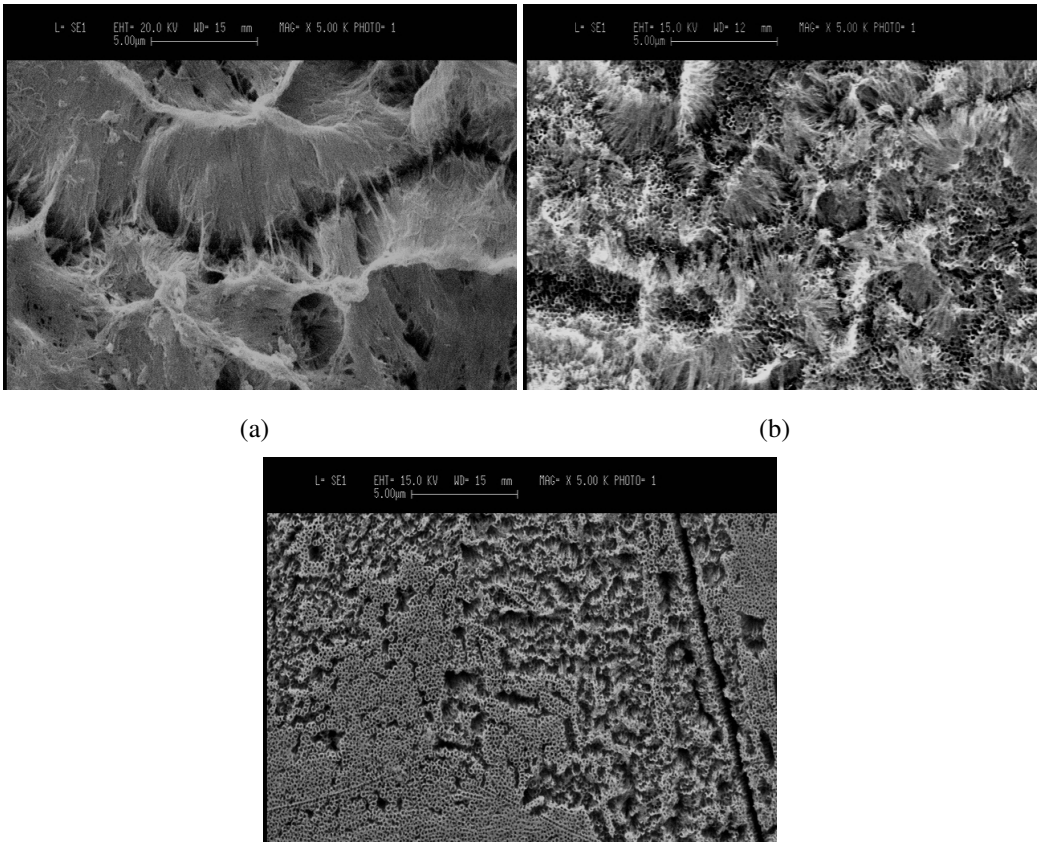

Figura 10: Campioni anodizzati a 60 V per 6 h aventi diverse rugosità: (a) 1, (b) 2 e (c) 3.

In particolare, il campione con la R_a minore risulta essere totalmente privo dei residui superficiali, ma lo strato di ossido formatosi ha mostrato una bassissima aderenza alla superficie di titanio sottostante e, perciò, per i successivi esperimenti sono stati utilizzati campioni con rugosità intermedia.

E' emerso successivamente che trattare i campioni per 20 secondi in ultrasuoni, alla fine del processo di anodizzazione, porta alla quasi totale rimozione dello strato di nanograss, consentendo l'ottenimento di nanotubi scoperti senza dover passare per un pretrattamento come quello di elettrolucidatura. Questo metodo, tuttavia, risulta efficace solo per anodizzazioni con una durata superiore alle 2 ore, poichè trattare il campione per un tempo minore porta superficialmente alla formazione di uno strato poroso compatto che non viene rimosso dagli ultrasuoni. Anodizzando, inoltre, più campioni per 2 ore a diversi voltaggi si è osservato che è possibile rimuovere lo strato superficiale se al sistema sono stati applicati almeno 50 V.

Per quanto riguarda le dimensioni dei nanotubi, è stato provato che prolungando il processo di anodizzazione si può aumentare lo spessore dello strato nanotubolare, il quale come i diametri può essere incrementato anche applicando una maggiore differenza di potenziale.

Una volta valutato come le dimensioni dei nanotubi fossero influenzate dai vari parametri

di processo, sono stati selezionati i parametri che consentissero la produzione due gruppi di campioni anodizzati a due diversi voltaggi, e quindi aventi nanotubi con dimensione dei diametri differenti (Fig. 11).

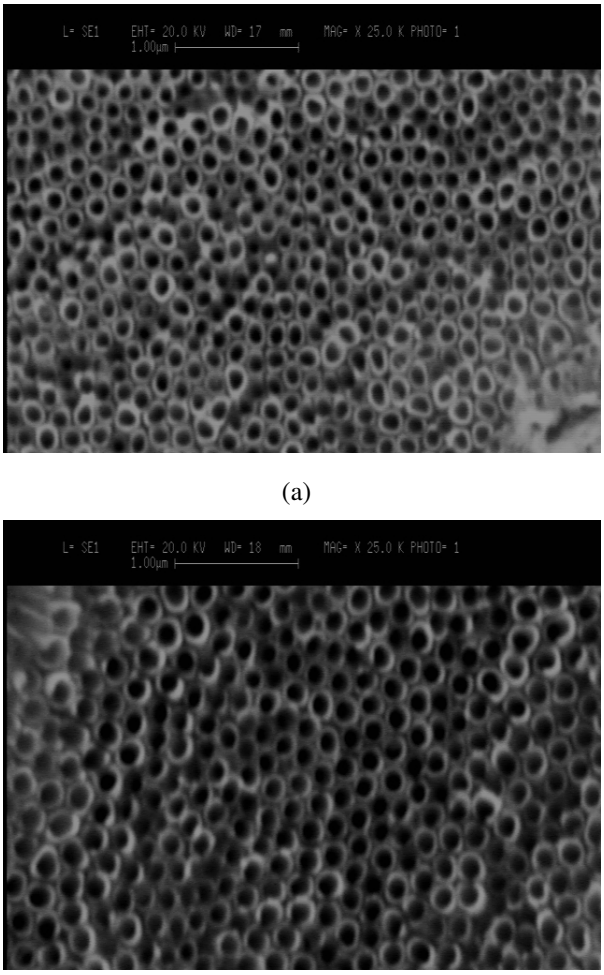

(a)

(b)

Figura 11: Esempio della struttura nanotubolare ottenuta. Campioni anodizzati in una soluzione a base di etilen-glicole, per 2 ore e applicando una differenza di potenziale di (a) 50 V e (b) 70 V.

Test di bagnabilità della superficie hanno permesso di osservare che l'idrofilicità delle superfici nanotubolari è più elevata rispetto a quella del titanio puro ed aumenta per nanotubi di diametri maggiori.
Per quanto riguarda il rilascio di farmaco, in linea con lavori precedenti, l'andamento di genisteina e genistina da parte dei nanotubi presenta inizialmente un rilascio istantaneo ed elevato ed una successiva fase di rilascio dopo circa 24 ore. A parità di concentrazioni utilizzate per caricare i campioni, i campioni anodizzati hanno mostrato una maggior quantità di molecole rilasciate rispetto al titanio non trattato ed, inoltre, l'ammontare di farmaco caricato risulta crescente con le dimensioni dei nanotubi ottenuti, specialmente per quanto riguarda la molecola genisteina.
La coltura di cellule osteoblastiche sui diversi campioni ha mostrato che, per quanto ri-

guarda l'adesione e la morfologia cellulare, in colture della durata di 24 ore gli osteoblasti rimangono tra loro isolati e presentano, rispetto a quelli su titanio puro, una forma più arrotondata, tipica delle prime fasi di adesione cellulare. Prolungando la coltura oltre 48 ore, la linea cellulare assume una forma più squadrata, appiattita e sono visibili interazioni tra cellule adiacenti, soprattutto sui campioni con nanotubi più piccoli.
Per quanto riguarda la proliferazione cellulare, essa aumenta in presenza dei soli nanotubi, mentre diminuisce sui dischetti ricoperti con l'estratto di soia. In particolare, questi effetti sono più marcati sulle superfici con nanotubi di dimensione maggiore.

Considerando i campioni caricati con gli isoflavoni, invece, attraverso lo staining dei filamenti di actina mediante falloidina non si notano particolari differenze morfologiche rispetto agli altri campioni. Tuttavia, dall'analisi SEM dei dischetti riportata in figura 12 sembra che in presenza del rivestimento le cellule siano maggiormente estese e comunicanti tra loro, specialmente sui campioni anodizzati a 50 V.

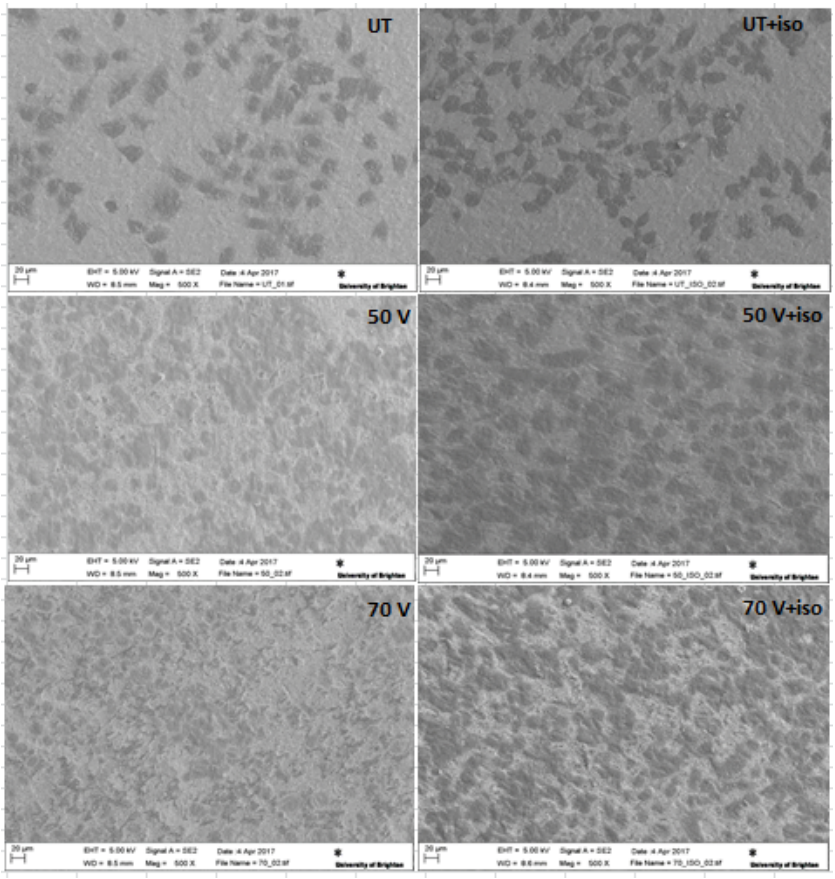

Figura 12: Analisi al SEM di cellule colitvate ore 65 ore su Ti non trattati (UT) e anodizzati non ricoperti (50 V e 70 V) e ricoperti con un estratto di soia (UT + iso, 50 V + iso, 70 V + iso).

Questo progetto ha permesso di definire come, nel set-up a disposizione, la morfologia e le dimensioni di nanotubi in ossido di titanio fossero influenzati dai parametri del pro-

cesso di anodizzazione con cui questi vengono prodotti. Inoltre, le prove effettuate hanno condotto alla definizione di un set di parametri che consente la produzione di uno strato nanotubolare con spessore dell'ordine della decina di micrometri e diametri modulabili tramite la variazione del potenziale applicato. Questa nanostruttura favorisce l'adesione e aumenta la proliferazione di cellule osteoblastiche di linea. Inoltre, può essere utilizzata come sistema di rilascio di farmaco, poichè è in grado di caricare e poi rilasciare molecole che possono favorire ulteriormente la produzione di matrice ossea fin dalle prime ore dopo l'impianto.

Sarebbe interessante in seguito esplorare tempi di anodizzazione più lunghi, per valutare se sia possibile per durate maggiori ridurre il potenziale applicato e quindi produrre nanotubi con diametri minori. Questo consentirebbe di ampliare lo studio relativo al rilascio di farmaco in relazione ai diametri dei nanotubi ed il loro effetto su cellule osteoblastiche.

Inoltre, l'analisi dell'attività della fosfatasi alcalina sulla linea cellulare saos-2 in presenza dei nanotubi e degli isoflavoni sarebbero utili per dimostrare quantitativamente come i diversi substrati influiscano sulla produzione di matrice ossea, sul differenziamento osteoblastico e quindi sull'effettiva osseointegrazione dell'impianto.

Contents

List of Figures

List of Tables

Chapter 1

Introduction

1.1 Titanium

Titanium is one of the most widespread element on the Earth, indeed, it constitutes the 6% of its total weight and it's the fourth metal element for diffusion after aluminium, iron and magnesium. It has atomic number 22, the melting point at 1668°C and it has, at ambient temperature, an hexagonal compact (EC) crystalline structure (α phase) that becomes a body-centred cubic (BCC) structure at 885°C (β phase).

Titanium is usually used in two different forms: commercial pure (CP) titanium and alloys. This is a very interesting material for those applications which need high mechanical properties, corrosion resistance and low weight in the same time. In particular, commercial pure titanium is so used cause it has very low density, Young's modulus and thermal conductibility and expansion; but in the same time it is really resistant to loads (as the steel and twice more than aluminium) and corrosive environments. Moreover, this metal has a brief radioactive half-life, a very high melting point, it isn't magnetic and it is extremely biocompatible, which makes this material one of the most used also in biomedicine.

Titanium alloys differ from CP titanium because of their higher mechanical characteristics and elasticity, but they're more sensible to corrosion and their processing is harder and more expensive [32].

1.1.1 Titanium applications

Titanium was initially used and developed for aeronautic and aerospace fields [33] owing to their high strength to weight ratio and excellent corrosion resistance. Today this

metal and his alloys are used also in the energy industry [34], in transport vehicles [35], in electro-chemistry [36] and sportive goods [37].

Commercially pure titanium is considered to be the best biocompatible metallic material because its surface properties result in the spontaneous build-up of a stable and inert oxide layer. The main physical properties of titanium responsible for the biocompatibility are: low level of electronic conductivity, high corrosion resistance, thermodynamic state at physiological pH values, low ion-formation tendency in aqueous environments and an isoelectric point of the oxide of 5–6. In addition, the passive-film-covered surface is only slightly negatively charged at physiological pH, and titanium has a dielectric constant comparable to that of water with the consequence that the Coulomb interaction of charged species is similar to that in water [38].

For these reasons, most recently titanium and titanium alloys gained big popularity and diffusion in the biomedical field. Particularly, they're used for implant devices replacing failed hard tissue. Examples include artificial hip joints, artificial knee joints, bone plates, screws for fracture fixation, cardiac valve prostheses, pacemakers and artificial hearts [39].

1.2 Implant failure

An implant-supported restoration offers a predictable treatment for bone replacement. Success rates for implants are high but, despite the low number, failures occur most of the time unexpectedly [19, 22].

A distinction should be made between early (weeks or months after implant installation) and late failures (after loading). Early failures may be the result of one or several aetiological factors during the healing phase. Late failures are characterised by failure once the implant is stably integrated and may be caused by pathological processes involving the biomechanical or the biological equilibrium [40].

The major reported predictors for implant success are generally divided into patient-related factors, implant characteristics and clinician's experience. Particularly, factors dependent from patient are his age [23], bone quality and quantity [24], the presence of any systemic disease [41] and hygiene [25]. Furthermore, for what concerns the implant characteristics, the correct integration between it and surrounding tissues can be affected by implant site and design (like sizes or superficial properties) [26]. At last there are factors that depend on the clinician, like the time of implant loading [23].

1.3 Surface modification of titanium

The clinical success of oral implants is related to their early osseointegration.

After the installation of implants, titanium surface interact with biological fluids and tissues and there are two possible responses that may occur in host tissues: an acute or chronic inflammatory process, with the formation of a fibrous soft tissue capsule around the implant that does not ensure proper biomechanical fixation and cause early implant failure, or living and functional bone tissue formation around the implants without an intervening connective tissue layer [42]. This biological fixation is considered to be a prerequisite for long-term success of orthopaedic and dental implants. The rate and quality of osseointegration in titanium implants are related to their surface properties. Surface composition, hydrophilicity and roughness are parameters that may play a role in implant–tissue interaction and osseointegration [2].

For this reason, in last years many treatments have been developed in order to create a micro-rough surface and improve the osseointegration of titanium surfaces. In the following sections are described some of the most used methods to create a rough surface and improve the osseointegration of titanium implants: plasma spray, grit-blasting, acid-etching techniques and the anodization treatment.

1.3.1 Plasma spray technique

A titanium plasma-spraying (TPS) consists in injecting titanium powders into a plasma torch at high temperature. Titanium particles condense and fuse together on the implant surface forming a uniform film of 40-50 μm which has a surface roughness of around 7 μm (Fig. 1.1) and increases the surface area of the implant [2].

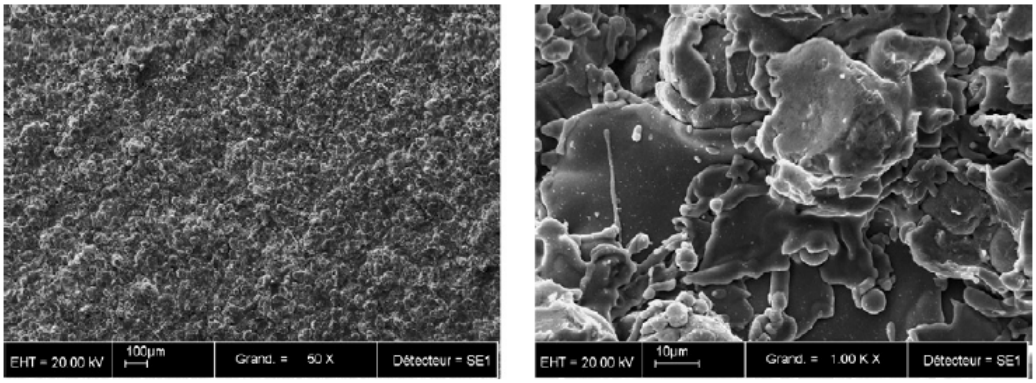

Figure 1.1: SEM micrographs of a titanium plasma-sprayed (TPS) surface [2]

This three-dimensional topography can increase the tensile strength at the bone-implant surface [43]. Some other works reported the presence of metallic wear particles, from endosseous implants in different sites or organs [44], that may be the product of dissolution, fretting and wear, and may be a source of concern due to their potentially harmful local and systemic carcinogenic effects [45].
However, the local and systemic adverse effects of the release of titanium ions have not been universally recognized [46].

Nowadays, there is a consensus on the clinical advantages of implanting moderately rough surfaced implants (in the micro-metric range) rather than using rough plasma-sprayed implant surfaces [47].

1.3.2 Grit-blasting technique

Another approach for roughening the titanium surface consists in the grit-blasting technique. It consist in projecting hard ceramic particles at high velocity by means of compressed air. Different surface roughnesses can be produced on titanium implants depending on the size of the ceramic particles. The blasting material should be chemically stable, biocompatible and should not affect the osseointegration of the titanium implants [2].

Various ceramic particles have been used, for example alumina (Al_2O_3) produces surface roughness varying with the granulometry of the blasting media. However, alumina is hard to remove from the titanium surface and it could give some problems to the integration of implant. For example, in some cases, these particles have been released into the surrounding tissues and have interfered with the osseointegration of the implants; moreover this chemical heterogeneity of the implant surface may decrease the excellent corrosion resistance of titanium in a physiological environment [48].

For blasting titanium prosthesis it's possible to use also titanium dioxide which could produce a moderately rough surface in 1–2 μm range using particles with an average size of 25 μm (Fig. 1.2).

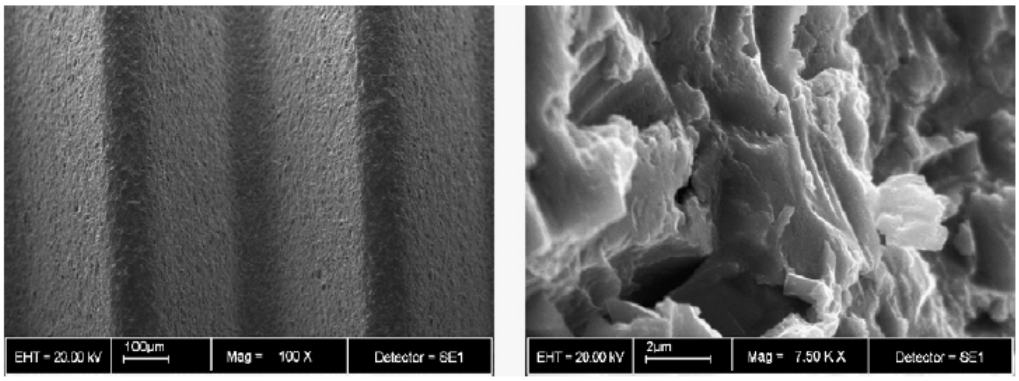

Figure 1.2: SEM micrographs of a TiO blasted surface [2]

Different experimental studies have shown a significant improvement for bone-to-implant contact (BIC) [49, 50] and survival rates [51, 52] for the TiO_2 blasted implants in comparison with machined surfaces. Wennerberg et al. [53] demonstrated with a rabbit model that grit-blasting with TiO_2 or Al_2O_3 particles gave similar values of bone–implant contact, but drastically increased the biomechanical fixation of the implants when compared to smooth titanium.
The problem is that these studies corroborate that roughening titanium implant surface increases their mechanical fixation to bone but not their biological fixation.

Another possibility for roughening titanium with the grit-blasting technique consists in using calcium phosphates such as hydroxyapatite, beta-tricalcium phosphate and mixtures: a biocompatible, osteoconductive and resorbable blasting material. These materials are resorbable, leading to a clean, textured, pure titanium surface. Experimental studies have demonstrated a higher BIC with these surfaces when compared to machined surfaces [54, 55] and similar to that observed with other blasting surfaces [56].

1.3.3 Acid-etching technique

Another way to treat titanium surface to improve osseointegration with the surrounding tissue is acid-etching, which consists in the immersion for few minutes of titanium in a solution with nitric, hydrochloric, sulphuric or hydrofluoric acid. This technique produces micro pits on titanium surface with sizes ranging from 0.5-2 μm in diameter [57].

Acid etching could also be made in a mixture of two different acids (dual acid-etching) heated above 100°C to enhance bone-to-implant contact, because of the pro-

duction of a homogeneous micro-porous surface, and less bone resorption with dual acid-etched surfaces compared to machined or TPS surfaces [58].

Another approach involves treating titanium surfaces in fluoride solutions. Titanium is very reactive to fluoride ions, forming soluble TiF_4 species. The surface produced has a micro-rough topography (Fig. 1.3) and there's fluoride incorporation which is favourable to the osseointegration of implants because it enhances osteoblastic differentiation [59]. Fluoridated rough implants also withstood greater push-out forces and showed a significantly higher torque removal than the control implants [60, 61].

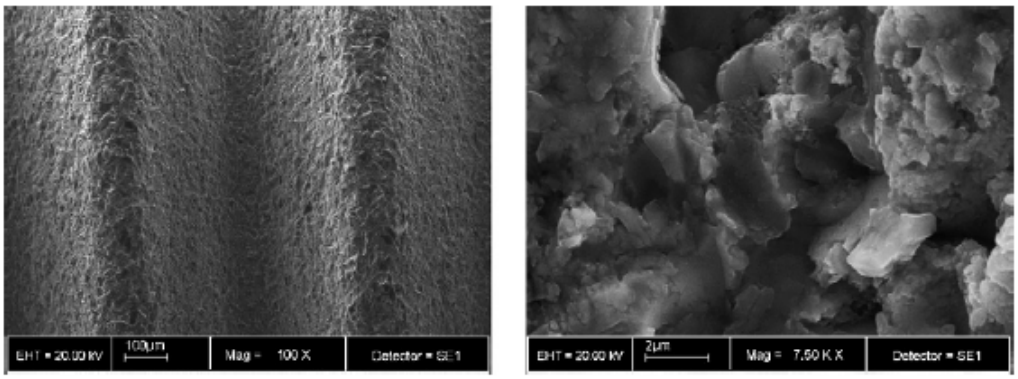

Figure 1.3: SEM micrographs of a titanium surface etched in a fluoride solution [2]

Nevertheless, chemical treatments might reduce the mechanical properties of titanium. For instance, acid-etching can lead to hydrogen embrittlement of the titanium, creating micro cracks on its surface that could reduce the fatigue resistance of the implants. This hydrogen embrittlement of titanium is also associated with the formation of a brittle hybrid phase, leading to a reduction in the ductility of the titanium. This phenomenon is related to the occurrence of fracture mechanisms in orthopaedic prosthesis [62].

1.3.4 Anodization

Anodization is an electrolytic passivation process used to increase the thickness of the natural oxide layer on the surface of metal parts which form the anode of an electrical circuit. This process could be performed under potentiostatic or galvanostatic conditions, in case you want to keep constant the potential difference or current intensity, in a strong acid solution. The oxide layer will be thickened during the process, but it dissolves along current convection lines creating micro or nano-pores on the titanium surface [3].

The anodization process is rather complex and depends on various parameters such as current density, concentration of acids, composition and electrolyte temperature. Anodized surfaces result in a strong reinforcement of the bone response with higher values for biomechanical and histomorphometric tests in comparison to machined surfaces [4]. Two mechanisms have been proposed to explain this osseointegration: mechanical interlocking through bone growth in pores and biochemical bonding [63, 64].
Modifications to the chemical composition of the titanium oxide layer have been tested with the incorporation of magnesium, calcium, sulfur or phosphorus. It has been found that incorporating magnesium into the titanium oxide layer leads to higher removal torque value compared to other ions [63].

Moreover, the anodization treatment could also be used on titanium surfaces to obtain a very regular nano-tubular structure.
The discover of this kind of structure was made on aluminium surfaces by Keller et al. fifty years ago [65]: they realised that anodic treatment of aluminium in neutral or alkaline solutions leads to the formation of a flat, compact oxide, but when anodized in acid electrolytes regular porous oxide structures could be obtained.
Some years later [66] was reported that, under specific experimental conditions, pores that show an high degree of self-organization could be achieved (Fig. 1.4).

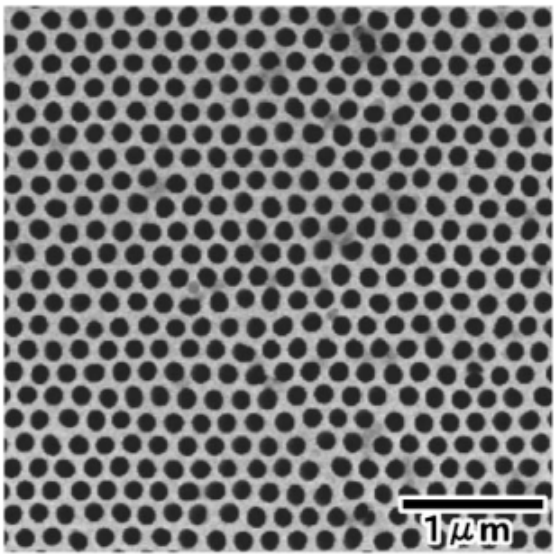

Figure 1.4: SEM micrographs of a alumina nanotubes [67]

1.4 Titanium dioxide nanotubes

Many of the principles and mechanisms for self-organized porous alumina can be transferred to the formation of self-organized tubes or pores on other metals, taking into account some specific differences in the chemical character of the different metal oxides. Particularly, in 1979 Kelly et al. [68] studied the influence of fluoride on the passivity of titanium and concluded that porous oxide layers could be obtained for low fluoride concentrations. Unfortunately, they did not perform electron microscopy at a sufficient high resolution to notice the presence of self-organized TiO_2 nanotube layers.
In 1999, Zwiling et al. reported the first self-organized anodic oxides on titanium for anodization in chromic acid electrolytes containing hydrofluoric acid [28]. This work showed organized nanotube layers with considerable sidewall inhomogeneity and not highly organization, but the most important thing is that they proved that small additions of fluoride ions to an electrolyte are the key to form these self-organized oxide structures on titanium surfaces.

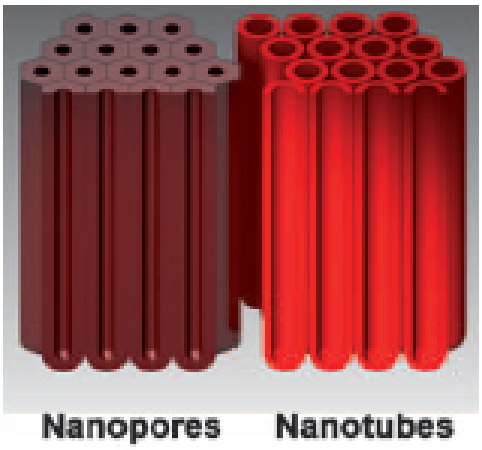

Figure 1.5: Self-ordered oxides [69]

After the discover that titanium dioxide nanotubes could be obtained by an anodization treatment in a fluoride-containing solution, many groups tried to find out which are the process variables that mostly affect the regularity of nanotubes structures. For example, first Makak et al. demonstrated that the electrolyte pH plays an important role in the thickness of tubes layers: NTs are longer if treated with a neutral solution [70, 71].
After that was proved that in non-aqueous electrolytes nanotubes appear with smooth

sidewall and are really more ordered than the ones obtained in aqueous or acid solutions [6]; it's even possible to obtain an ideal hexagonally arranged tube layer (Fig. 1.6) through a two-step anodization process [72].

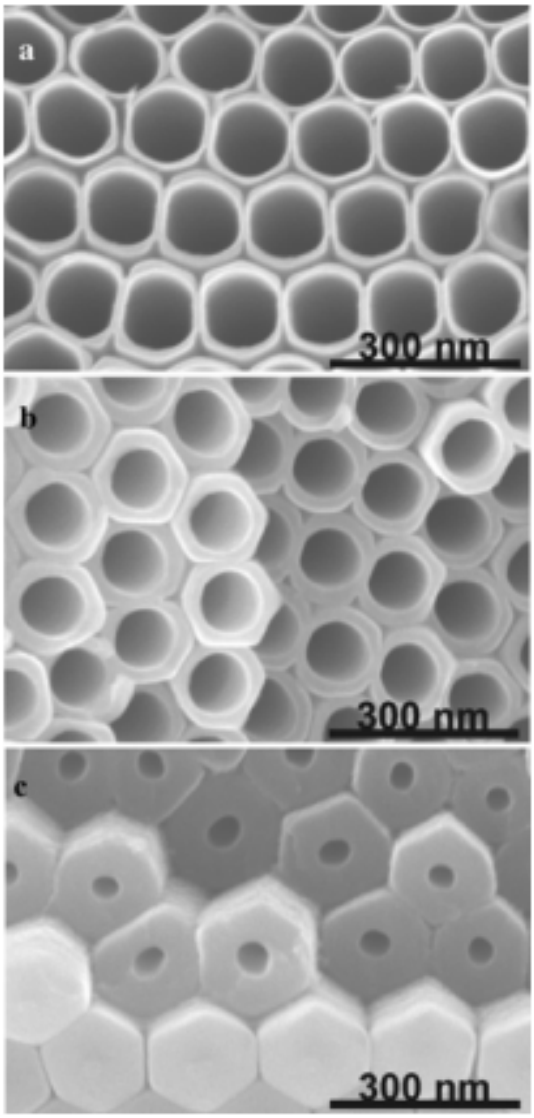

Figure 1.6: SEM images of close-packed hexagonal TiO2 nanotubes taken from the upper part of the layer (a), in the middle (b) and at the bottom of the layer (c). [69]

Then it was demostrated that titanium dioxide NTs coul be formed also in ionic liquids [73] or other protic solvents [74], but no further significant enhancement could be achieved. Regarding nanotubes, may also be encountered self-ordered surface dimples [75], which are metallic surfaces from which the tube layers have been ultrasonically removed (Fig. 1.7).

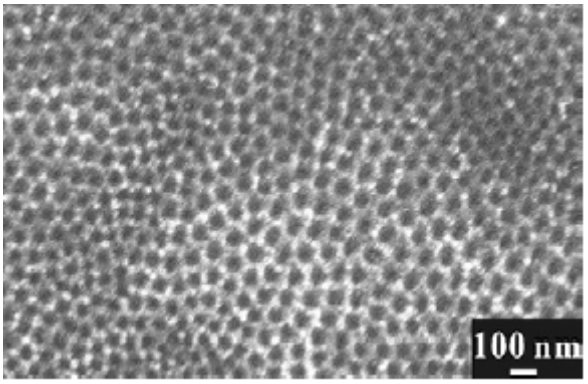

Figure 1.7: SEM images of Ti foil surface after ultrasonic removal of the NTs layer. [75]

1.4.1 Growth of TiO_2 nanotubes

Self-organized titanium dioxide nanotubes could be obtained trough an anodization process in a fluoride-containing electrolyte that is either water-based or organic. A titanium sheet is used as an anode in a two- or three-electrode configuration and voltages in the range of a few up to a several hundred volts are applied.

In absence of fluoride ions a compact oxide layer forms on the TiO_2 surface according to the following equations:

$$M \rightarrow M^{z+} + ze^- \tag{1.1}$$

$$M + \frac{z}{2}H_2O \rightarrow MO_{\frac{z}{2}} + zH^+ + ze^- \tag{1.2}$$

$$M^{z+} + zH_2O \rightarrow M(OH)_z + zH^+ \tag{1.3}$$

$$M(OH)_z \rightarrow MO_{\frac{z}{2}} + \frac{z}{2}H_2O \tag{1.4}$$

In the same time hydrogen evolution takes place at the cathode:

$$zH_2O + ze^- \rightarrow \frac{z}{2}H_2 \uparrow + zOH^- \tag{1.5}$$

This is the classical anodization scheme, involving ion formation [$Ti_4{}^+$; (1.1)], reaction with O_2 (created by deprotonation of H_2O or OH; (1.2), (1.3), (1.4)) and highfield ion migration of $Ti_4{}^+$ and O_2 through the oxide.
Subsequently, the growth of an anodic oxide layer is determined by the field-aided

transport of mobile ions through the oxide (Fig. 1.8).

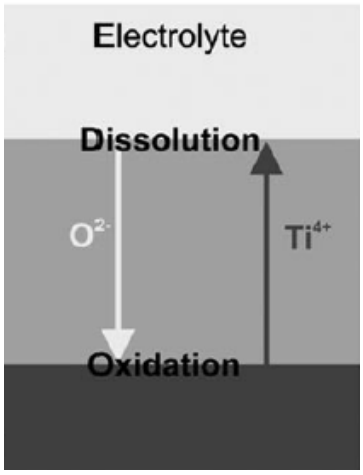

Figure 1.8: Schematic drawing showing field-aided transport of mobile ions through the oxide layers in the absence of fluoride ions. [69]

Depending on the migration rate of the involved ionic species ($Ti_4{}^+$, O_2), compact anodic oxide layers may in principle grow at either the interface between metal and oxide or at the interface between oxide and electrolyte, but under most experimental conditions oxide proceeds at metal-oxide interface.
Under a constant voltage U, the field $F = \frac{U}{d}$ reduces with increasing film thickness d. This lead to an exponential drop in the anodic current with the time until the field effect is lost and, from this moment, a determinate thickness which depends on the anodization voltage is reached [69].

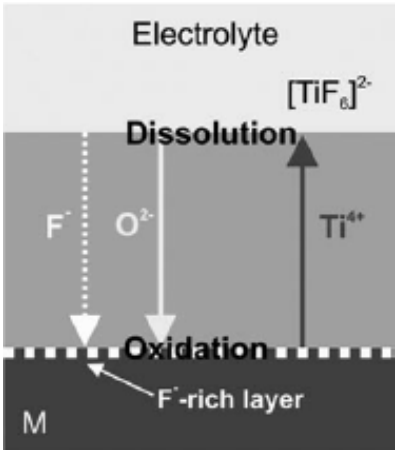

Figure 1.9: Schematic drawing showing fieldaided transport of mobile ions through the oxide layers in the presence of fluoride ions. [69]

In the case of fluoride-containing solutions, the second important anion (besides $O_2{}^-$) that migrates through the growing compact oxide is fluoride. It has been reported that fluoride ions can migrate through anodic oxide layers at twice the speed of the oxygen anions [76]; this allow fluorides to form Ti-fluoride compounds ($[TiF_6]^{2-}$) at the metal-oxide interface (Fig. 1.9). On one hand, complexation occurs with $Ti_4{}^+$ ions that are ejected at the oxide–electrolyte interface (1.6) and on the other hand by chemical attack of the formed TiO2 (1.7).

$$Ti^{4+} + 6F^- \rightarrow [TiF_6]^{2-} \tag{1.6}$$

$$TiO_2 + 6F^- \underrightarrow{H^+} [TiF_6]^{2-} + 2H_2O \tag{1.7}$$

Looking at current–time curves taken in a typical tube-forming electrolyte, using different anodization voltages (Fig. 1.10), could be noticed that during the formation of the compact layer (stage I), an exponential decay of the current occurs that is virtually the same as in absence of fluorides.

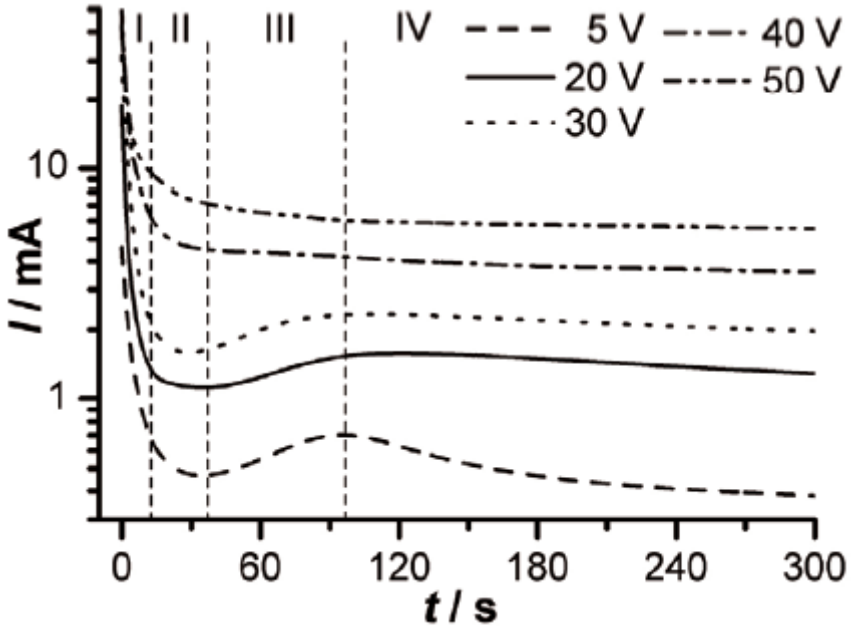

Figure 1.10: Current intensity trend in time for different applied voltages in an anodization process in the presence of fluoride ions (regions I, II, III, IV represent stages of TiO2 nanotube growth). [77]

After this first phase, that lasts less than 60 seconds, there's the formation of nanoscopic pores into the initial oxide especially at surface defects, and then they grow and widen

in time (stage II–III). The formation of these nanopores is not an entirely sequential process: it occurs concurrent with the first anodization stage but becomes only clearly detectable by SEM during the second stage where the current density deviates from an exponential decay due to the formation of these pores and the accompanying area increase.

When the primary pore survives and becomes large enough it will give birth to a nanotube underneath the initial compact oxide (stage III–IV), but should be noticed that not all these pores survive and become nanotubes. There is a competition between them, and the fastest growing pore wins by expanding under the initiation layer and closing access to metallic titanium for other pores.

As the transition from an initially porous layer to a stable tube growth occurs, the current density increases (stage III).

The increase in current is influenced by the specific anodic conditions, for example at higher anodization potentials this "drop and increase" behavior of the current becomes less clear due to a fast transition of processes through stages I–III.

In the last stage (IV), the TiO_2 nanotubes grow with a speed proportional to the current passed through the system [77], until the etching action of fluorides (permanent thinning of the tube tops) becomes apparent [78] and a steady-state situation between tube formation at the bottom and etching at the top according to equation (1.7) is established. For extended anodization, the growth may be determined by diffusional effects [78] and thus agitation [79] and viscosity (influence on the diffusion constant [6]) may become important.

Should be noticed that, when tubes are growing in stage IV (Fig. 1.10) the magnitude of the current is higher than when a compact oxide is formed at the same voltage. In terms of the driving force, this implies that an accordingly higher field must be present over the tube bottom, as the ion-migration rate is controlled by this oxide layer. A main role of fluorides is thus to maintain a thinner bottom oxide layer [80] by chemical etching of the oxide layer and immediate complexation of $Ti_4{}^+$ species (1.6) arriving at the oxide–electrolyte interface.

As a result, a fluoride-rich layer is formed at the metal–oxide interface.

The tube layers overall have a considerable fluoride ion content but the fluoride content decays strongly upon annealing [81].

1.4.2 Process parameters influence

Great attention should be given to any anodization parameter cause they all influence the final geometry and arrangement of the obtained TiO_2 nanotubes.

It is now accepted that growth occurs exclusively at the metal-oxide interface, whereas oxide dissolution is uniformly distributed over the whole of the NTs, especially in aqueous media. Preferential paths for the electrolyte are possible in organic media and non-uniform dissolution of the oxide can occur. The balance between oxide growth and dissolution is fundamental and can be altered by modifying the growth parameters. In addition to the nature of the electrolyte (i.e. aqueous or organic) there are several other key factors, such as pH, fluoride content, ageing of the electrolyte, anodizing potential and time, current density and temperature, that need to be taken into account when growing anodized TiO_2 NTs

1.4.2.1 Electrolyte

The nature of electrolyte used for the development of TNT strongly influences the formation of the graded structure.
It was demonstrated that, under the same conditions, different electrolytes produce different electric field intensity and so different kinds of nanotubular structures.

It was shown in previous work of Schmuki et al. [82] that the porosification process in HF electrolytes is essentially based on a competition between the pore formation at the metal-oxide interface and a chemical dissolution of the oxide at the outer interface.

This dissolution of titania is required for the pore formation, but on the other hand avoids the thickening of the porous layer, because when the pH is low the dissolution rate is too high [70].
More recently for the first time were obtained high-aspect ratio self-organized nanotubular titania layers, with thickness higher than $2\mu m$, by tailored anodization in neutral electrolytes containing NH_4F instead of HF [71, 29]. Thereby was exploited the slower chemical etching of titania: the hydrolysis reaction at the pore tip produces an acidic environment by adjusting the dissolution current and thereby the pH profile along the TiO_2 nanotubes in a manner that local acidification occurs at the pore tip while the pH-values established at the pore mouths are higher due to the buffer species NH_4F [83].
Further progress was recently achieved by using a viscous electrolyte containing fluoride ions. Prior experiments showed that nanotubes with very smooth tube walls and

length of several micrometers can be achieved using an organic solution [6].

After this, many studies were carried out to define how the water and the fluoride concentrations can affect the nanotubes geometry. In 2006, Grimes et al. defined the ranges of water and fluoride concentrations that could lead to the formation of a regular nanotubolar structure. Particularly they discovered that, increasing the water content, the lenght of nanotubes increases until the percentage volume of H_2O is lower than the 2 %, then it starts to decrease. The same behaviour could be observed varying the F^- concentration up to 0.3 % wt [84, 85]; the results of these studies are summarized in the following table (Tab. 1.1).

	0.1 wt % NH_4F	0.3 wt % NH_4F	0.5 wt % NH_4F
1% vol H_2O	54	67	47
2% vol H_2O	85	165	106
3% vol H_2O		136	85

Table 1.1: NTs lenght (μm) obtained by varying the concentration of H_2O and NH_4F in ethylene glicol (anhydrous), anodization performed at 60 V for 17 h.

Considering growth in organic solutions, another factor to be taken into account is the 'ageing' of the electrolyte [86] which helps to synthesize well defined NTs. It is generally observed that by reusing an organic electrolyte its electrical conductivity increases (Fig. 1.11) as a result of (i) a higher $TiF_6{}^{2-}$ content built-up during previous anodization cycles and (ii) a higher water content, which eventually reaches saturation due to moisture adsorption. A higher $TiF_6{}^{2-}$ concentration translates into a lower rate of chemical dissolution; hence it is important in establishing the condition required for maximizing oxide growth. Furthermore, the higher conductivity also enhances the growth rate of NTs, as it facilitates the passage of the current required to form the oxide. The importance of 'ageing' the anodizing solution is clearly demonstrated by the study from Raja et al. [87], since in anhydrous media the NTs could be only be formed by allowing sufficient uptake of moisture by the electrolyte.

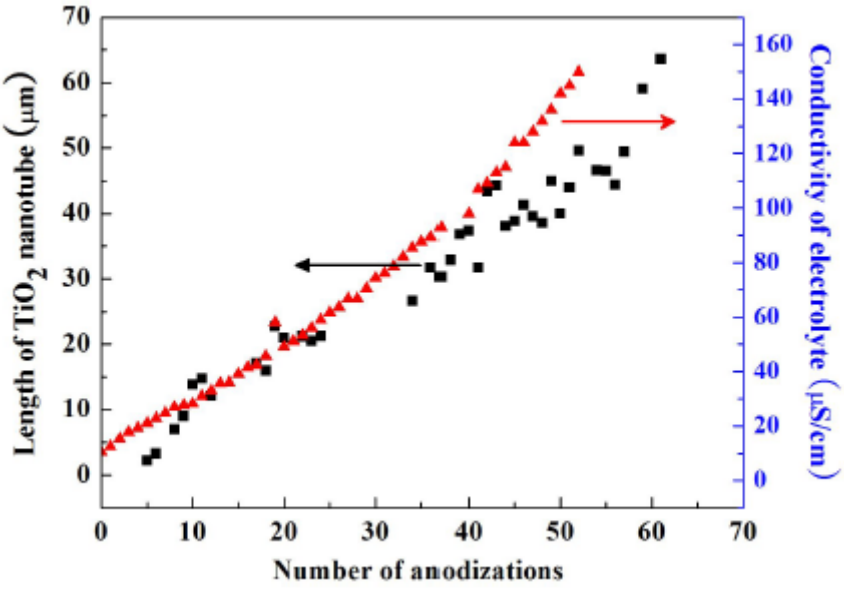

Figure 1.11: Variation of the solution conductivity with the iterative number of anodizations [88]

1.4.2.2 Anodising potential and current density

Self-ordering titanium dioxide nanotubes could be formed both with potentiostatic or galvanostatic method, which mean maintaining respectively anodization voltage or current constant [89].

The galvanostatic approach has been less investigated; work by Taveira et al. [90] showed that during constant current anodization the voltage indeed increases and fluctuates: the fact that the voltage may change with time leads to the loss of control over the tube diameter.

Most of experiments are performed applying a constant voltage and monitoring the current, cause was demonstrated that the tube diameters and the layer thickness depend on the steady-state voltage and under potentiostatic control highly ordered TiO_2 nanotubes with tunable dimensions can be obtained. Indeed, applied potential determines the electric field strength across the oxide, thus affecting the migration of ions and ultimately the nanotube diameter. A linear relationship between the applied potential and the diameter of the NTs was demonstrated in 2010, in a work made by Albu et al. [77]. They also noticed that increasing the anodising potential the outer diameter increases really more respect the inner diameter which remains almost constant (Fig. 1.12).

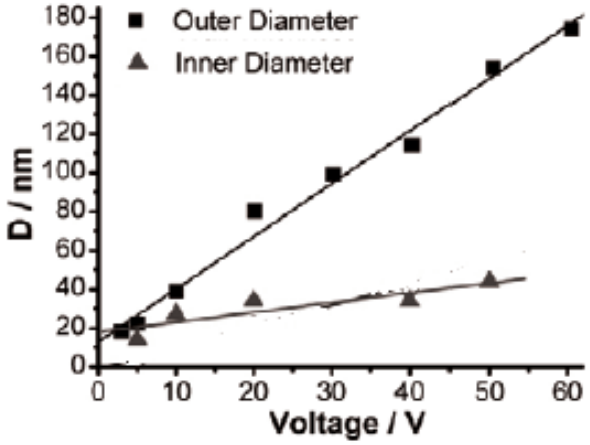

Figure 1.12: Diameter–voltage dependence of the nanotubes grown in ethylene glycol with addition of 0.1 M NH_4F and 1 M H_2O [77]

Later Schmuki et al. verified that the slope of the linear relationship between the diameter and the applied voltage changes in different electrolytes (Fig. 1.13).

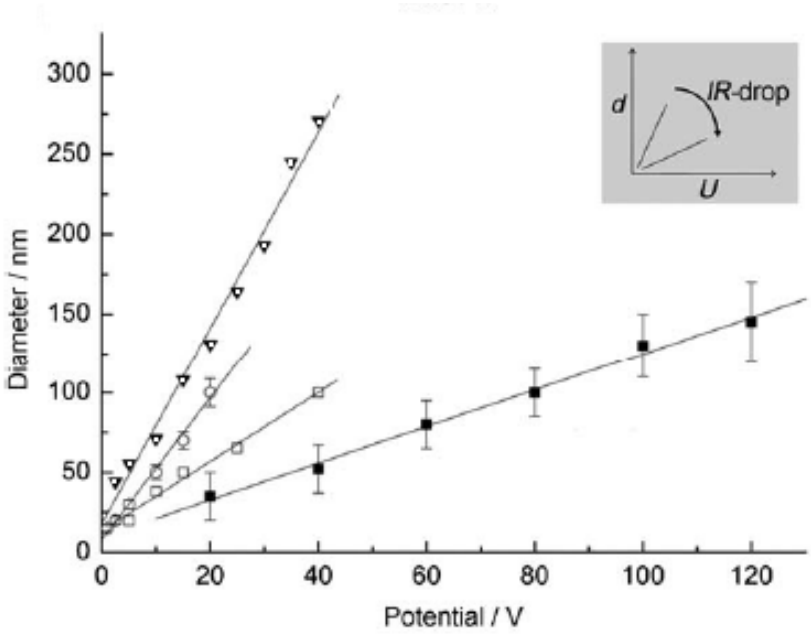

Figure 1.13: Diameter–voltage dependence of the nanotubes grown in different electrolytes, where ◯ stays for water-based electrolyte, ▽ for glycerol/water 50:50, □ glycerol, ■ ethylene glycol. Anodization voltage for ethylene glycol electrolyte held at 60 V, and 40 V for other electrolytes [69]

A linear dependence relationship also exists between the thickness of the barrier layer at the base of the NTs and the applied potential [8], but as illustrated in figure 1.14 this correlation is inverted for voltage larger than 60 V.

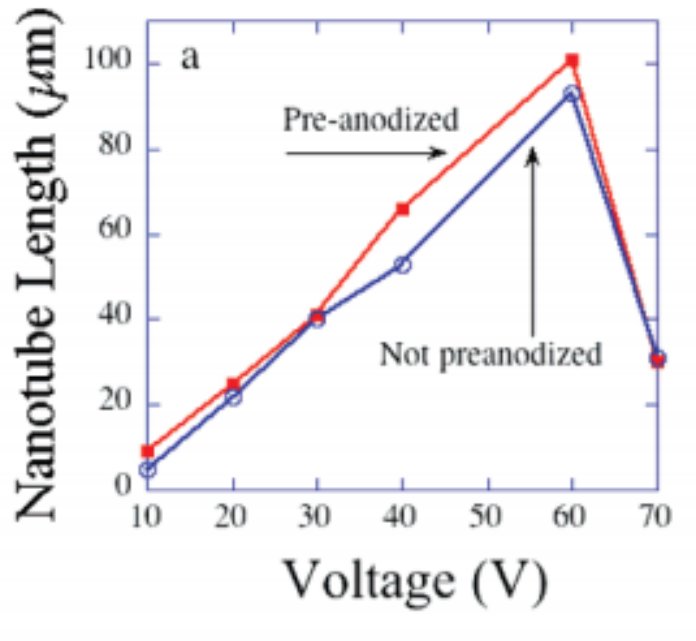

Figure 1.14: Variation of TiO_2 nanotube array length as a function of applied voltage for a 70 h anodization using 2% HF-DMSO electrolyte with and without a pre-anodization step to template the surface [91]

Clearly the anodizing potential and the modality by which it is applied (i.e. the potential may be established after sweeping or stepping up to a constant value, which is then maintained for the remainder of the anodizing process) have also an influence on the current density. For example, by applying a sweep in the range of 100 $\frac{mV}{s}$ to 1 $\frac{V}{s}$ it is possible to obtain a higher current density and longer NTs than by using slower sweep rates [92].

1.4.2.3 Anodization time

The anodization time influence most of all the length of the obtained nanotubes for every kind of electrolyte; indeed, NTs are generally longer if the treatment lasts more. Hence, to extend the maximum length of NTs for a given set of conditions, the optimal anodizing time should be identified.

Using an aqueous media, the conditions are too aggressive to allow the NTs to grow any longer than a few micrometers [93]. This length is reached within minutes from the start of anodization, but the process time could reach also 2 hours to allow the structure to rearrange itself and increase self-order.

Instead, the growth process in organic electrolytes is much slower and dissolution phenomena are not as significant as in water, although conditions still need to be tuned

for optimal growth. As a result, by extending the anodization time from several hours up to a day, it is generally possible to obtain NTs with a length up to hundreds micrometers [7].
In figure 1.15 could be noticed the great difference in terms of obtained lengths between using an aqueous or an organic electrolyte.

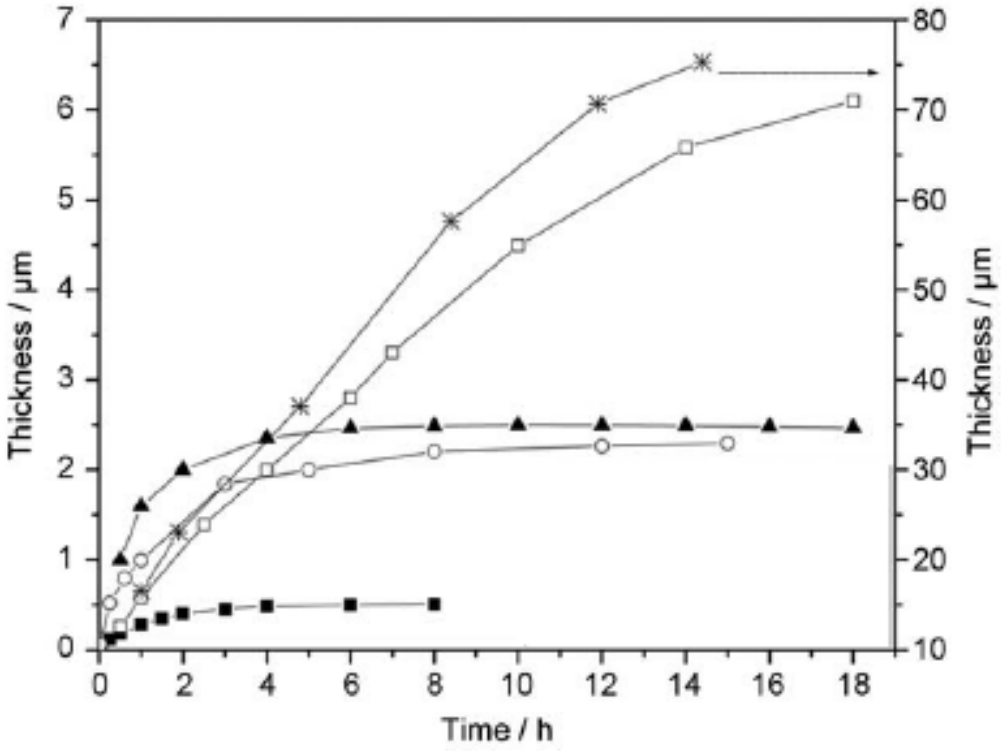

Figure 1.15: Length-time dependence of the nanotubes grown in different electrolytes, where ■ stays for water-based acidic electrolyte, ▲ for water-based neutral (left axis) and □ for glycerol, ◯ for glycerol/water 50:50, ∗ for ethylene glycol (right axis) [69].

1.4.2.4 Temperature

The temperature of the electrolyte affects the dissolution rate of the NTs which are normally grown at room temperature (20-25°C).

It has been shown that in aqueous media the diameter on the NTs does not depend on the anodizing temperature; instead, when using an organic electrolyte the diameter of the NTs is larger at a higher anodizing temperature since at a low temperature leads to higher viscosity and reduces both ion migration and especially the dissolution of TiO_2 and Ti by F^- ions [94].

Instead, the length of nanotubes increases with the electrolyte temperature (Fig.

1.16). Schmuki et al. in 2006 showed that for glycerol-based electrolytes the length of NTs is higher when the temperature increases from 0 to 80°C, but over 60°C the structure is not regular any more [95].

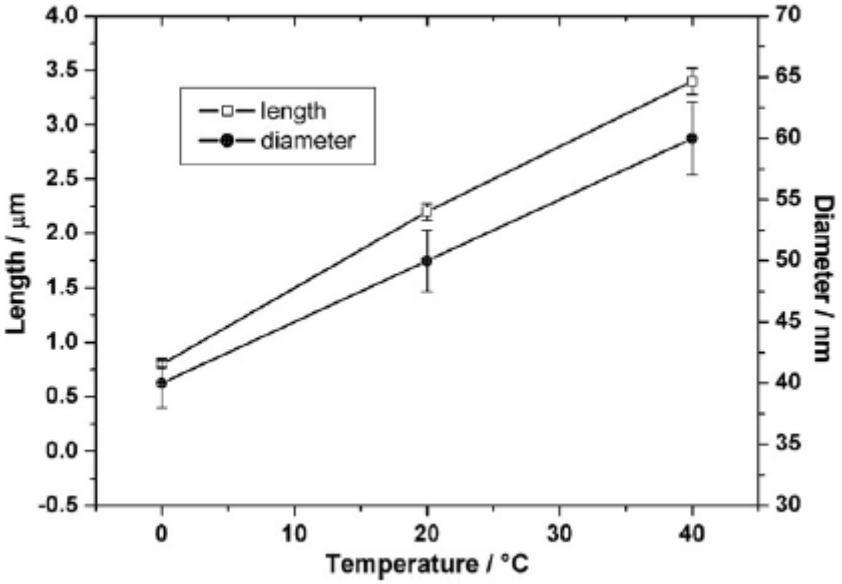

Figure 1.16: Lenght-temperature dependence in glycerol-based electrolyte. Anodization performed with a three-electrode configuration. [95]

1.5 Titanium dioxide nanotubes biological characterization

Nowadays titanium dioxide nanotubes (TiO_2 NTs) are used for many different applications because of their unique features, like outstanding charge transport properties, which make them suitable for a variety of advanced applications, including their use in sensors [96], dye sensitized solar cells [84, 97], and in hydrogen generation by water photo-electrolysis [84, 98]. Furthermore materials with aligned porosity in the submicron regime are of great interest for application in organic electronics, microfluidics, molecular filtration, drug delivery [99], and tissue engineering [12].

Concerning the biomedical applications, studies have shown that TiO_2 NTs provide more advantages than micro-rough TiO_2 or bare cpTi, including enhanced bioactivity and biocompatibility, appropriate biomechanics with bone, ease of functionalization and tailorable drug loading and releasing performances [100]. Numerous $in\ vitro$ and $in\ vivo$ studies have established these features of TiO_2 NTs, which make them an attractive implant modification strategy [101, 102].

Moreover, it was expected that nanotube dimensions will differentially affect the behaviour of cells adjacent to the implant. Indeed, some works have concluded that decreasing the pore size under 30 nm enhances cellular adhesion and proliferation, while larger pores (> 90 nm) demonstrate the least cell adhesion and proliferation characteristics but increasing cells differentiation [10, 11]. Anyway, another previous work showed that the Alkaline Phosphatase activity and the elongation of mouse osteoblasts become higher increasing the nanotubes size and this might lead to a change in cytoskeletal stress, thus promoting osteogenic differentiation of human BMMSCs and mouse MC3T3 cells [103].

Then, titanium dioxide nanotubes provides enhanced bioactivity to the implant surfaces, but what's really interesting is that they could be loaded with a variety of therapeutics, including growth factors, antibiotics or anticancer drugs which can be released locally at the site of trauma upon implantation [9].

1.5.1 Titanium NTs as local drug delivery

Bone infection and poor osseointegration are the leading causes for implant related complications, demanding extensive but ineffective systemic therapy and re-surgery

[104]. Bone infection and osseointegration are related and achieving quick osseointegration can prevent bacterial attachment and invasion. Furthermore, as conceptualized by Buchholz et al. [105], local drug delivery from the surface of bone implants has the potential to target these challenges, bypassing systemic therapy needs and achieving effective local therapeutic effect [106]. The key is releasing active biomolecules directly at the site of trauma, inside the bone microenvironment.

The aims of controlled drug delivery are to administer the appropriate amount of drug to the relevant sites in the human body and regulate the drug delivery profile in order to optimize the therapeutic benefits. Moreover, a proper drug delivery system should posses the following characteristics: haemostatic properties, controlled inflammation potential, lack of toxicity and stimulation of tissue cell activity [18].
Despite of the good properties of, for example, biodegradable polymeric coatings, such as collagen, chitosan and alginate this materials still do not offer any significant clinical advantage, unless they are loaded with expensive growth factors and biomolecules [107]. Then, because of those non satisfactory clinical outcomes of the products currently available, physicians continued to ask for biomaterials that could enhance tissue regeneration effectively having a reasonable cost.

In last years, was proved that titanium dioxide nanomaterials (like nanotubes, nanowires or nanoparticles) are suitable for drug-eluting implants and their drug delivery properties spur potential applications in the biomedical field [18], particularly owing to the large open volume.
In 2010, Gultepe et al. [108], demonstrated that the titanium nanotubular structure showed, after an initially high release rate, a nearly constant release which can be maintained over a long period of time, similar to the one typical of polymeric devices, but without dangerous degradation debris. Moreover, Peng et al., demonstrated the dependence of the release rate and times from nanotubes length and diameter sizes: nanotubes topography is directly responsible of drug elution [109].
Then, the new drug delivery systems composed of titanium nanotubes have the following advantages: high delivery efficiency, control of the dose varying the nanostructure geometry, prolonged exposure to drugs up to months, and reduced toxicity.
Moreover, different kinds of drugs such as antibacterial agents [110, 111], anticancer drugs [112] and genes [113] can be delivered by nanostructured TiO_2.
For example, the loading of drug into the nanotubes could be obtained by integrating TiO_2 nanotube arrays with polymeric micelles and biopolymer coatings [114]. About this, in the 1990s, the research groups at the School of Pharmacy and Biomolecular Science, University of Brighton, UK, and at the Institute of Composite and Biomedical

Materials, National Research Council (CNR), Italy, recognised a potential in the use of soy components in the tissue engineering field. The properties of the soy were compared with that of other natural biomaterials and was found the possibility to use it as biodegradable coating for applications in tissue regeneration.

1.5.1.1 Soy isoflavones

Soybean (*Glycine max*) is a leguminous plant belongs to the fabaceae family. It is the most widely grown and utilised legume in the world. As a consequence of its long story as a food used by many civilizations and countries, soy is among the most studied of natural materials [115]. Once harvested soybeans are usually dehulled and processed to make soy flour which is composed of proteins, carbohydrates, oil and minerals (Fig. 1.17).

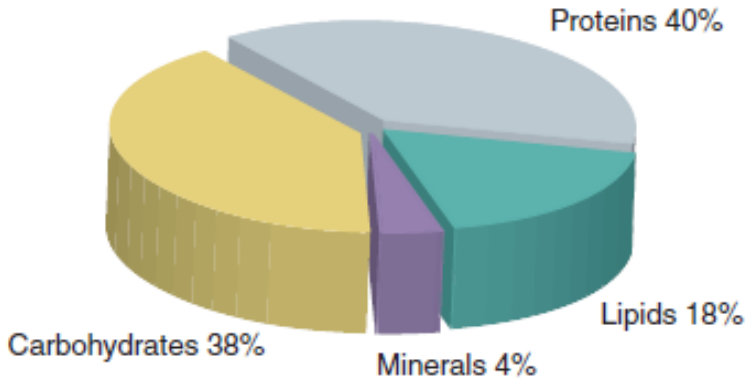

Figure 1.17: Soy flour composition [13].

Specifically, soy naturally contains the isoflavones, a class of plant produced steroidal compounds, with ascertained effect on immune and tissue cells [116]. There are 12 isomers of isoflavones which have been found in soybeans in 4 different isoforms, aglycones (Fig. 1.18) and three glucoside conjugates: the acetyl- β- glucoside, the malonyl- β- glucoside and the β-glucoside [117].

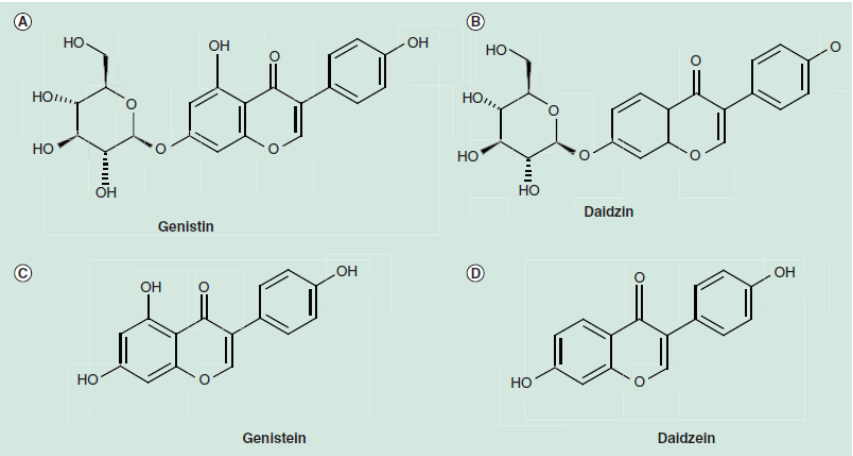

Figure 1.18: Isoflavone structures: glycosylated nonactive forms (A and B) and nonglycosylated bioactive forms genisteine and daidzein (C and D) [13].

Soy proteins and peptides have been reported to interact, activate and modulate biochemical and cellular components of the human body. Particularly, focusing the interest on the molecule genistein, many works were performed to find out which benefits this substance could have on the body cells.
This isoflavone has been shown to have an inhibitory effect on protein tyrosine kinases [118, 119] and more recently it has been shown that genistein has an anabolic effect on bone metabolism inhibiting bone loss in the tissue culture system in vitro [120] and on ovariectomized rats [121, 122].
Moreover, because of their relatively high hydrophobicity, non-glycosylated isoflavones are able to penetrate the cell and to interact with the estrogens receptors on the cell nuclear membrane. Their preferential interaction with the estrogen receptor β, rather than the α, leads them to block the cell proliferation cycle, by inhibiting the topoisomerase II enzyme, explaining their antitumoral effect [13].Then some works showed that this interaction with estrogen receptors gives to the isoflavones an estrogenic effect on osteoblasts and stem cell differentiation and their stimulation to produce mineralized bone noduli in vitro [14]. As for inflammatory cells, was proved that isoflavones inhibit the activation of the osteoclasts, the cells responsible for bone resorption during tissue remodelling [15, 16].

1.5.1.1.1 Soybean-based hydrogels

The researcher at the University of Brighton and CNR, Naples, have optimized a novel class of biodegradable soybean-based biomaterials that could offer a solution of many

of the problems currently experienced in the regeneration of broken bones and damaged tissues [15].
Using defatted soybean flour, those biomaterials can be obtained in form of membranes, granules, gels, pastes and bioglue and provided in different formulations such as injectable product (Fig. 1.19). All the formulations are protected by patent applications [123] and they're prepared from soy flour defatted through optimized methods that are able to completely remove the oil fraction.

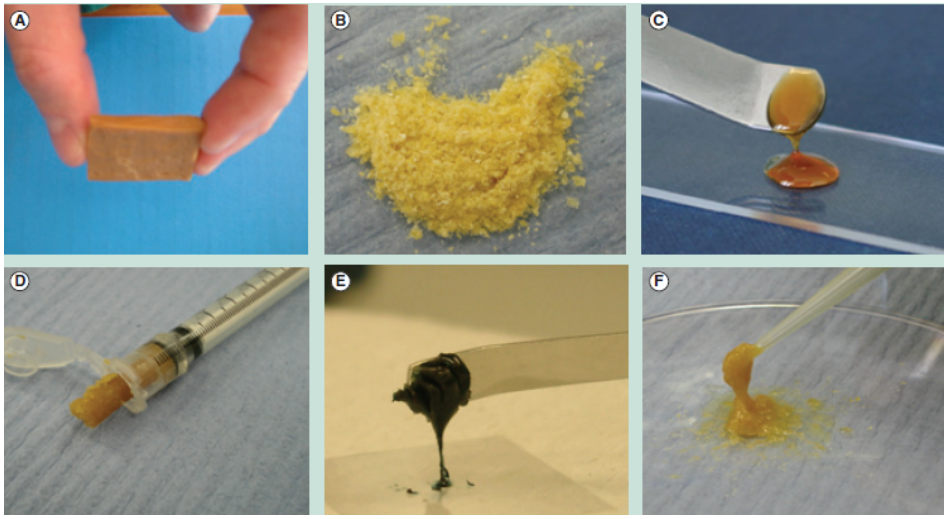

Figure 1.19: Soybean-based biomaterial formulations: blocks (A), granules (B), hydrogel (C), paste (D), bioglue (E) and injectable paste (F) [13].

Specifically tallking about soybean-based hydrogels, they're obtained by an extraction method where defatted soy flour is extracted in cosolvent system, such as ethanol and water (80/20, v/v), which allows the control of the concentrations of isoflavones in the final biomaterial [123]. Briefly, the soluble extract undergoes filtration to eliminate sediments and it's finally freeze-dried to obtain a very fine powder which is then resuspended in a cross-linking solution.
In vitro studies [15] showed a gradual release of isoflavones upon biomaterial swelling and degradation. Moreover, unpublished data obtained by researchers of the University of Brighton, showed a pattern of isoflavone release, whereby the nonactive glycosilated forms of these molecules are released at higher levels than the non-glycosilated ones, but gradually transformed into these bioactive molecules. Then, these findings offered the possibility to obtain soybean-based biomaterials where the gradual release of glycosilated isoflavones and their later transformation into non-glycosilated forms may ensure a protracted bioactivity upon implantation [13].

1.6 Aim

Despite of the great improvements achieved in the last years concerning the improvement of biomaterials for dental and orthopaedic applications, there are still open problems that have to be addressed about the implant/bone interface and implant fixation. Among the possible strategies, a possibility is to consider drug release systems applied to metallic biomaterials capable to deliver drugs or active biomolecules from the implanted device. Such systems, usally polymers or biopolymers applied as coating at the implant surface, usually lack of adhesion and the kinetic release is not fully predictable. In this perspective, a proper modification of the implant surface topography at the nanoscale could provide a proper reservoir for a proper drug release, possible with no or low drawbacks for bone cells adhesion, differentiation an implant fixation.

Indeed, cell to surface interactions, at the nanoscale, may represents a promising strategy to precisely control cell functions and differentiation to improve implant to bone interface, exploiting a a proper hierarchical interaction of the cells to the implant surface. Titanium dioxide nanotube arrays provide a highly regular nanostructure, and the possibility to tune nanotubes geometric parameters showed promising opportunity for future clinical applications. Titanium dioxide nanotubes can be easily formed on titanium surface by proper anodic oxidation processes, applicable to both flat and porous surfaces.

This project aims to optimize the titanium anodization process to obtain an ordered nanotube interface at the titanium surface to increase adhesion to enhance cell adhesion and differentiation, improving implant fixation. The project was particularly focused on the research of the treatment parameters to obtain different nanotube geometries. In particular, we want to set up an anodic oxidation process capable to coat the titanium surface with a strong and stable layer of nanotubes, around ten microns thick, with regular diameters, capable to uptake and release a drug. Moreover, the possibility to obtain two different diameter size was considered.

An anodic oxidation treatment was considered to obtain two different diameter titanium dioxide nanotubes. The obtained structures were characterized and functionalized with a biomolecule. A biological characterization was performed as well using osteoblast cell line.

The developed nanotube geometries were coated using soybean-based gels, a novel class of biomaterials, developed to further increase osteoblasts adhesion to the implant and to enhance osteoblastic differentiation. In particular, the different nanotube dimensions were compared in terms of soybean isoflavone release.

Chapter 2

Materials and methods

The anodization process optimization was carried out at the Department of Chemistry, Materials and Chemical Engineering 'Giulio Natta' of Polytechnic of Milan while nanotubes functionalization was made at the Department of Pharmacy and Biomolecular Science of the University of Brighton.

Samples were anodized in an inorganic solution with water and salt and in an organic electrolyte.
For both solutions, were made different experiments modulating voltage, current density, anodization time and kind of sample.

2.1 Samples

Titanium (grade 2) disks with a diameter of 12 mm and thickness of 0.7 mm were used for the experiments. Those disks came from sheets which presented different roughnesses that are reported in table 2.1.

Sheet	Ra [μm]	Rmax [μm]
S1	0.99	5.48
S2	0.22	1.98
S3	0.12	0.97

Table 2.1: Parameters obtained from the profilometric analysis of samples taken from different sheets.

Samples taken from sheet 1 underwent a pre-treatment in acid solution to wash

them: samples were deep for 25 s in a solution containing 5% of hydrofluoric acid and 30% of nitric acid in dH_2O and after that they were washed in ethanol (70%).
Were used also disks obtained from a commercial sheet (Sheet 2), which underwent a finer surface treatment than sheet 1, and from electropolishing process (Sheet 3).

2.2 Equipment

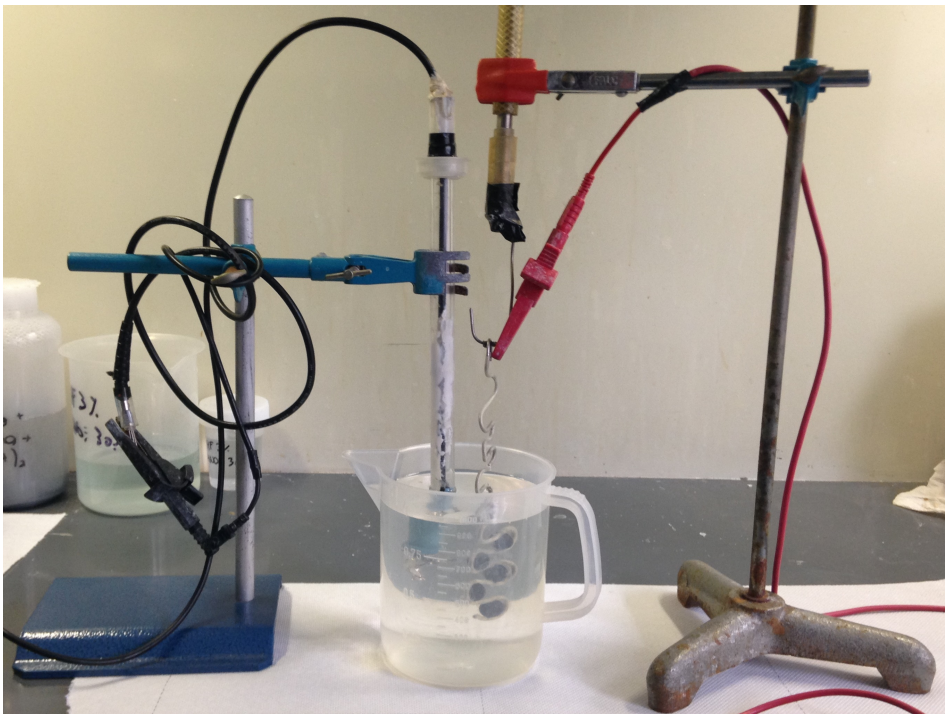

Figure 2.1: Anodization experimental set-up

The experimental set-up used for the synthesis of nanotubes is showed in figure 2.1. It includes an anode, which consists in the titanium disk, and a platinum cathode which was placed 2 cm distant from the other electrode, because this was the most used distance in literature [124, 125, 126]. The oxidative anodizations were all performed at room temperature [70, 83] because the temperature of the electrolyte could affect the nanotubes lengths, but from literature emerged that it's easier working at room temperature and varying the dimensions modifying other parameters like the anodization times and voltages. The samples were treated in two different solutions, an aqueous one (Tab. 2.2 and an organic one (Tab. 2.3): their compositions were chosen basing on the most used solvents and solutes concentrations contained in literature [127, 83], [84,

85]. The applied voltage and current density were controlled by a system DC power supply by Agilent technologies (N5772A; 600 V/2.6 A, 1560 W).
Concerning the choice of the organic solution, ethylene-glycol was used as electrolyte because from literature, working under the same parameters, this kind of solvent gave longer nanotubes in shorter time than glycerol [6]. Particularly, this electrolyte could be used to obtain a regular nanotubular structure, with a thickness around a dozen of μm, in less than 6 hours of treatment [69].

Solution 1	dH_2O	Sodium sulphate	Sodium fluoride
	2 L	1 M	0.5 wt %

Table 2.2: Aqueous solution composition.

Solution 2	Ethylene glycol	dH_2O	Ammonium fluoride
	1 L	2 wt%	0.3 wt%

Table 2.3: Organic solutions composition.

2.3 Experimental method

2.3.1 Aqueous solution

Samples coming from sheet 1 were anodised, both in potentiostatic and galvanostatic approach, for different times and voltages or current densities.
Two samples were then anodized under the same conditions, but one applying the needed voltage instantly and the second using a ramp of 0.3 V/s .
Furthermore, variation of nanotube geometry was studied keeping the solution motionless or under magnetic agitation.

Different tests are summarized in table 2.4, where 'A' indicates the use of aqueous solution, 'P' means potentiostatic approach, 'G' means galvanostatic approach and the numbers are respectively the used voltage and the anodization time.

Sample	P/G	Agitation	Voltage [V]	Current [mA]	Duration [h]
AP_20_2	P	Yes	20	14	2
AP_20r_2			20 (0.3 V/s)		
AP_25_2		No	25		
AG_3_2	G		70	3	
AG_3_4					4

Table 2.4: Aqueous solution tests parameters. P and G mean respectively potentiostatic or galvanostatic approach and 'agitation' refers to the solution which could be motionless or under magnetic stirring.

2.3.2 Organic solution

Samples were all anodized under a potentiostatic approach for a simpler future modulation of nanotube diameters and with the solution motionless.

Then, using samples from sheet 1, was evaluated the effect of different anodization times (2, 4, 6 and 8 hours) on nanotubes morphologies and lengths.
Samples coming from the three different sheets were tested under the same condition to study the effect of different initial roughness on the obtained nanotubes. After the choice of the best sheet, tests were carried out again to evaluate the effect of different anodization times (2, 4 and 6 hours) and voltages (10, 20, 30, 40, 50, 60 and 70 volt) on the geometries and dimensions of the obtained nanotubes.

The anodization tests are summarised in table 2.5, where 'O' stays for the use of organic solution, 'P' means 'potentiostatic approach' and the numbers are respectively the used sheet and anodization voltage and time.

Sample	Sheet	Voltage [V]	Duration [h]
OP1_60_8	1	60	8
OP1_60_6			6
OP1_60_4			6
OP1_60_6		60	
OP3_60_6	3		
OP2_60_6	2		
OP2_60_4		60	4
OP2_70_2		70	2
OP2_60_2		60	
OP2_50_2		50	
OP2_40_2		40	
OP2_30_2		30	
OP2_20_2		20	
OP2_10_2		10	

Table 2.5: Parameters of organic solution tests. All experiments were conducted with motionless solution, potentiostatic approach and with an intensity of current of 20 mA.

After the anodization, samples were maintained under stirring in ethanol (70 %) for one hour to remove organic residuals. Subsequently, they were treated with ultrasound in ethanol for 20 s, to remove surface residuals, and then dried at 37°C for at least 4 hours.

2.3.3 SEM analysis

The micro-morphology of the TiO_2 nanotubes was investigated by a scanning electron microscope (Stereoscan 360, Cambridge Instruments) with an extra high tension of 20 kV.
Before being observed samples were let to dry at ambient temperature and then metallized with gold. The average length and diameters of TiO_2 nanotubes were calculated using the Image J software with a number of 10 or more measures for each sample.

2.3.4 Statistical analysis

The statistical analysis of nanotubes sizes was made using the software 'Graphpad Prism'.
First of all, on each group of data was effectuated the D'Agostino-Pearson normality test to evaluate how close is that to the normal distribution. Indeed, it first computes the skewness and kurtosis to quantify how far from Gaussian the distribution is in terms of asymmetry and shape. It then calculates how far each of these values differs from the value expected with a Gaussian distribution, and computes a single P value from the sum of these discrepancies.
This test was useful to choose between the parametric or non parametric subsequent tests. The groups that passed the normality test were compared to evaluate if their averages were significantly different and for that kind of data the unpaired t-test or the one-way ANOVA test were used. Instead, groups that were too far from the Gaussian distribution, were compared using the non parametric tests of Mann-Whitney and Kuskal-Wallis.

2.3.5 Wettability test

A wettability test was performed, using the sessile drop method, to evaluate the differences in the surface hydrophilicity between the untreated titanium disk and the nanotubular structure and between the two dimensionally different nanotubes layer.
Then, images of DI water dropped on the surfaces were analysed through the Drop Shape Analyser software.
The static contact angle was obtained by estimating the tangent to the drop at its intersection with the surface, as shown in figure 2.2. The equilibrium contact angle θ, which results from a balance of interfacial forces acting on the contact line, can be calculated as described from equation (2.1), where γ_{LV} is the surface tension of the liquid-vapour energy, γ_{SV} is the surface tension of the solid-vapour in air and γ_{SL} is the interfacial surface tension of the solid-liquid [128].

$$\theta = \cos^{-1}\left(\frac{\gamma_{SV} - \gamma_{SL}}{\gamma_{LV}}\right) \tag{2.1}$$

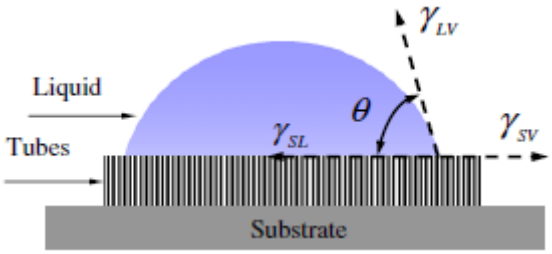

Figure 2.2: Contact angles of TiO_2 based on Young's equation [128].

2.4 NTs biological characterization and functionalization

Based on the results obtained from the anodisation process optimization, two types of samples were prepared for the biological characterization of titania nanotubes.
Particularly, samples from sheet 2 were treated for 2 hours using the organic solution at 50 and 70 V to obtain nanotubes with inner diameters of respectively 114.6 $\pm$ 8.0 and 151.9 $\pm$ 9.6 nm.

Samples were functionalised with soy isoflavones extracts. Then a viability test on 3T3 line murine fibroblasts was performed to optimize the sterilization and seeding process on samples to subsequently biologically characterized them with Saos-2 cell line.

2.4.1 Soy isoflavones extracts release experiment

Before doing the seeding experiment with osteoblasts on different samples, a functionalization of titania nanotubes with soy isoflavones extracts was performed.

In other authors works, the effect of different amounts of genistein dispersed in cell medium on MG63 human osteosarcoma osteoblasts was analysed [129, 130, 131]. Based on those results, and considering the amount of genisteine content in the used soy isoflavones powder [132], different soy based gels were prepared and they're showed in figure 2.3. Those gels were made resuspanding different amounts of soy isoflavones extracts powder in a solution with 70% of ethanol and 30% of dH_2O and sonicating them for 10 minutes.

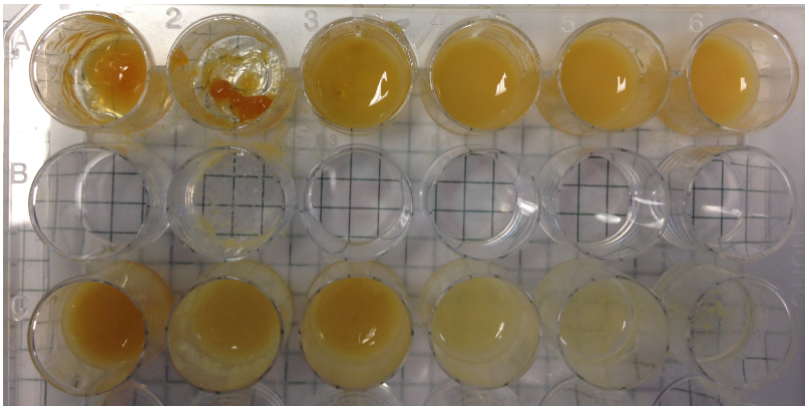

Figure 2.3: Gels made with different density of soy isoflavones extracts powder resuspanded in a solution made with 70 % ethanol and 30% dH_2O

Before coating samples with gels they were washed with pure ethanol and then let to dry.
The release experiment with samples was performed loading on the samples two gels with different densities which are summarised in table 2.6.

	Soy extracts powder concentration [mg/ml]
Gel1	208
Gel2	416

Table 2.6: Two different kind of gels used for the coating of samples.

For both kinds of gel were used three different samples: an untreated disk, one disk anodised at 50 V and another one treated at 70 V. The coating was obtained soaking the samples in the solutions, then they were placed in a 24-multiwell plate and left under hood for 24 hours to allow the solvents to evaporate.

When samples were dried, they were cleaned removing the excess material on edges with a scalpel and then each one of them was placed into one 15 mL-centrifuge tube with 1.5 mL of PBS.
All tubes were then placed into an ES-20 Orbital shaker incubator and left there for one week without motion and with a temperature of 37°C. During the incubation, in several moments, an aliquote of 100 μl of supernatant was taken and replaced with the same amount of fresh PBS.

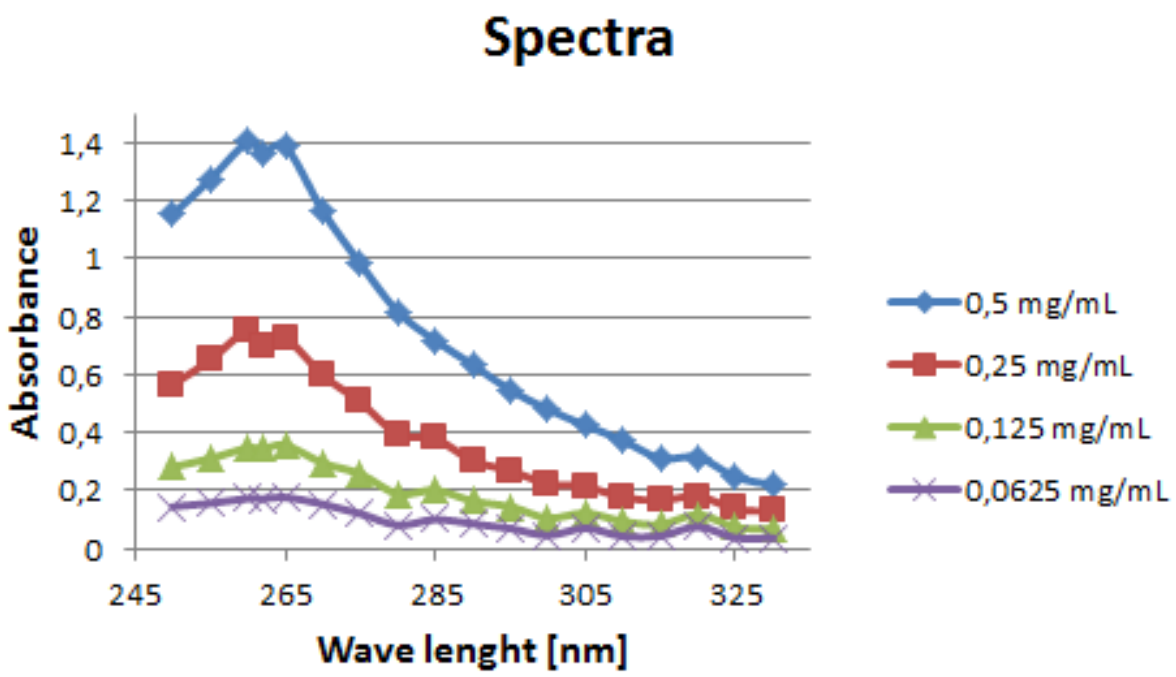

Figure 2.4: Absorbance spectra of four different known concentrations of soy isoflavones extracts in a solution with 70 % of ethanol

Using a 6305-Manual Spectrophotometer (Jenway) a calibration curve for solutions of soy isoflavones extracts and PBS was plotted reading the absorbance values (from 250 to 320 nm) of samples with a known concentration of soy extracts, the obtained spectra are rapresented in figure 2.4. The absorbance was read from 250 to 320 nm of wave lenght, because in this range should be contained the wave lenght corresponding to the genistein molecule [133].
Indeed, these curves showed two different peaks for the used solution at 260 and 265 nm: this suggested the peaks correspond to two different kind of molecules. From literature, the two molecules present in the soy isoflavones extracts that show absorbance peaks for wave lenght of 260 and 265 nm are respectively the genistin and its non-glycosilated form genistein [134, 133].

Using the absorbance values read at these wave lenghts two different standard curves were plotted (Fig. 2.5) and they were used to calculate the actual quantity of genistin and genistein released from the samples.

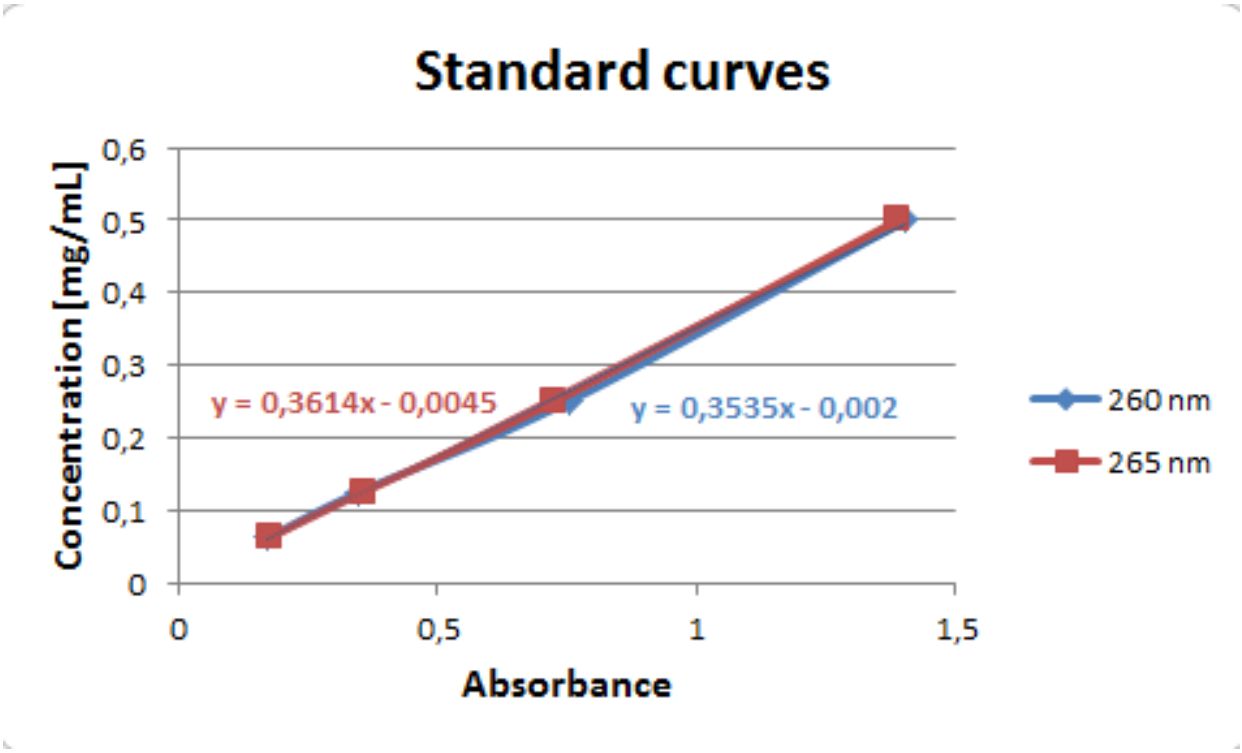

Figure 2.5: Standard curves plotted for soy isoflavones extracts concentration in dependence from the read absorbance.

2.4.2 Thin Layer Chromatography

Thin-layer chromatography (TLC) is a chromatography technique used to separate non-volatile mixtures and it was performed on the supernatants of each release sample to confirm that the extracts truly contain genisteine.

TLC was performed on aluminium foils, which were coated with a thin layer of adsorbent material, silica gel (Fluka analytical).

Using spotting capillaries, a small portion of each sample was spotted on the plate which was then placed into a 150mL beaker with the sides lined with Whatman 9 cm-filter paper as shown in figure 2.6. A solution of chloroform and methanol (10/1, v/v) was used as solvent and made travel up the plate. The filter paper keeps the air in the beaker saturated with solvent so that it doesn't evaporate from the plate.

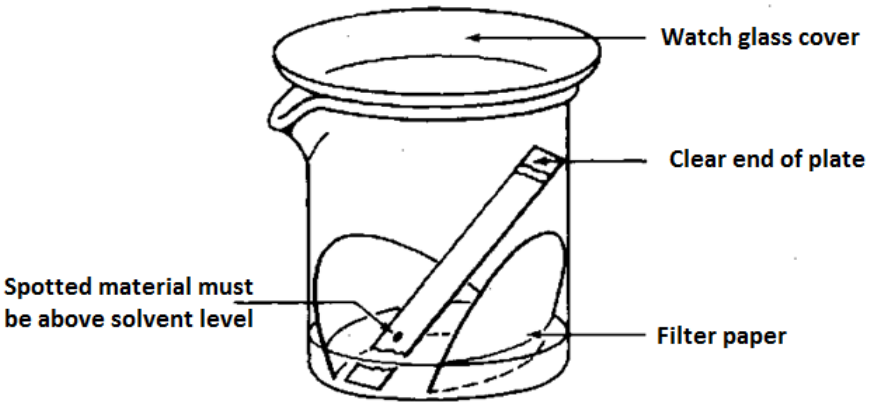

Figure 2.6: Thin-layer chromatography set up

When solvent reached the end of the run, the plate was immediately removed from the beaker and let to drain on a glass.
Every sample was then examinated and compared with the run of a known solution of soy isoflavones and PBS, watching the plates through a non-destructive visualization under a UV light box. The Rf values were then calculated using the software ImageJ.

2.4.3 Murine fibroblast line culture

Cells used to optimize the seeding process were 3T3 mouse embryonic fibroblast purchased from ATCC uk. They were cultured in T75 flasks using Dulbecco's modified eagle medium (purchased from Gibco) with 5 % of fetal bovine serum (from Sigma).

Every time that cells reached 80 % of confluence they needed to be moved in another flask and so thepassages were performed using trypsin-EDTA purchased from Gibco.
The seeding density should be chosen depending on the available surface and the needed incubation time, but before the optimization of the seeding procedure, the proliferation of 3T3 fibroblasts should be evaluated.

Using a 24-multiwell culture plate, murine fibroblasts were seeded with four different densities and cultured for 24 hours. The aim of this experiment was to find the right amount of cells that, after 24 hours of culture, could have covered most of the available area without exceeding the 80-90 % of confluence.

In figure 2.7 are represented cells after 24 hours of confluence and in the following table (2.7) are summarized the percentages of area covered by cells at the end of the experiment.

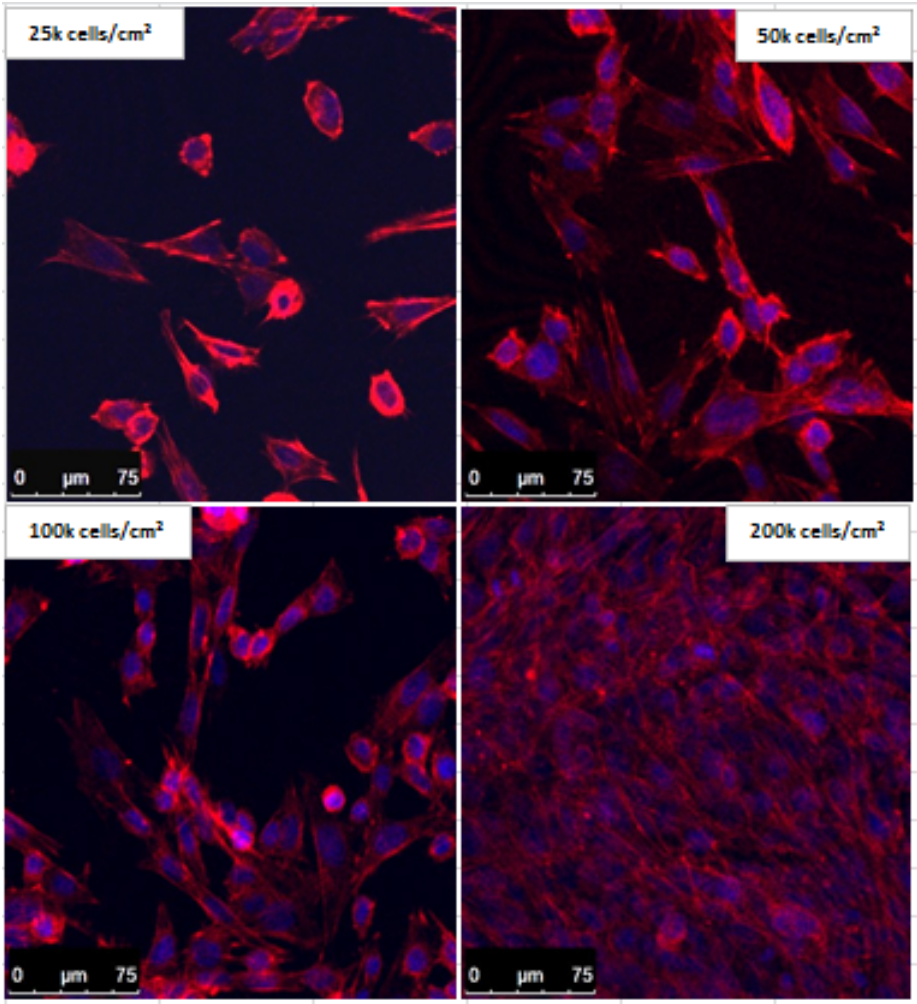

Figure 2.7: 3T3 fibroblast seeded on the tissue culture plate with different densities and cultured for 48 hours. After the culture cells were fixed and colored with phalloidin and DAPI.

Seeding density [$\frac{cells}{cm^2}$]	**Covered area [%]**
25 k	12.3 ± 1.3
50 k	30.6 ± 1.3
100 k	39.0 ± 0.8
200 k	99.9 ± 0.15

Table 2.7: Percentage of covered area after 24 hours of culture starting from different seeding densities.

Based on these results, the accettable seeding densities were 50 k and 100 k $\frac{cells}{cm^2}$. Anyway, considering that an incubation of more than 24 hours could be subsequentely used for the biological characterization, 50 k $\frac{cells}{cm^2}$ was chosen as seeding density.

2.4.4 Sterilization and seeding procedures

One 24 culture multiwell plate was prepared to optimize the seeding procedure and evaluate the viability of murine fibroblast cell line to confirm the sterilization process of samples.
Before seeding cells, samples were sterilized: they were immersed in ethanol (70%) for 3 hours and then left under hood for 1 hour to dry. After that, both surfaces of the titanium disks were sterilized for one hour under an UV lamp.

The first seeding experiment was performed seeding on each sample 1 mL of medium containing 50 k resuspended cells, but in this way almost all cells migrated out of the samples on the tissue culture plate.
To avoid this problem, another seeding method was used: each well was washed with 500 μl of medium and one drop of 50 μl containing 50 k cells was seeded on each sample. After that, samples were incubated for 90 minutes to allow cells to adhere to the substrate. Then 1 mL of medium was added in each well and cells were incubate for 24 hours with a temperature of 37°C and and 5% CO_2.
The problems this time were that washing samples with medium before the seeding the drop slipped on the wet surfaces and didn't remain confined on the samples and, in addition, a drop of 50 μl was too big for the samples.
Therefore, the seeding procedure was modified as follow: one drop of 15 μl containing 50 k cells was seeded on dried samples and lead in incubator for 1 hour to allow cells to adhere to the surface. Subsequentely, 1 mL of medium was added in each well and the culture plate was incubated for 24 hours.

2.4.5 Stainings and fixation

All the stainings used in this section were purchased from Sigma UK and to watch results an optical-fluorescence microscope (Axioskop, ZEISS) was used. The pictures of cells seeded on materials different from the tissue culture plate were all taken with a 20X magnitude, so specific consideration about cells morphology weren't make, but just consideration about their distribution and general shape.

After 24 hours of incubation, all medium was removed from each well which were washed twice with 500 μl of Phosphate Buffered Saline. Then, working in dark, in each well were added 100 μl of a solution containing calcein and ethidium homodimer-1.
Calcein acetoxymethyl is a widely used green fluorescent cell marker. Calcein AM is membrane-permeant and thus can be introduced into cells via incubation. Once inside

the cells, calcein AM, a nonfluorescent molecule itself, is hydrolyzed by endogenous esterase into the highly negatively charged green fluorescent calcein.
Instead, ethidium homodimer is a membrane-impermeable fluorescent dye which binds to DNA. When cells die, the plasma membranes of those cells becomes disrupted. Because of this, ethidium homodimer may enter those cells and bind to DNA within those cells. Because live cells do not have a compromised membrane, the ethidium homodimer can't enter. After a cell sample has been stained with ethidium homodimer, the dead cells may be viewed and counted under a UV-light microscope.
Therefore, covering the plate with aluminum foil, it was incubated for 10 minutes to allow the stainings to penetrate cells.
Then the staining solution was removed and samples were observed at the fluorescence microscope to monitored the fluorescent signals.

After that cells viability on different samples was observed, cells needed to be fixed on materials and stained with phalloidin to observe their morphology and distribution. Phalloidin is a rigid bicyclic heptapeptide that specifically binds at the interface between F-actin subunits, locking adjacent subunits together. Fluorescent derivatives of phalloidin could be observed through the fluorescence microscope, they emit red light and give the opportunity to observe the cytoskeleton of cells and analyze the morphology and distribution on different materials.
To create che correct fixation conditions for phalloidin binding, paraformaldehyde must be used as the fixative because it retains the quaternary proteine structure which is necessary for high affinity. Therefore, samples were washed twice with 0.5 ml of PBS and 80 μl of a solution with 3.7 % of formalin in PBS was added in each well to fix samples. The plate was left under hood for 10 minutes to allow paraformaldehyde to operate and then was washed again with PBS.
Working in dark, 80 μl of phalloidin based solution were added in each well and incubated for one hour.

To put in evidence cells nuclei, samples were also stained with DAPI (4',6-diamidino-2-phenylindole), a molecule that can pass through an intact cell membrane and binds strongly to A-T rich regions in DNA. It absorbs the ultraviolet light and emits in blue.

2.4.6 Saos-2 cell line culture

Cells used for the experiment were Saos-2 cell line purchased from ATCC .
Saos-2 is a cell line derived from the primary osteosarcoma of an 11-year-old Caucasian girl in 1973 by Fogh et al.

In 1987 Rodan et al. determined that Saos-2 cells possess several osteoblastic features and could be useful as a permanent line of human osteoblast-like cells and as a source of bone-related molecules [135].
They resemble human osteoblasts in their ability to express osteogenic markers, to react to Ti particles, etc. They have been reported to express osteocalcin, osteonectin, osteopontin, bone sialoprotein, decorin, type I collagen, procollagen I, and type V and type X collagens. In Saos-2 cells, ALP activity was detected, which increased significantly after reaching cell confluence. Saos-2 cells represent a mature phenotype of osteoblasts, and have high mineralization capacity. They are sensitive to hormonal administration, and express cytokines and growth factors similar to human osteoblasts [136].
Saos-2 cells bind to material surfaces via $\beta 1$, $\alpha 5$, $\alpha\nu$ subunits of integrin receptors. Saos-2 cells were used for studying cell–material interaction on Ti, Nb, and TiNb alloy with different surface morphology, topography, roughness, and charge distribution. Osteogenic differentiation markers reach maximum level after 7 or 14 days in vitro [137]. For tissue-engineering purposes, it is important to study osteogenic differentiation at shorter time intervals, as early onset of osteogenic differentiation and bone formation on a biomaterial surface is crucial for successful implantation in vivo. In addition, at longer time intervals, the difference between different samples usually decreases or even disappears [138].

This cell line was cultured in a T75 flask (Thermo scientific) using McCoy's 5A medium (GE Healthcare) with 15 % of fetal bovine serum.
When cells reached 70-80 % of confluence they needed to be moved in another flask and for this trypsin-EDTA (gibco) was used.

2.4.7 Samples characterization with Saos-2 cell line

To evaluate the effect of both different titania nanotubes and soy isoflavones extracts on Saos-2 cell line, several kind of samples were needed. Three different 24-multiwell culture plates were prepared with two disks for each kind of sample: control samples (i.e. the tissue culture plates), untreated disks and disks anodized at 50 and 70 V.

First of all, samples were sterilized with immersion in ethanol for three hours and then let to dry for one hour.
Then, always working in sterile conditions, half of samples were coated with gel 1 as described in 'Soy isoflavones extracts release experiment'. When the coated samples

were ready, they were placed under UV light for one hour for each side of disks to sterilize them.
After that, cells were seeded on samples as described in 'Sterilization and seeding procedures optimization' in all the multiwell plates, they were then incubated respectively for 24, 48 and 65 hours. After incubation, every sample was fixed and coloured with phalloidin as described in section 'Stainings and fixation' to be able to observe them with the fluorescence microscope and analyse cell morphology, migration and proliferation.
Samples with nanotubes were also used to perform an Alamar blue viability test: Saos-2 cells were cultured on different samples for 72 hours and then washed twice with 0.5 ml of medium. Then, they were incubated for 2 hours in medium containing 1/10 (v/v) of 0.2 mg/ml of resazurin in PBS. Resazurin is a non-toxic, cell permeable compound that is blue in color and virtually non-fluorescent. Upon entering cells, resazurin is reduced to resorufin, a compound that is red in color and highly fluorescent. Viable cells continuously convert resazurin to resorufin, increasing the overall fluorescence and color of the media surrounding cells.
Absorbances of each sample of treated medium were measured with a spectrophotometer at 570 nm.

2.4.7.1 Cell count

Cells were seeded on materials depositing one drop of them and leaving to adhere to the substrate before adding 1 mL of medium per well. At the beginning of culture cells were all clumped at the center of disks and then slowly migrated toward sample edges. Because of this drop, cells count was made considering the area surrounding it to estimate how many cells had migrated from the drop toward material edges. Two samples for each kind were used for the count.

2.4.8 SEM analysis

The cells distribution and morphology were also investigated by a field emission gun-scanning electron microscope (ZEISS 300, Sigma) analysis. Before being observed, samples were dehydrated through several immersions of 10 minutes in a series of four solutions of ethanol and dH_2O, which concentrations went from 25% (v/v) to 100% (v/v). Images were taken with an extra high tension of 5 kV and several magnitudes; two sample for each kind were observed.

2.4.9 Statistical analysis

The statistical analysis of cells number was made using the software 'Graphpad Prism'. First of all, on each group of data was effectuated the D'Agostino-Pearson normality test to evaluate how close is that to the normal distribution. This test was useful to choose between the parametric or non parametric subsequent tests. The groups that passed the normality test were compared to evaluate if their averages were significantly different and for that kind of data the unpaired t-test or the one-way ANOVA test were used. Instead, groups that were too far from the Gaussian distribution, were compared using the non parametric tests of Mann-Whitney and Kuskal-Wallis.

Chapter 3

Results

3.1 Anodization process

Using different samples and set-up parameters, several anodization tests were carried out to find the experimental conditions that could offer an opened and regular nanotubolar structure with length around a dozen of μm and homogeneous diameter values, that could be modulated by varying the applied voltage.

The experiments were performed using an aqueous based solution and an organic one. The second should give better nanotubes in terms of regularity of the structure, smoothness and definition of their walls and bigger dimensions.

3.1.1 Aqueous solution

Cosidering the experiments performed in the aqueous based solution (Tab. 2.2), the used samples were all taken from sheet 1 (Tab. 2.1) and prepared as described in section 2.3.1.
Because all the experiments described in this section were performed in the aqueous-based solution, for simplicity letter 'A' was removed from samples names.

The difference between applying a galvanostatic approach or the potentiostatic one was studied. Therefore, two samples were anodised in solution 1 under magnetic agitation with a current intensity of 3 mA for 2 and 4 hours (Tab. 2.4, G_3_2 and G_3_5). A macro visualization of the sample is showed in figure 3.1 and reveals that not the entire disk area is covered by the nanotubolar structure wich is distributed just on the light spot visible on the surface.

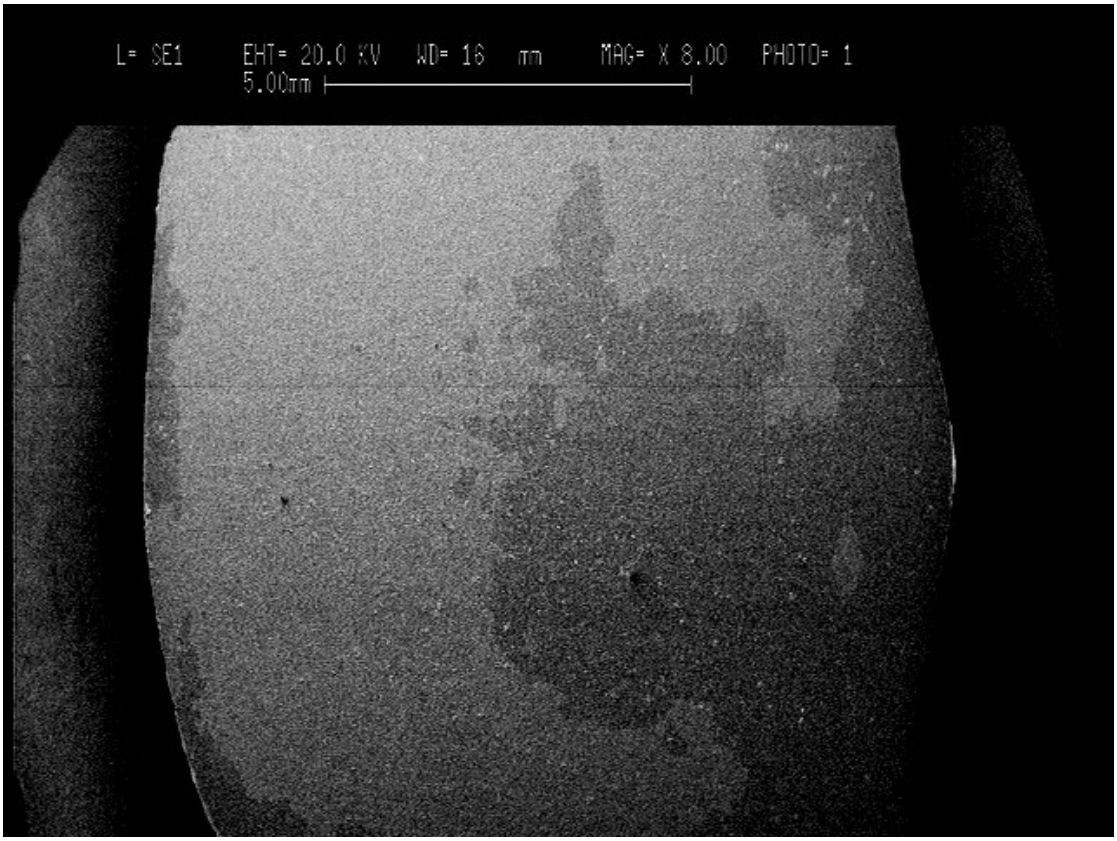

Figure 3.1: Macro view of G_3_2 (Tab. 2.4) sample. The lightest spot is the only area covered by nanotubes.

The SEM analysis of these samples are rapresented in figure 3.2 and, specifically the sample anodised for 2 hours, showed that, as reported in the state of art [89], the galvanostatic approach could offer a nanotubolar structure regular and homogeneous. Moreover, when the duration of the experiment was doubled (G_3_4), an irregular nanoporous structure was obtained again.

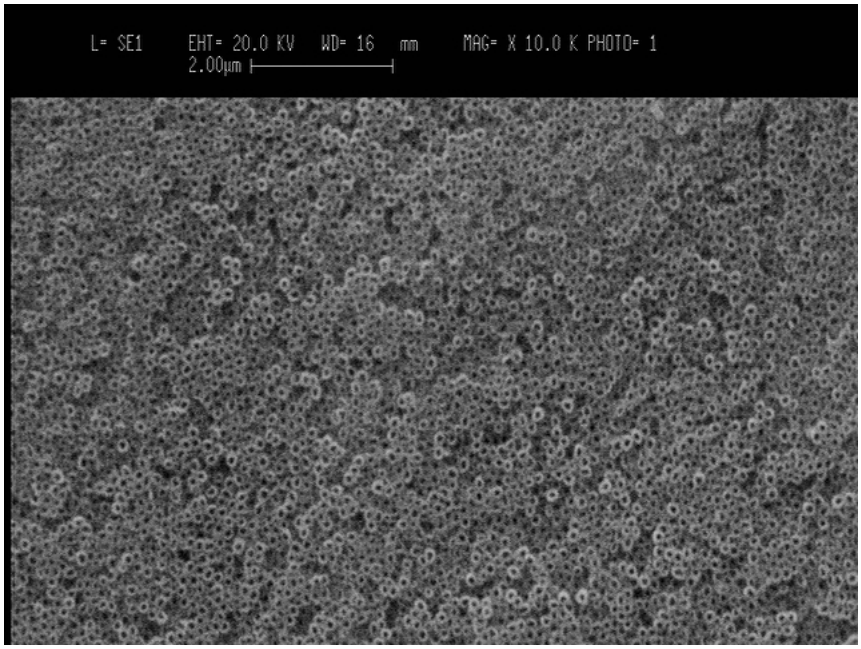

(a)

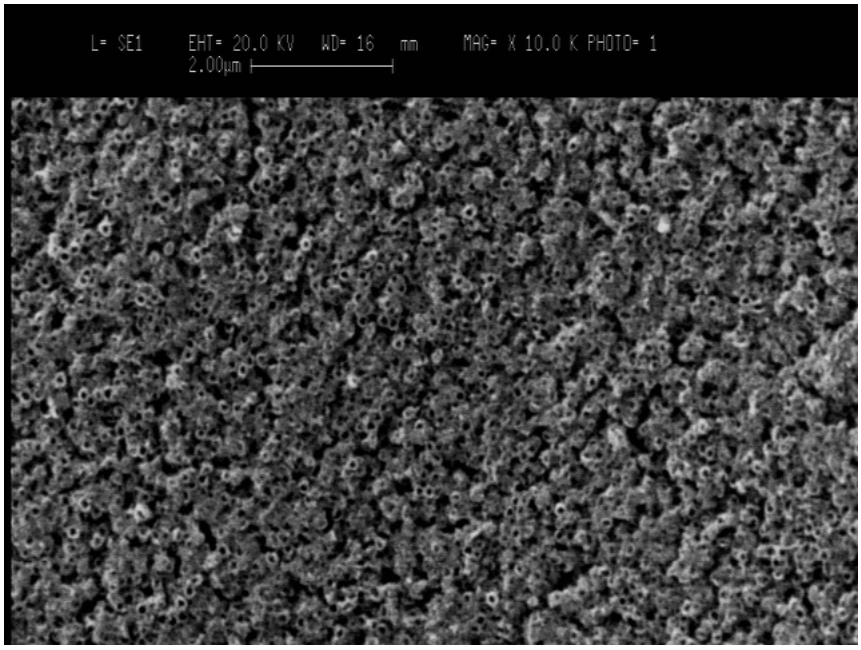

(b)

Figure 3.2: SEM images of samples anodised in the aqueous based solution with a galvanostatic approach at 3 mA for 2 (a) and 4 (b) hours.

However, a lateral view of obtained nanotubes, showed in figure 3.3, revealed that they have a lenght lower than 2 μm and rough and pierced walls.

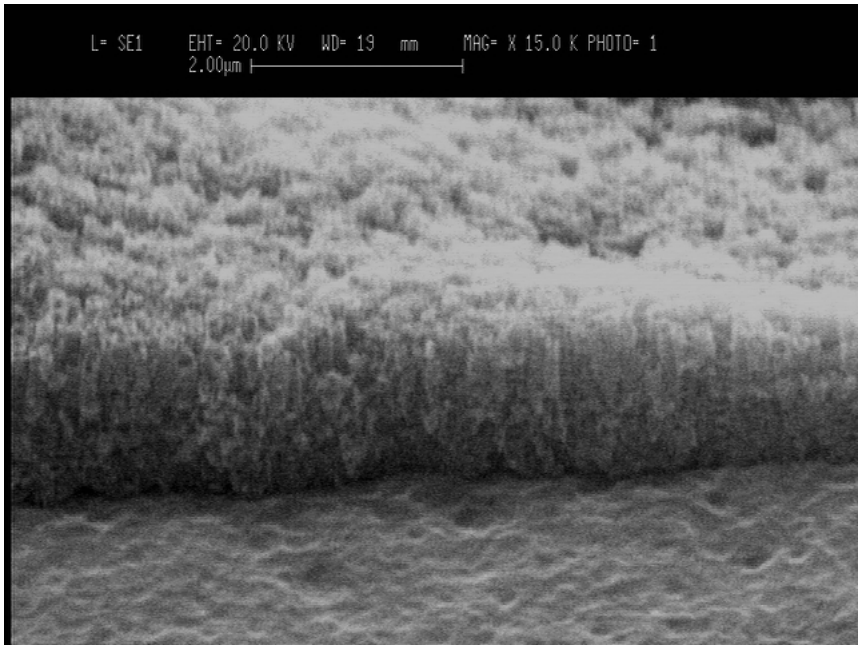

Figure 3.3: Lateral view of nanotubes obtained using galvanostatic approach for 2 hours and a current intensity of 3 mA.

Based on those results was confirmed that the galvanostatic approach could be used to obtain a pretty regular nanotubolar structure with rough walls and a thickness of maximum 2 μm. However, under this approach the intensity of current was kept constant instead of the potential value and this generated voltage oscillations that did not allow the direct modulation of nanotubes sizes, i.e. lenghts and diameters, varying the applied current density.

Tests were then carried out using a potentiostatic approach and was also evaluated the difference between applying the voltage value instantly or with a ramp of 0.3 $\frac{V}{s}$. Samples P_20_2 and P_20r_2 (Tab. 2.4) were respectively obtained, anodizing them for 2 hours with the solution under magnetic agitation, and their morphology was obseved through the SEM analysis shown in figure 3.4.

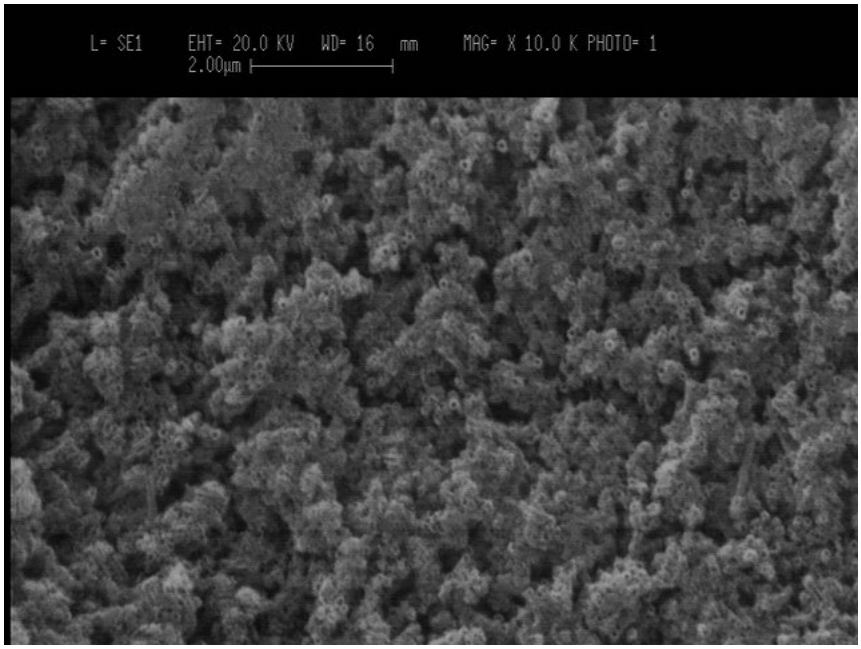

(a)

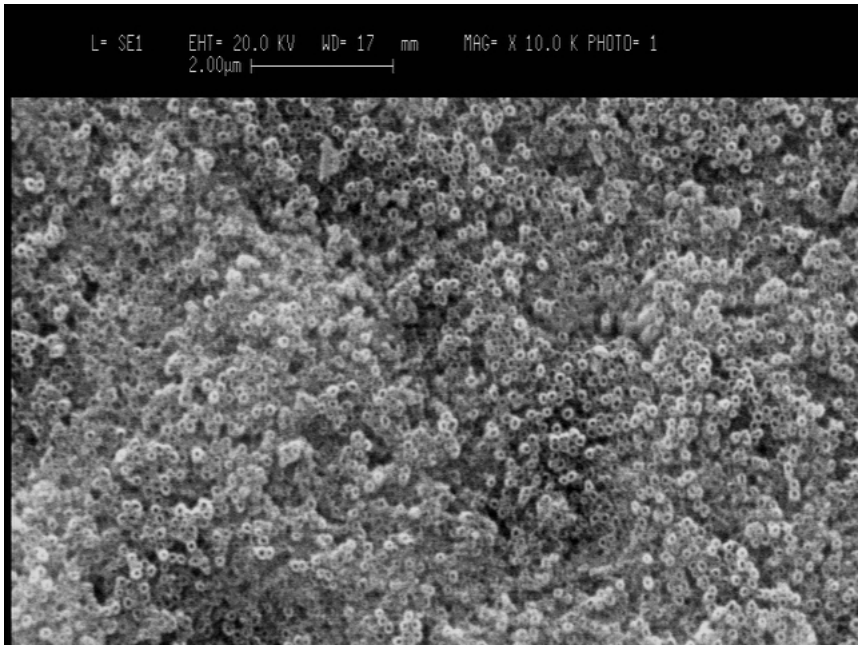

(b)

Figure 3.4: Samples anodised for 2 hours applying instantly 20 V (a) or through a ramp of 0.3 $\frac{V}{s}$ (b).

In line with the literature about the use of an aqueous solution [93], on both samples the obtained nanotubes had really small dimensions, i.e. maximum lenght of 1 μm, and their walls were rough but more defined than other samples. Moreover, their distribu-

tion was irregular and seemed to follow the microstructure of the undelying surface. Both the two samples appeared more nanoporous than nanotubolar, but disk treated using the ramp of potential looked slightly more homogeneous than the other one as expected [92], but the difference between the two structures was not great enough.

The sample P_20_2 was then produced again keeping the solution without magnetic agitation and results are shown in figure 3.5.

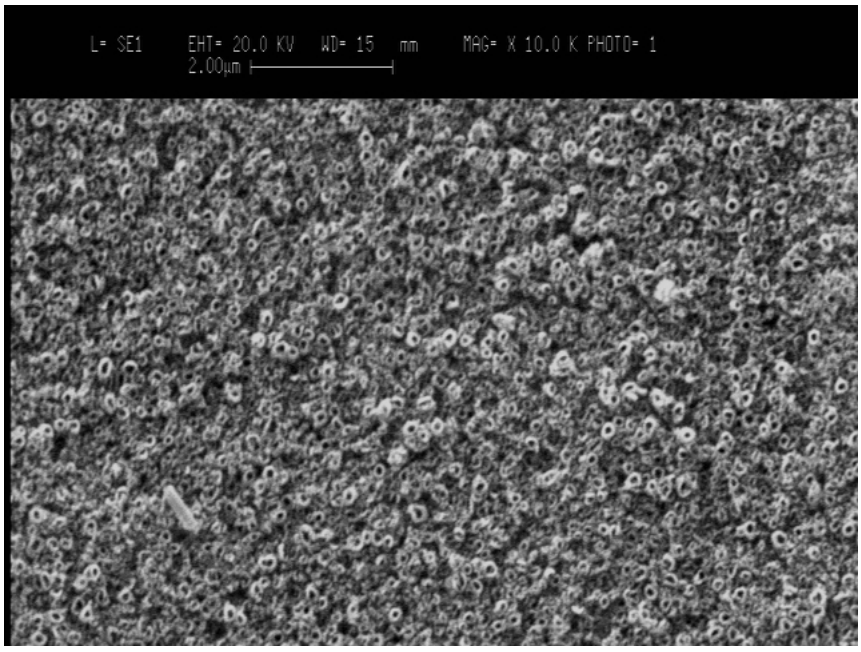

Figure 3.5: Samples anodised for 2 hours at 20 V with the aqueous based solution motionless.

The SEM analysis of sample treated with the motionless solution showed a structure almost nanotubolar and more regular than the previous one.

Then, from this moment of the study only the potentiostatic approach was used applying directly the chosen voltage value and keeping the solution motionless.

3.1.2 Organic solution

In this section are summarised the results obtained through the anodization tests performed in the organic solution (Tab. 2.3) varying several parameters.
Comparing to the anodization in water-based solution, this kind of electrolite needed higher voltage values and anodization times to give an homogeneous nanotubolar layer. However, it also should give a more regular structure, than the one obtained through the inorganic solution, nanotubes with smoooth and well defined walls and bigger dimensions in terms of nanotubes layer thickness [6].

Because all the experiment performed from this moment were carried out using the organic solution and under a potentiostatic approach, letters ‘OP’ won’t be reported in samples names.

3.1.2.1 Top layer morphology

The experiments were performed with the aim to evaluate the effects of different anodization times.

First of all, three samples were anodised in the organic solution at 60 V, for different times: 4, 6 and 8 hours.

The first thing which should be said is that, as expected [126] using an organic elettrolite, the anodised samples appeared superficially covered by a disordered layer made of thin nanotubes that is called ”nanograss” and is shown in figure 3.6.

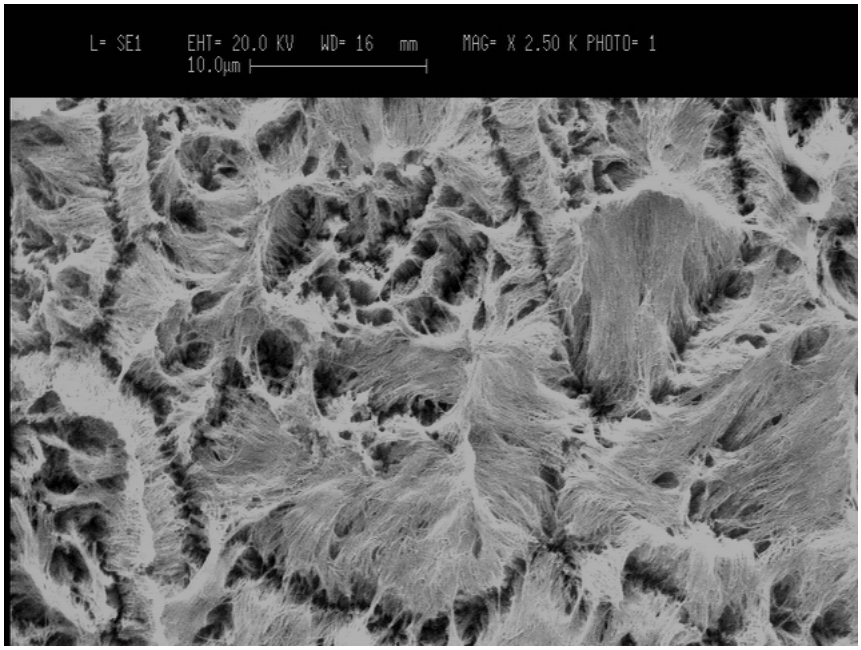

Figure 3.6: Example of sample anodised in solution 2 (Tab. 2.3) at 60 V for 8 hours (Tab. 2.5, 1_60_8).

In figure 3.7 are represented the differences between this overlying structure obtained in different anodization times.

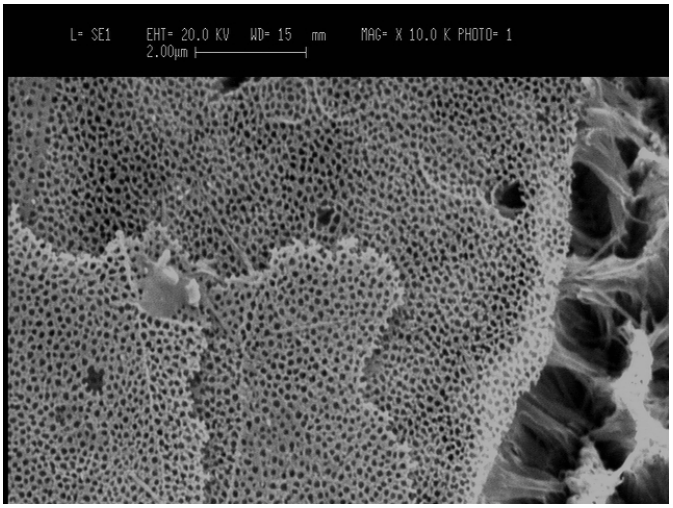

(a)

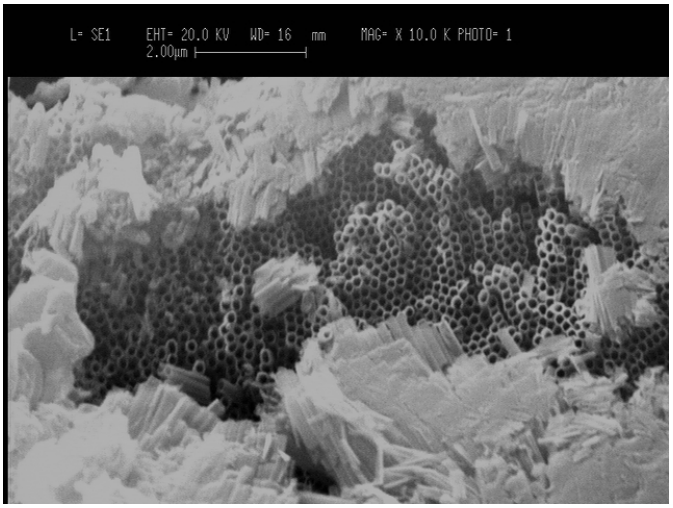

(b)

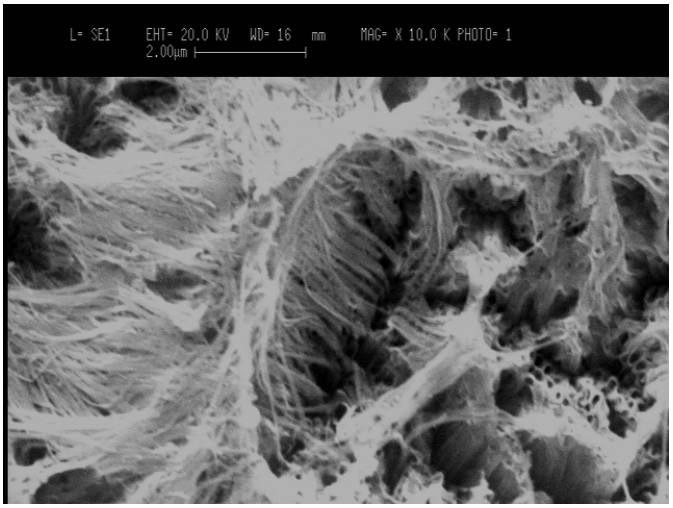

(c)

Figure 3.7: Samples anodised for in solution 2, at 60 V for 4 (a), 6 (b) and 8 (c) hours.

Sample treated for 8 hours were totally covered by this collapsed structure as well as sample anodized for 6 hours, a part of few opened zones. Instead, sample treated for 4 hours had part of the surface covered by those debris and the rest of the nanotubolar structure presented an overlying porous and compact layer, which could be an intermediate stage between nanotubes and nanograss.
Anyway, in figure 3.8 could be seen that nanotubes obtained with the organic solution have smooth and defined walls and they are really more regular, for what concern their diameter sizes, than the ones anodised in the aqueous solution, confirming the state of art concerning the use of organic solutions [6].

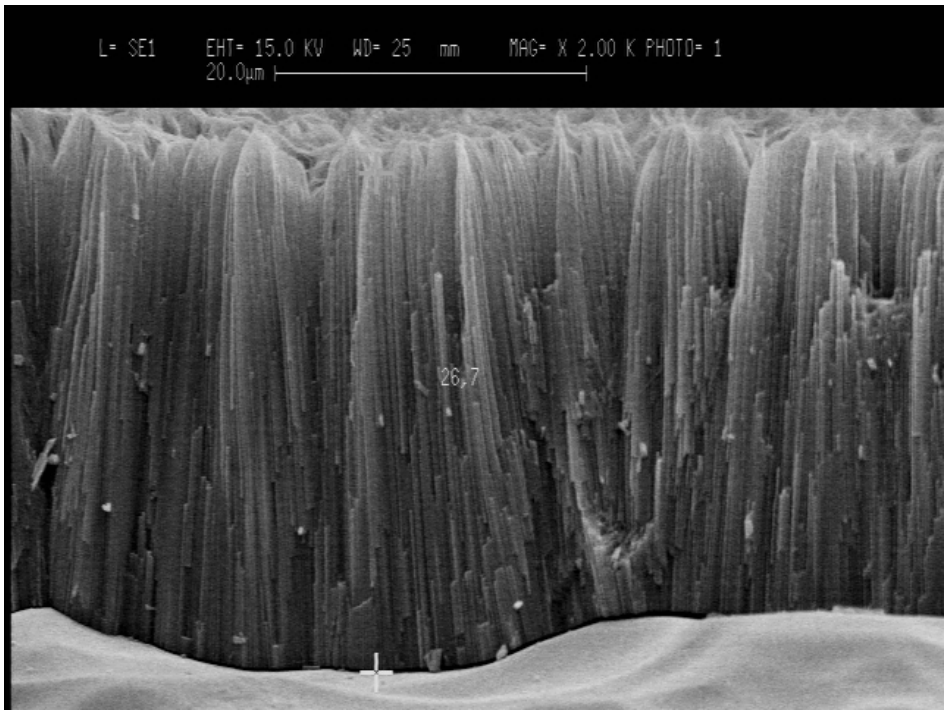

Figure 3.8: Lateral view of sample anodised in solution 2 (Tab. 2.3) at 60 V for 4 hours (Tab. 2.5, 1_60_4).

Moreover, increasing the anodization time should increase the thick of the obtained nanotubolar structure [69], but the measures taken from those three samples reveals an unusual trend for the nanotubes lenghts rapresented in figure 3.9.

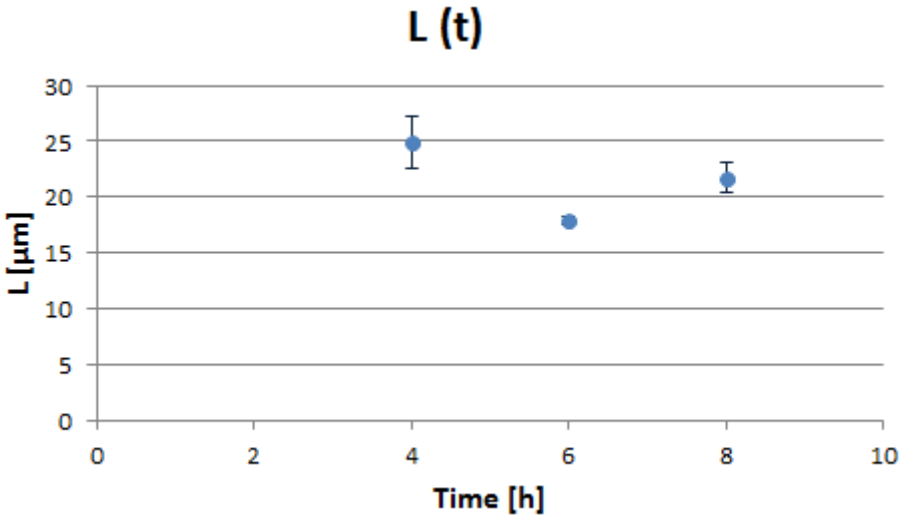

Figure 3.9: Trend of nanotubes lenghts in dependence of time for samples coming from sheet 1, treated in solution 2, at 60 V and for three different times (Tab. 2.5; 1_60_4, 1_60_6 and 1_60_8). Data summarised in appendix A, table A.1.

Specifically, these measures confirmed that, using an organic solution, nanotubes with a lenght higher than a couple of micrometers could be obtained [7]. Netherless, samples treated for the shorter time possessed the biggest length, but should be said that these values could be not so accurate, because of the fact that the initial sample surface presented a very irregular macro structure so not all nanotubes started to grow from the same level.

3.1.2.2 Initial surface roughness

After the evaluation of how the anodization time modify the nanotubolar structure, the attention was focused on studying the differences obtained using samples with different surface roughnesses. Based on literature, using samples taken from sheets with a better surface quality should give a nanotubular structure with less nanograss [17].
Because of the intermediate top morphology and accettable lenghts values for our purpose, experiments were performed anodizing samples for 6 hours.

Three samples taken from sheets with three different roughnesses (Tab. 2.1) were anodised in the organic solution, at 60 V for 6 hours (Tab. 2.4, 1_60_6, 2_60_6, 3_60_6) and results are showed in figure 3.10.

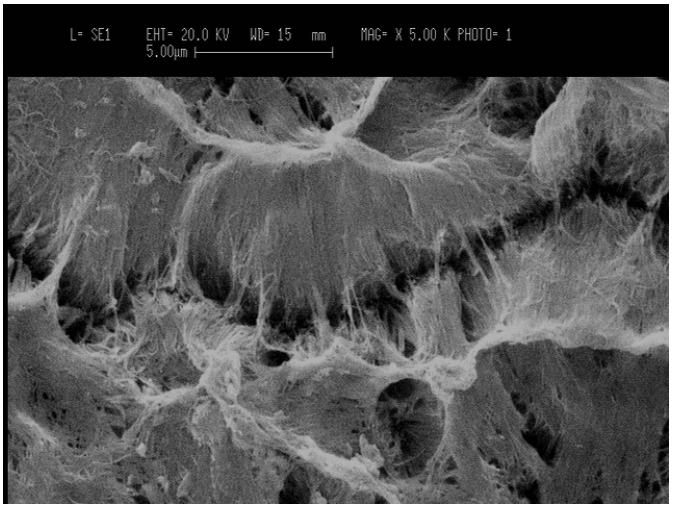

(a)

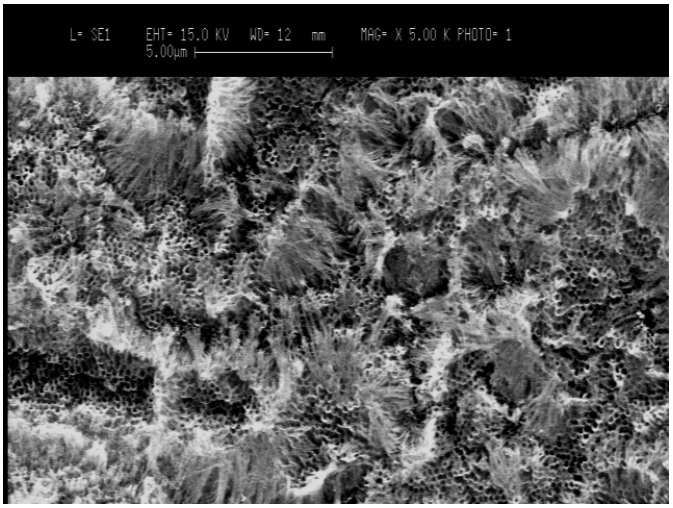

(b)

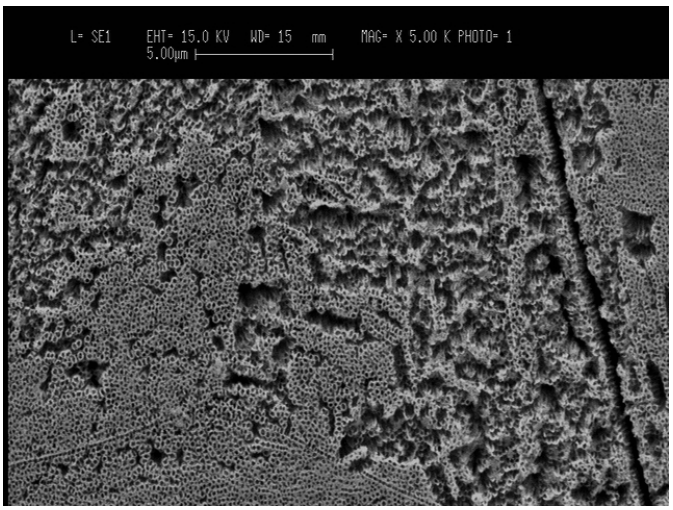

(c)

Figure 3.10: Samples taken from (a) sheet 1, (b) 2 and (c) 3 anodized for 6 hours at 60 V.

Considering sheets 1 and 2, both the samples still appeared superficially covered by nanograss, but the sample coming from sheet 2 presents more nanograss-free zones than the other one and this could be due to the finest surface quality of the second sheet.
Anodizing under the same conditions (i.e. in the organic solution, at 60 V and for 6 hours) an electropolished disk, it appears completely free from the overlying disordered structure. This confirm the fact that anodizing samples in an organic elettrolite, the presence of an overlying nanograss structure depends on the surface roughness of the used substrate.
Anyway, the nanotubolar layer obtained on the elettropoolished sample easily slipped away from the titanium surface revealing a very low adherence to the underlying titanium surface. In figure 3.11 are shown the closed bottoms of the nanotubolar structure.

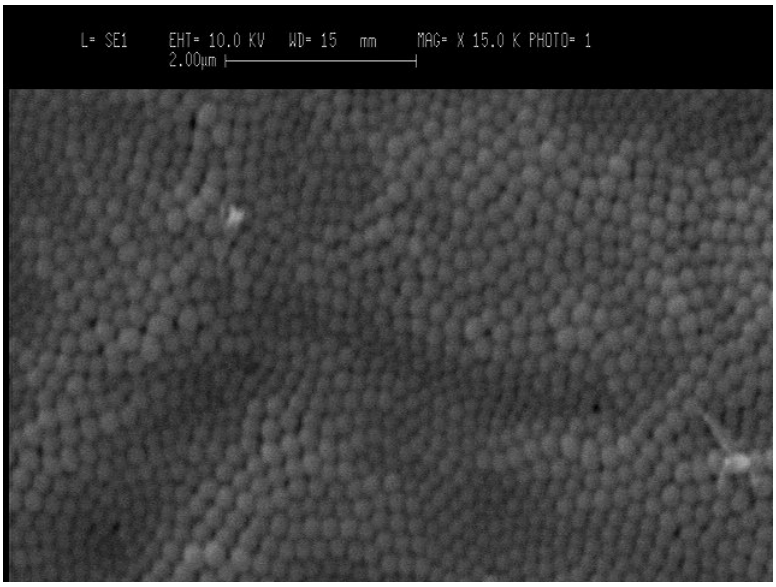

Figure 3.11: Bottom view of the nanotubolar structure obtained with an anodization in organic solution, for 6 hours at 60 V of the elettropolished sample (3_60_6).

These results showed how working on a sample with better surface quality led to the formation of a more regular and homogeneous nanotubular structure and give the possibility to obtain nanotubes without the overlying debris layer.
Anyway, if the initial surface R_a is too low, the produced nanotubular structure reveals a very low adherence to the substrate and, for this reason, from this point of the study all treated samples were taken from sheet 2.

3.1.3 Ultrasound post-treatment

The effect of a post-anodization process to remove nanograss was evaluated to produce titania nanotubes without the presence of overlying disordered structure.
For this reason, basing on literature [84], samples taken from sheet 2, anodized for 6 hours at 60 V (2_60_6) after a washing for 1 hour in ethanol was treated with ultrasounds for 20 seconds and then washed again for 5 minutes.
As could be seen in figure 3.12 the ultrasounds post-treatment was really effective on this kind of sample: almost all the natubes are uncovered and their mouths are now open.

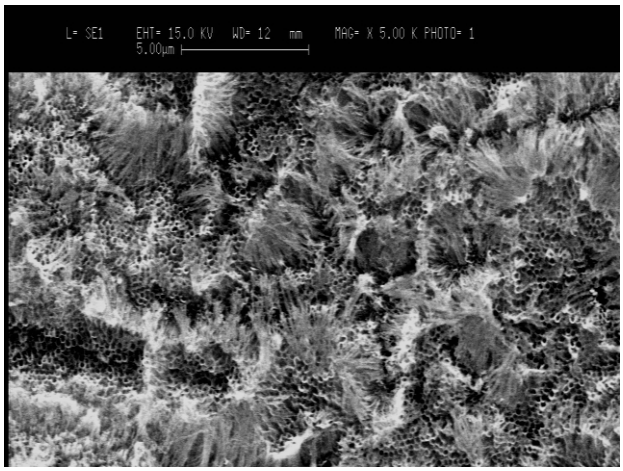

(a)

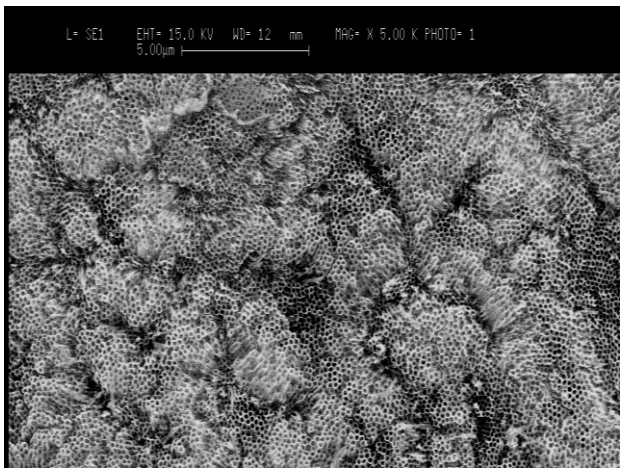

(b)

Figure 3.12: Sample coming from sheet 2 anodized for 6 hours at 60 V in the organic solution (over) before and (under) after a treatment of 20 s in ultrasuonds.

3.1.4 Anodization parameters optimization

Several anodization treatments were carried out on sample taken from sheet 2 and post-treating them in ultrasound. The aim was to evaluate both the minimum time needed to obtain a nanotubular structure with opened top, both the different geometries and dimensions obtained on sheet 2 depending on the potential value used.
Because all samples from this point of the experiments were performed in the organic solution, with a potentiostatic approach and using samples from sheet 2 then, from now, also the sheet number will be removed from samples names.

3.1.4.1 Treatment time

Three samples were anodized at 60 V for different times (1, 2, 4, 6 hours) to study the influence of the duration of the process on the nanotubular structure.

Nanotubes dimensions in dependence of anodization time for samples coming from sheet 2 are summarised in figures 3.13 and 3.14.

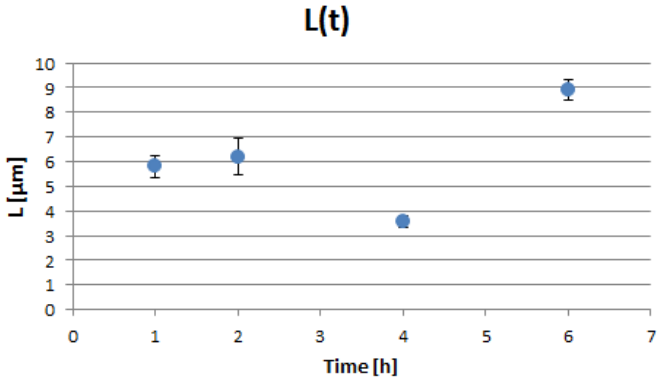

Figure 3.13: Trend of nanotubes lengths in dependence of time for samples coming from sheet 2, treated in solution 2, at 60 V and for four 1, 2, 4 and 6 hours.

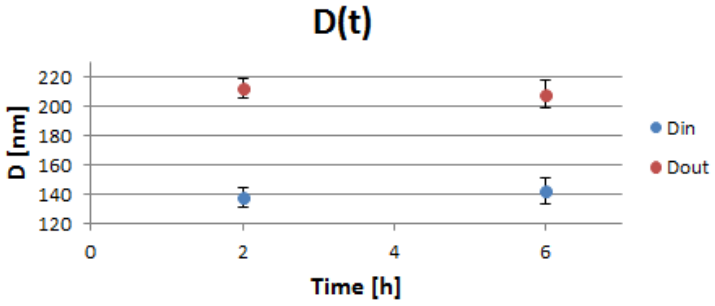

Figure 3.14: Diameters values for samples treated in solution 2, at 60 V, for 2 and 6 hours.

As reported in literature [7] the thickness of the nanotubular layer should have increase using a longer anodization time and this was true for samples anodised for 1, 2 and 6 hours which dimensions were statistically different between each others (p_{value}<0.0001).
However, the thickness of the sample treated for 4 hours resulted too short in respect of other values. This could be due to the difficulties found in taking longitudinal measures of nanotubes and then these values could not reflect the actual nanotubular layer thickness.
Instead, in figure 3.14 is showed that both the diameters sizes were not affected by the duration of the process and the average values for different samples did not result significantly different.

Considering now the nanotubular morphology, from picture 3.15, could be notice that sample anodized for just one hour did not present a regular nanotubular structure, but a nanoporous one which is also covered by a quite thick layer of crust that couldn't be removed with ultrasounds.

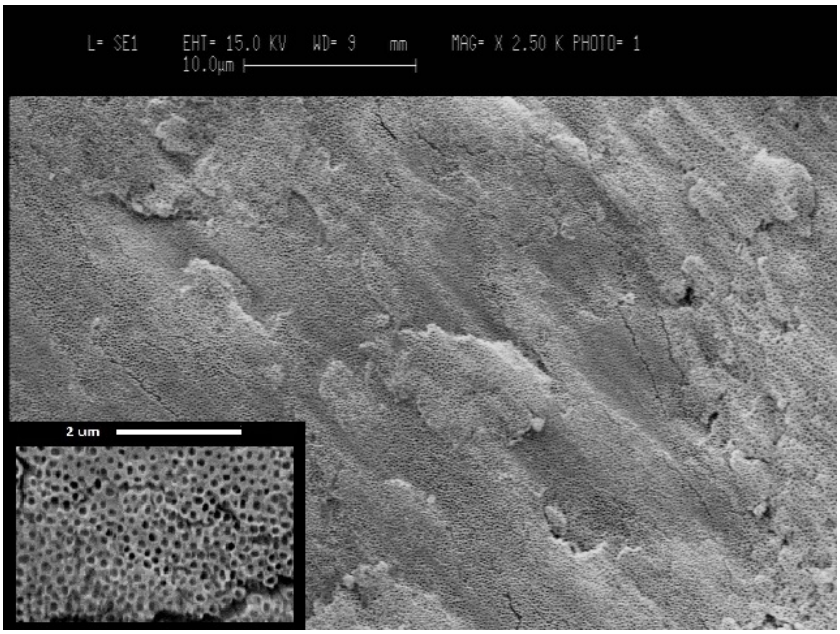

Figure 3.15: Sample coming from sheet 2 anodized for 1 hour at 60 V in the organic solution after a treatment of 20 s in ultrasound. The compact overlying layer couldn't be removed through the ultrasounds and is still well visible.

In the previous section, was confirmed that the ultrasound post-treatment was really effective on sample anodized for 6 hours at 60 V (Fig. 3.12).
In figure 3.16 are rapresented the anodised samples before and after the ultrasound treatment.

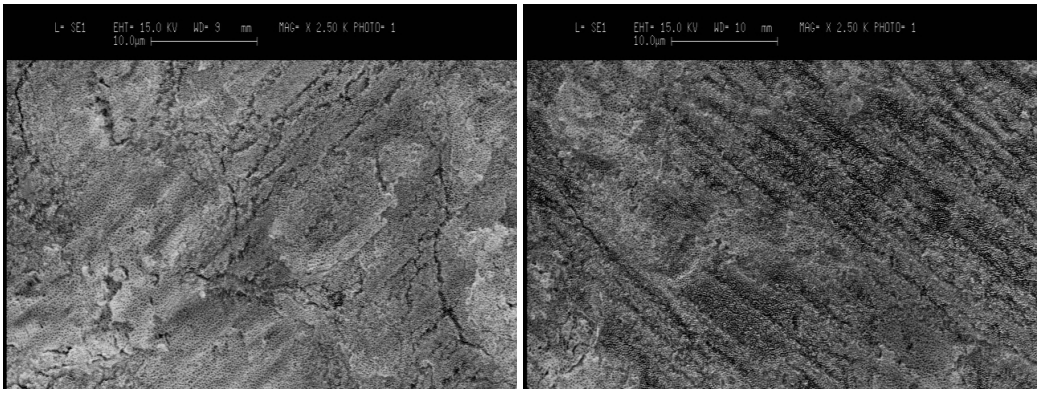

(a)

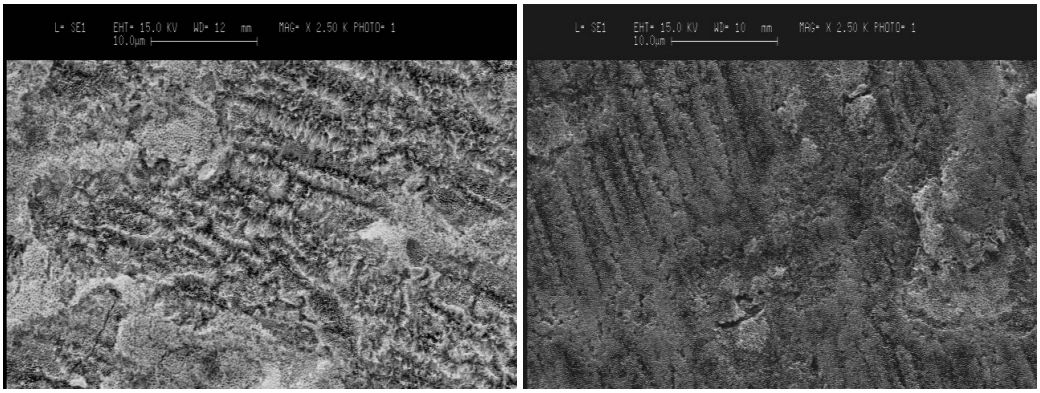

(b)

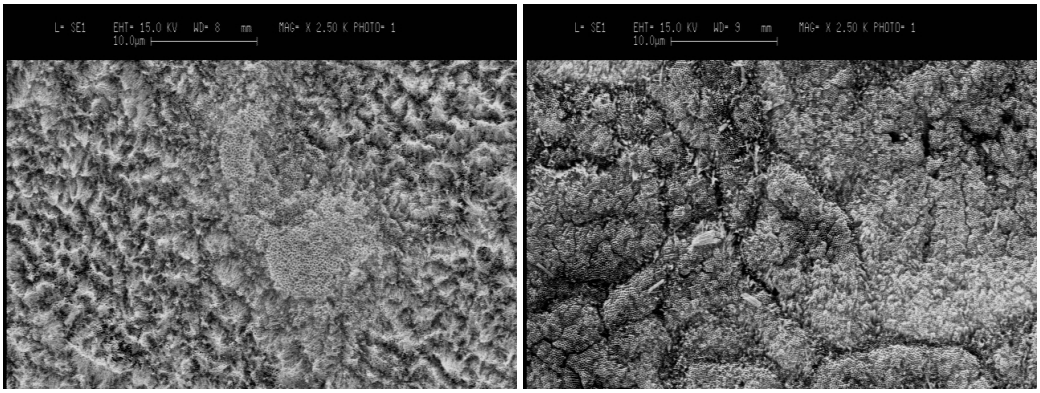

(c)

Figure 3.16: Sample coming from sheet 2 anodized for (a) 2, (b) 4 and (c) 6 hours at 60 V in the organic solution (left) before and (right) after a treatment of 20 s in ultrasounds.

However, at this point was observed that, on samples treated for less than 4 hours, the disordered overlayer that covered the nanotubular structure is more compact than the one formed on disk anodized for longer times and not so easily removable.
Particularly, could be observed that on sample treated for 2 hours the compact overlying

layer was almost completely removed through the ultrasounds and the same happened with an anodization time of 4 and 6 hours. After this tests, could be said that the disordered layer could be removed from samples treated at 60 V just if the anodization time is higher than one hour, because with this duration the overlying structure resulted too compact to be easily detached with ultrasounds.

Because of these results, from this moment samples were all anodized for 2 hours, but with several applied potentials with the aim to find a range of voltage values that could led to the formation of an opened nanotubular structure.

3.1.4.2 Applied voltage

Several samples were anodized in the ethilen-glicol based solution for 2 hours and a voltage range that goes from 10 to 70 V ($\Delta V = 10V$) was explored to evaluate the influence of applied potential on the overlying layer and nanotubes dimensions.

Nanotubes obtained on all the samples treated at more than 10 volt were measured and these sizes are summarized in figures 3.17 and 3.18.

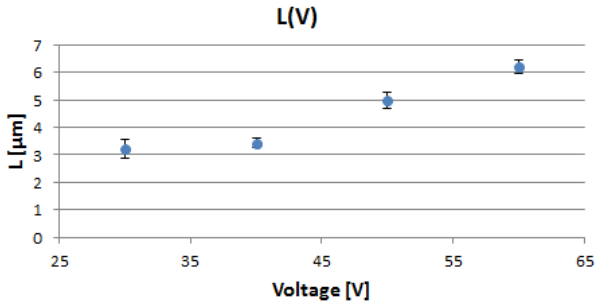

Figure 3.17: Nanotubes lenghts trend for samples, anodised for 2 hours at 30, 40, 50, 60 and 70 V.

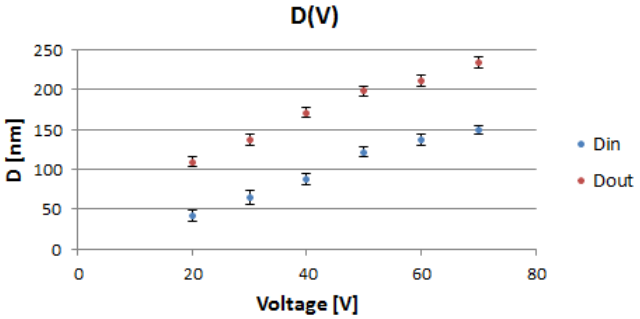

Figure 3.18: Diameters sizes for samples, anodised for 2 hours at 20, 30, 40, 50, 60 and 70 V.

As expected [8], lengths values increased increasing the anodization potential, but

their mean values were lower than the data reported in literature under similar working conditions, specifically they went from around 3 μm to 6 μm at respectively 30 and 60 V and were significantly different (p_{value}<0.0001).
The same happened to the diameters: both sizes became bigger increasing the applied voltage from 20 to 70 V and the differences between their average measures resulted statistically significant (p_{value}<0.0001). However, from literature seemed that the increasing rate of the outer diameter in dependence of the potential value should be very higher than the one of the inner size [77], entailing the growing of walls thickness applying higher voltages.
Instead, these data showed that the increasing rates of the inner and outer diameters seemed to be almost the same and then the thickness of the nanotubes walls was almost constant varying the potential.

In figure 3.19 is showed that anodizing a sample for 2 hours at 10 V, a disordered and heterogeneous structure resulted and so wasn't possible to measure sizes for those nanotubes.

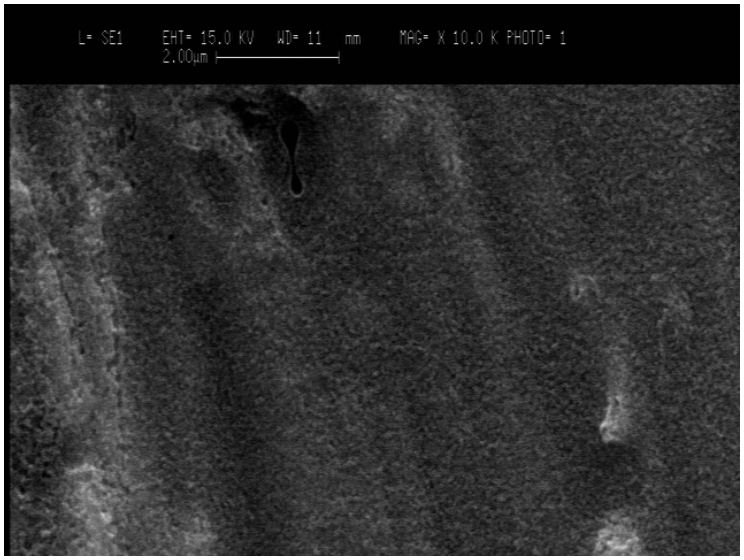

Figure 3.19: Structure obtained anodizing sample for 2 hours at 10 V (Tab. 2.5; 10_2).

In figure 3.20 are showed samples anodized for different applied voltage, after the treatment in ultrasound.

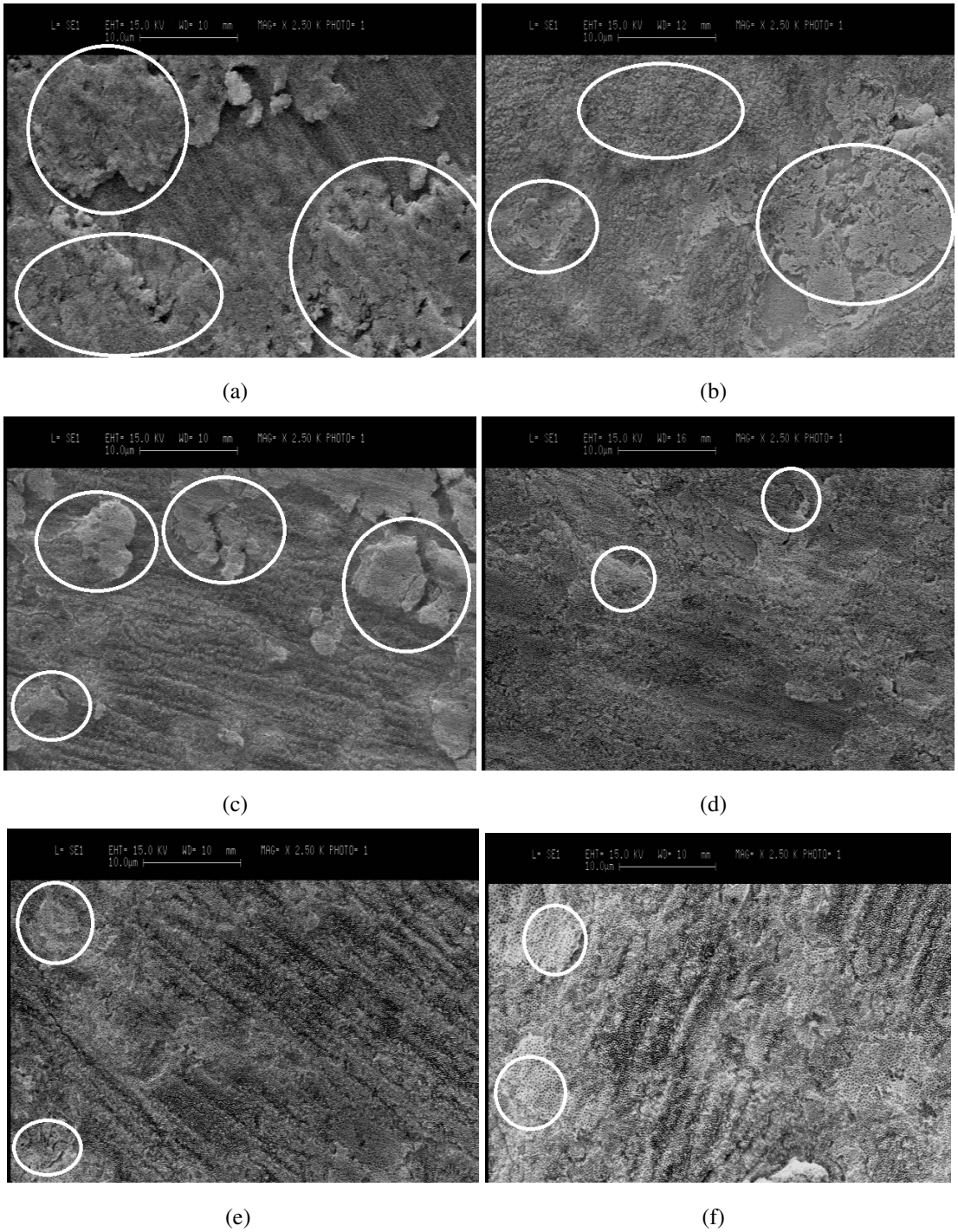

Figure 3.20: SEM images of samples anodized for 2 hours at (a) 20 V, (b) 30 V, (c) 40 v, (d) 50 V, (e) 60 V and (f) 70 V and post-treated for 20 s in ultrasound. Circles indicate the crust layer.

Could be seen that, on samples anodized for two hours with a potential equal or lower than 40 volt, wasn't possible to remove the compact layer that covered the nanotubular structure; while this overlying layer almost completely disappeared on samples

treated at 50, 60 and 70 volt.

Because of these results, several samples were now anodized with the same experimental parameters to evaluate the repeatability of the treatment and, subsequently, to choose two voltage values that could offer two dimensionally different nanotubular structures.
Then samples were anodized for 2 hours at 50 and 70 volt and, specifically, many sample were treated simultaneously using a multisample holder.
Their structures resulted dimensionally equal and their dimensions are summarised in table 3.1.

V	L [μm]	D_{in} [nm]	D_{out} [nm]
50	5.0 ± 0.2	114.6 ± 8.0	190.7 ± 8.4
70	6.2 ± 0.7	151.9 ± 9.6	233.2 ± 13.9

Table 3.1: Sizes of samples treated in solution 2 for 2 hours at 50 and 70 V.

From previous experiments, emerged that to have a regular nanotubular layer with a thickness in the order of a dozen of micron, the minimum anodization time to obtain an opened structure is 2 hours. Then, with this duration of the treatment, the minimum voltage that should be applied to allow the remotion of the nanograss layer with the ultrasound post-treatment resulted 50 V. For there reasons, 50 and 70 V were chosen as applied potential values to produce two dimensionally different nanotubular structure that will be subsequently used for the nanotubes biological characterization and functionalization.

3.1.4.3 Wettability test

A wettability test was then performed on the untreated titanium disk and on samples chosen for the biological characterization (i.e. 50_2 and 70_2) to define and compare the hydrophilicity of the different surfaces.
Drops deposited on different samples are represented in figure 3.21 and the respective measured contact angles are summarized in the following table (3.2). The surface wettability increased on the anodized samples and, particularly, the hydrophilicity of the surface is higher on sample with bigger nanotubes.

Sample	Contact angle [°]
UT	102.5 ± 6.6
50 V	63.1 ± 8.7
70 V	50.8 ± 6.1

Table 3.2: Contact angles measured on different samples.

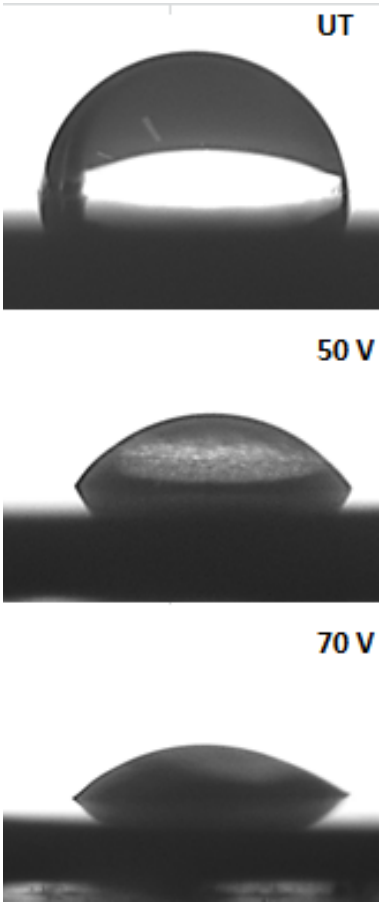

Figure 3.21: Drops deposited on different samples to measure the contact angles.

These results are in accordance with literature, which says that the nanotubular structure should be more hydrophilic than the untreated titanium and moreover this behaviour should increase increasing nanotubes diameter. Different works showed how this feature could be varied tuning the experimental parameters as the anodization time [128] or the applied potential [139, 31].

3.2 NTs functionalization and biological characterization

3.2.1 Soy isoflavones release experiment

Using the absorbance values and the obtained standard curves (Sec. 2.4.1, fig. 2.5), for each kind of sample were plotted two curves showing the release trends of genistin and genistein in dependence of time and they're represented in figures 3.22, 3.23, 3.24 and 3.25.

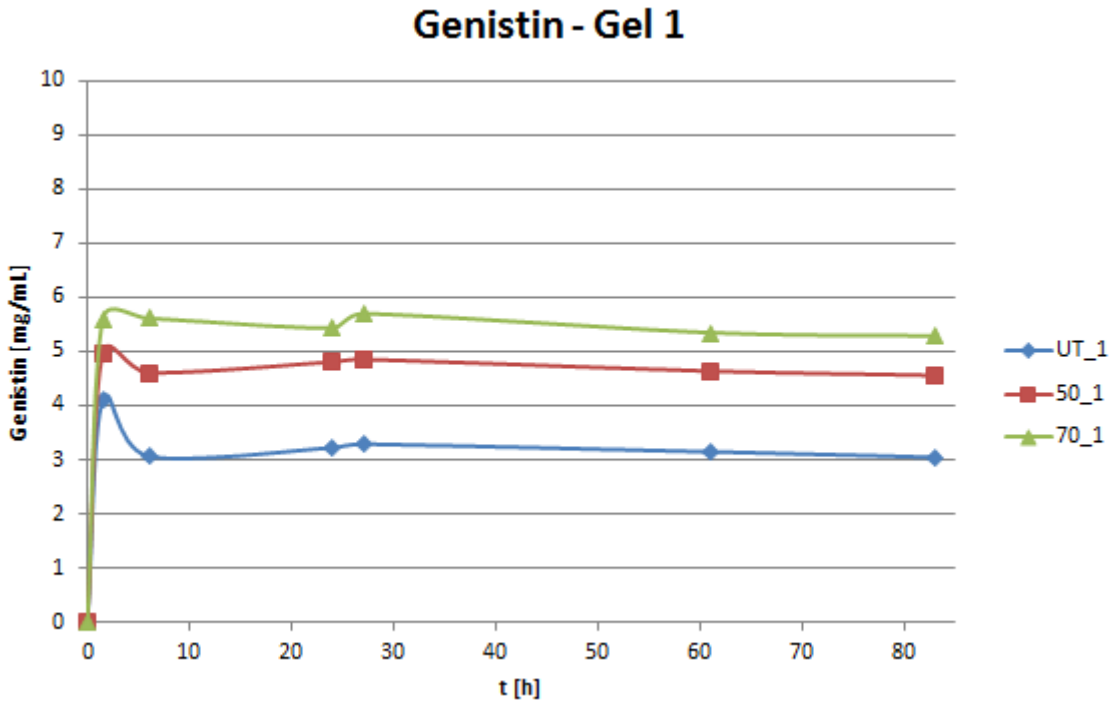

Figure 3.22: Genistin release, from samples coated with gel1, in dependence of time.

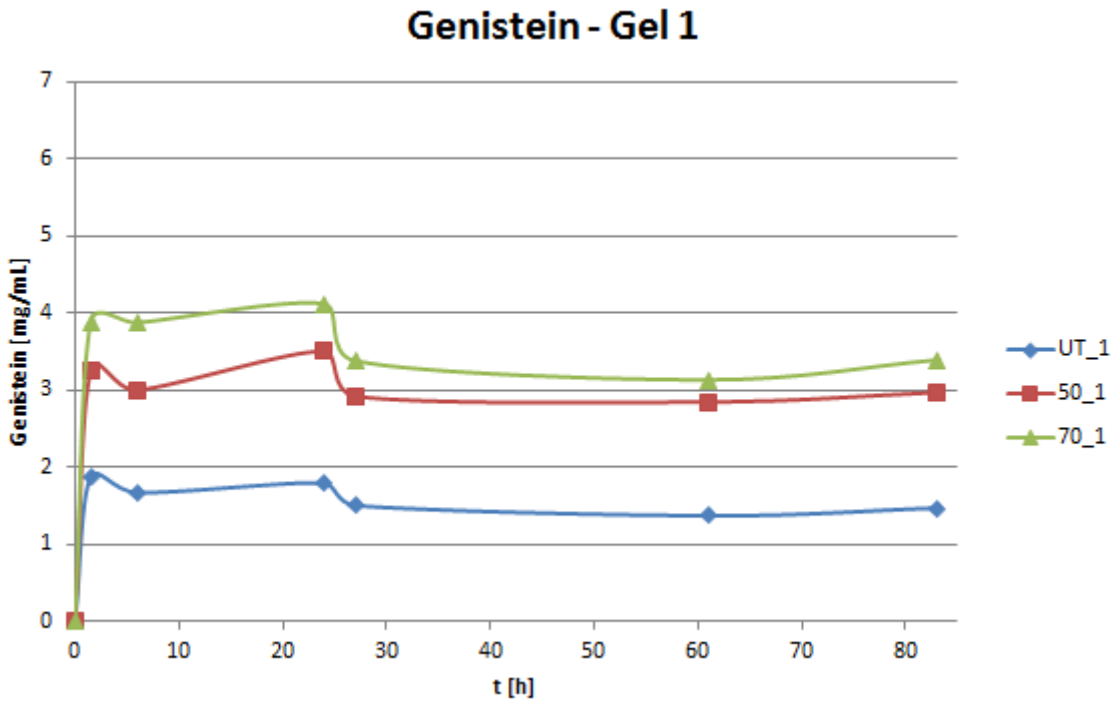

Figure 3.23: Genisteine release, from samples coated with gel1, in dependence of time.

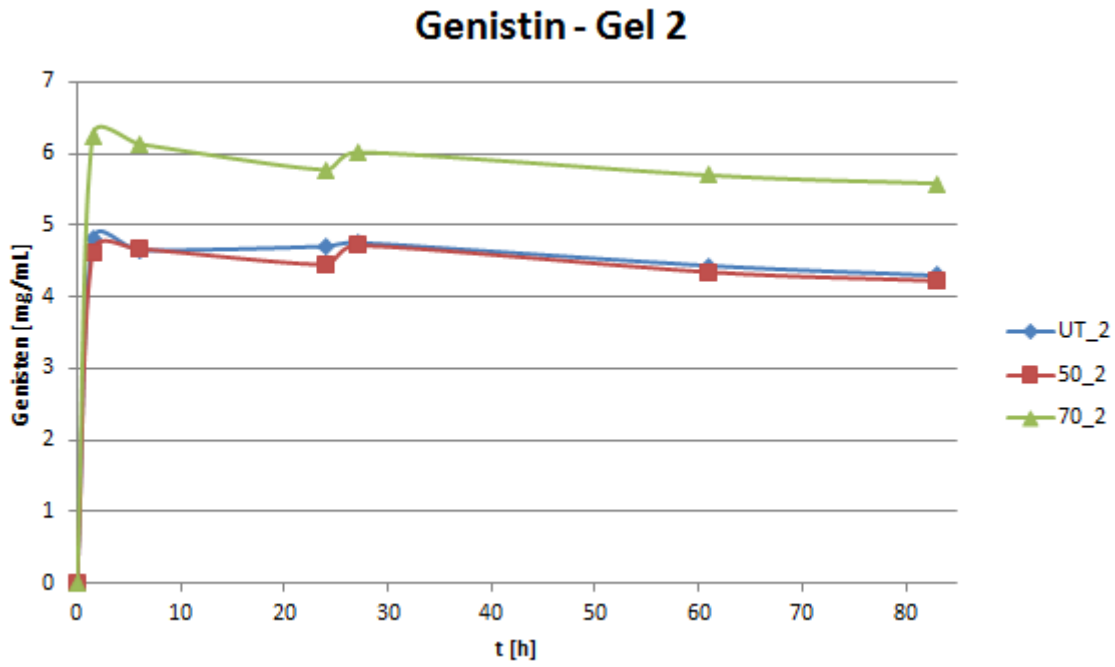

Figure 3.24: Genistin release, from samples coated with gel2, in dependence of time.

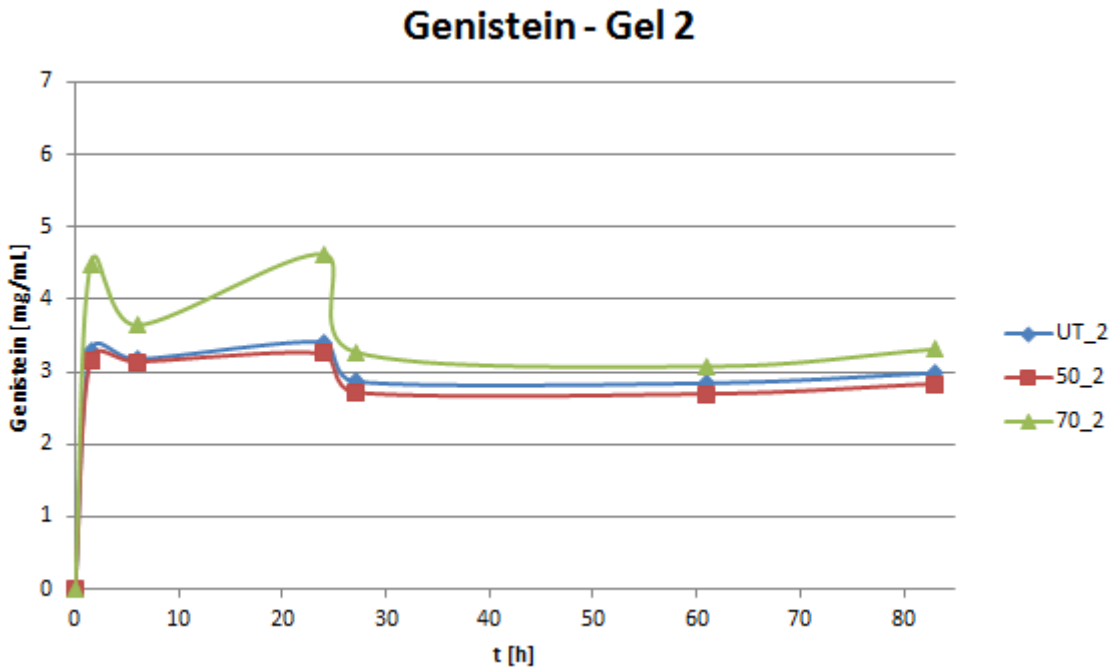

Figure 3.25: Genisteine release, from samples coated with gel2, in dependence of time.

First of all, what could be noticed comparing the trends of genistin and genistein concentrations in dependence of time is that both molecules releases showed a trend that present an initial fast high release. Concerning genistin, this first phase is followed by a partial resorption of this molecule that could be then slowly released during following days.

Instead, considering genistein, after the first high release

Genistein release presents a drop after 24 hours and this could be due to a partial reabsorbtion of the loaded substance; particularly, this reabsorbtion is more evident on sample with bigger nanotubes and this could be due to the higher hydrophilicity of this surface. Moreover, this second low release phase is followed by a partial resorption of molecule that is then slowly released during next days.

Considering the differences in the release of one molecule between the untreated and the anodised titanium loaded with gel 1, could be said that the quantity of substances released by the treated samples is higher than on pure titanium. The loaded quantity results the lowest for the untreated titanium and the highest for the sample treated at 70 V, i.e. with the bigger nanotubes, confirming that nanutubular structure topography is directly responsible of drug elution [109]. Specifically, the genistin and genistein concentration peaks are respectively 21.1 % and 95.5 % higher on samples treated at 50 V than on the untreated one and respectively 36.5 % and 129.6 % on the 70 V. This

is really interesting, because the presence of nanotubes enhance particularly the loading of the genistein molecule that is the active form of genistin, which needs an enzymatic action to have an effect on cells.

Instead, comparing the same samples coated with different gels, we could notice that using a gel with double density of soy extracts to coat samples has not a remarkable effect on the loaded quantity. Indeed, isoflavones concentrations peaks measured on 70 V sample coated with gel 2 are higher of just the 12.1 % than the peak reached when gel 1 was used. For this reason, to coat samples for the experiments with Saos-2 cell line the gel 1 was used. Moreover, from the release experiment with gel 2 emerged that there's no difference between the quantity of molecules released from the untreated sample and the one anodized at 50 V. Could be that the treated sample reached the maximum amount of loaded genistein and so doubling the concentration of loading gel does not have an effect on it.

3.2.1.1 Thin Layer Chromatography

After that the Thin Layer Chromatography (TLC) was performed as described in section 2.4.2, the used plates were watched through a non-destructive visualization under a UV light box.
The TLC analysis was made on the supernatants of samples, used for the release experiment and coated with gel2, to confirm that the used soy isoflavones powder truly contain genistein.

Before analysing release samples, this procedure was conducted on two known concentrations of solute: they were prepared dissolving in PBS respectively 208 and 416 mg/ml of soy isoflavones powder and their TLC plates are represented in figure 3.26.

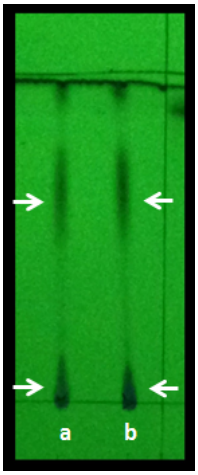

Figure 3.26: TLC analysis performed on standard samples: (a) 208 mg/ml of soy isoflavones powder in PBS and (b) 416 mg/ml.

From the UV analysis of samples could be notice that there are two spots corresponding to two molecules with different polarity, particularly the higher one is a bit elongated and this is due to the presence of many similar molecules in the extracts.
TLC was performed on the supernatants coming from the release experiment conducted on disks coated with gel 2 and it showed in figure 3.27 that the three different samples contained the same chemical species.

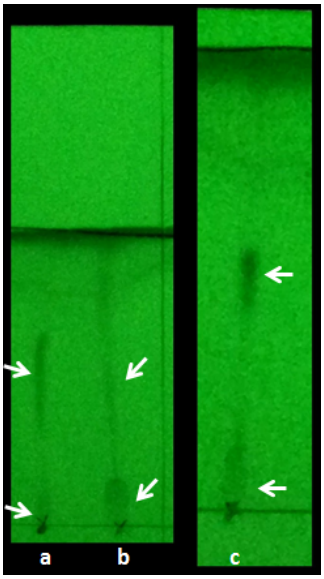

Figure 3.27: TLC analysis performed on supernatants of samples taken from the release experiment and coated with gel2. (a) represent the untreated titanium, (b) the disk treated at 50 V and (c) the one anodised at 70 V.

Specifically, considering the run of the solvent coming from the disk with bigger nanotubes (c), could be noticed that the intensity of the spot is higher for this sample and this means that the concentration of genistein in this supernatant is higher than the others, confirming the results coming from the release experiment (Sec. 3.2.1).
In the following table (3.3) are summarized the Rf values calculated for the standard solutions and release samples.

Standard samples	Rf_1	Rf_2
208 mg/ml in PBS	0.49	0.07
416 mg/ml in PBS	0.51	0.06
Release samples	Rf_1	Rf_2
UT	0.51	0.06
50	0.44	0.08
70	0.51	0.07

Table 3.3: Rf values of standard samples and of samples used for the release experiment and loaded with gel2 (release samples). Number 1 is referred to the higher spot and 2 to the lower one.

Basing on literature, the Rf value for genistein is 0.5 [140] and then these values confirm that the material loaded on samples contain this molecule.
Anyway, the higher spots on the plates appear elongated and this could be due to the fact that the extracts contain many other molecules similar to the genistein one, like genistin, daidzein and daidzin, indeed, they have Rf values about 0.5. Moreover, the lower spot should represent the malonyl-forms of genistein and daidzein that showed an Rf of 0.1 [141].

3.2.2 Test for fibroblasts viability and distribution

3.2.2.1 Calcein staining

The staining with calcein and ethidium-homodimer1 was used to evaluate the viability of murine fibroblast cell line on different kind of samples.
After 24 hours of incubation, the results obtained through those stainings are sum-

marised in figure 3.28, where 'TC' means the tissue culture plate, '50' the sample anodised at 50 V, '70' the one treated at 70 V and 'UT' the untreated titanium disk.

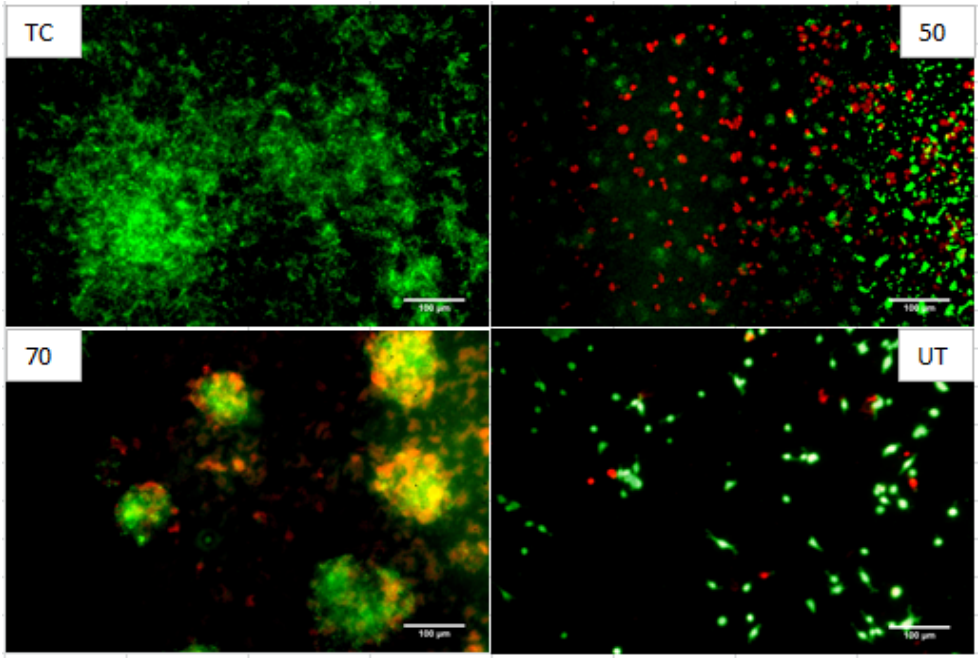

Figure 3.28: Results obtained from the viability staining with calcein (green) and ethidium homodimer-1 (red). 'TC' means the tissue culture plate, '50' the sample anodised at 50 V, '70' the one treated at 70 V and 'UT' the untreated titanium disk.

This picture shows that most cells (i.e. the green ones) are viable on each sample, but on disks with nanotubes there are more dead cells than on the others. This could mean that there was something on the nanotubular structure that differed from the untreated titanium surface and caused cells apoptosis.
However, all samples were stained in the same moment and the anodised two were watched at last at the fluorescence microscope after that the staining with calcein and ethidium homodimer-1 was done, therefore the presence of a larger amounts of dead cells could also may be due to the long exposition to those toxic substances.

3.2.2.2 Phalloidin and DAPI staining

The stainings with phalloidin and DAPI were used to evaluate the cells distribution on different kinds of samples and their shape.
The figures 3.29 were taken with the fluorescence microscope and they contain the results obtained after the staining with phalloidin and DAPI. When samples were watched looking for these stainings, calcein was still visible so was possible to overlap pictures

showing viability as well.

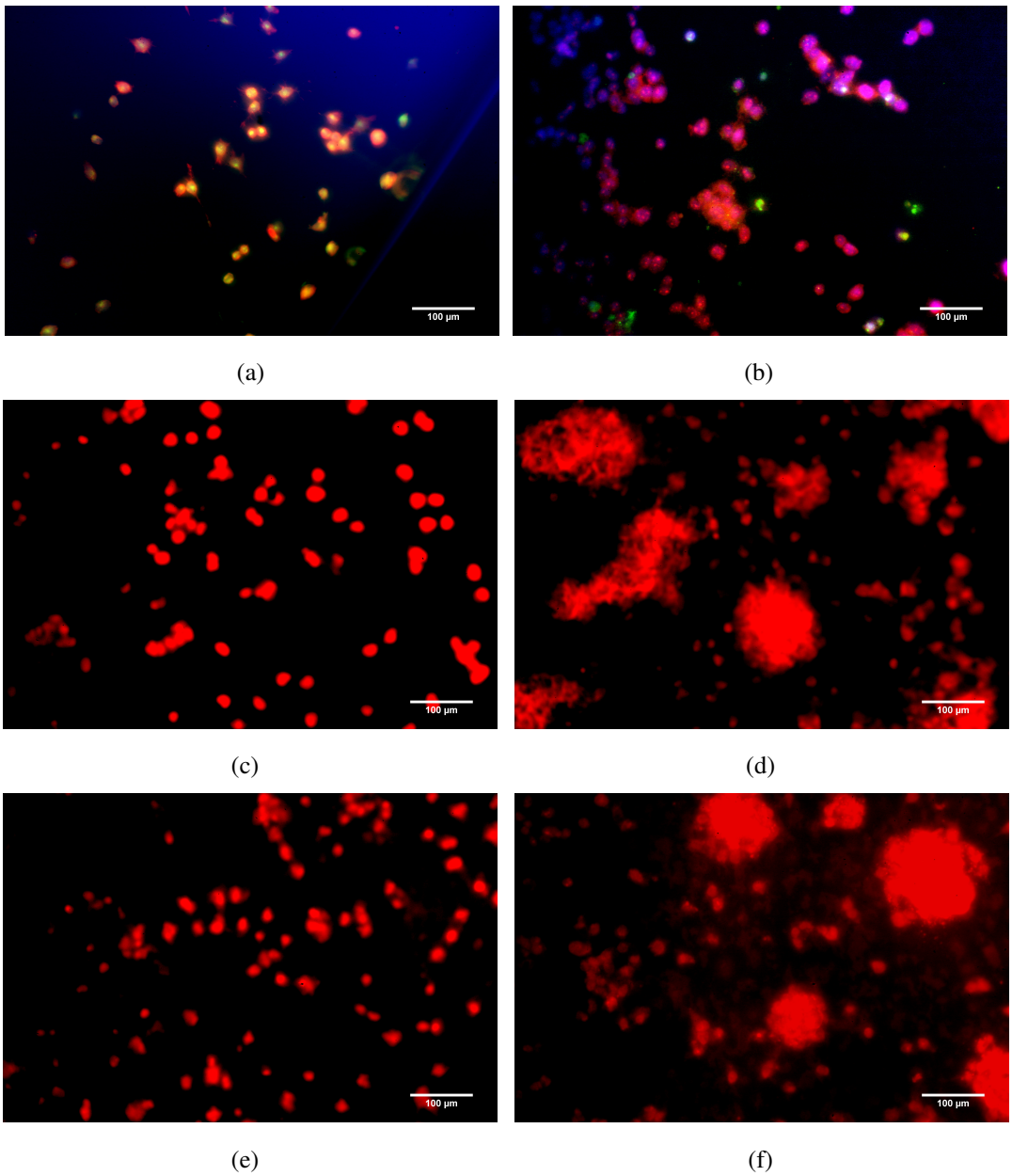

Figure 3.29: Results obtained after the staining with phalloidin (red), DAPI (blue) and calcein (green). (a) tissue culture plate, (b) untreated disk, (c) edges and (d) centre of sample anodized at 50 V, (e) edges and (f) centre of sample treated at 70 V.

From these pictures was possible to see that on each sample cells are present in large amount and they are distributed on almost all the available surface, also near the edges of the disks.

Furthermore, cells are evenly spaced on all the available surface on the tissue culture

plate and the untreated titanium as could be seen in figures 3.29(a) and 3.29(b) which are representative of the entire samples.
Moreover, cells cultured on the tissue culture plate have a more elongated shape than cells on titanium which did not show filopodium-like processes extending from them. This behaviour could be due to the fact that cells needed more than 24 hours to migrate away from other cells and find the space to extend themselves and their actin-stained filaments on different kinds of materials.
Instead, considering samples with nanotubes, cells are equally distributed near the edges of disks, but they formed rounded clusters at the centre of samples which are represented in figures 3.29(d) and 3.29(f). Indeed, some papers showed that on this kind of surface cells do not spread but rather form 3D spheroids of rounded cells [142, 143]. Those could be used to make spheroids of cells that are in a progenitor-like phenotype, rather than a differentiated one, and simulate a staminal niche.

3.2.3 Samples characterization with Saos-2 cell line

Three different 24 multiwell culture plate were prepared as described in section 2.4.7 and incubated for three different times: 24, 48 and 65 hours. After that cells were fixed and stained with F-actin phalloidin to make possible observing them under the fluorescence microscope and evaluate their number, shape and distribution on different kinds of samples.

3.2.3.1 Tissue culture plates

Cells morphologies on the tissue culture plates for different incubation times could be found in figure 3.30.

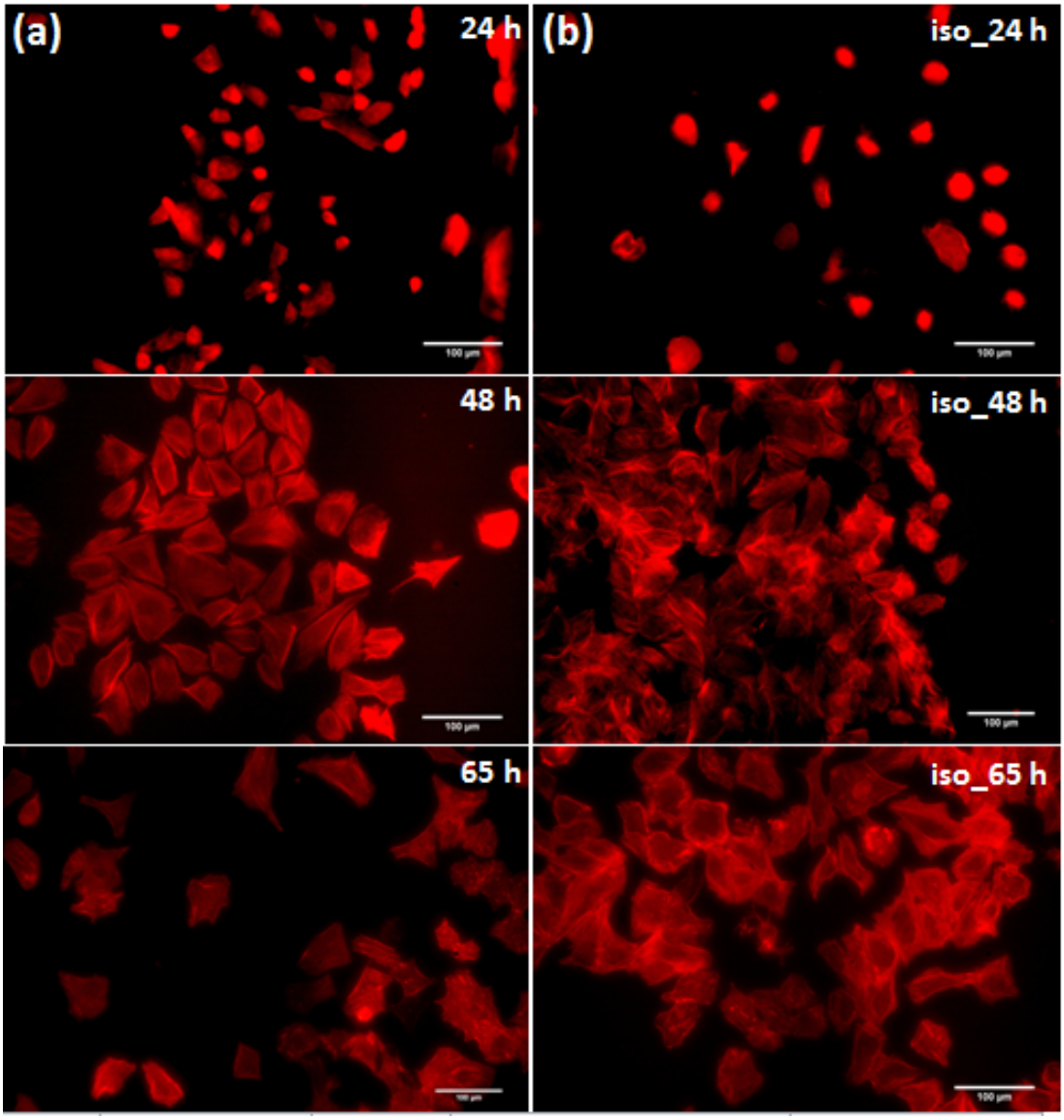

Figure 3.30: Phalloidin staining of Saos-2 cell line seeded on tissue culture plates and cultured (a) without and (b) with soy isoflavones extracts contained medium for 24, 48 and 65 hours.

After 24 hours of culture, cells were small, round shaped and isolated on both samples. Instead, after 48 hours could be seen that they were really bigger more elongated and less round shaped than before. Then, cells cultured with soy isoflavones extracts present filopodia like processes that represented the presence of an interactions with the substrate and other cells. Moreover, they are closer between each others than the ones cultured on just the tissue culture plate and some rounded shape cells are present in these groups. This suggest that, as reported in literature [14], osteoblasts treated with genistein have a tendency to form clusters.

3.2.3.2 Titanium disks with or without nanotubes

3.2.3.2.1 Cells count

Cells were count as described in section 2.4.7.1 and, for those reasons, the calculated cell amounts coming from here should not be considered an evaluation of how many cells were present on samples, but just an estimation of how many cells migrated from the drop toward the remaining surface. Furthermore, the fact that cells were count in the same way on each sample, gave the opportunity to compare the number of cells on different material morphology and chemistry.

In the following figure (3.31) are represented the number of cells, in dependence of time, evaluated on titanium disks untreated or with nanotubes.

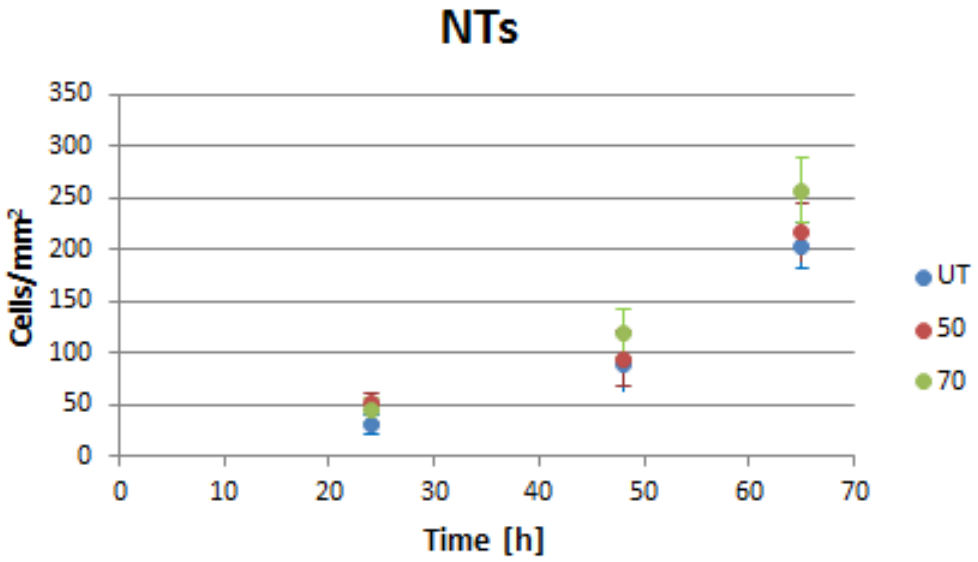

Figure 3.31: Trend of number of cells, in dependence of the incubation time, on untreated titanium disk (UT), sample treated at 50 V (50) and disk anodised at 70 V (70).

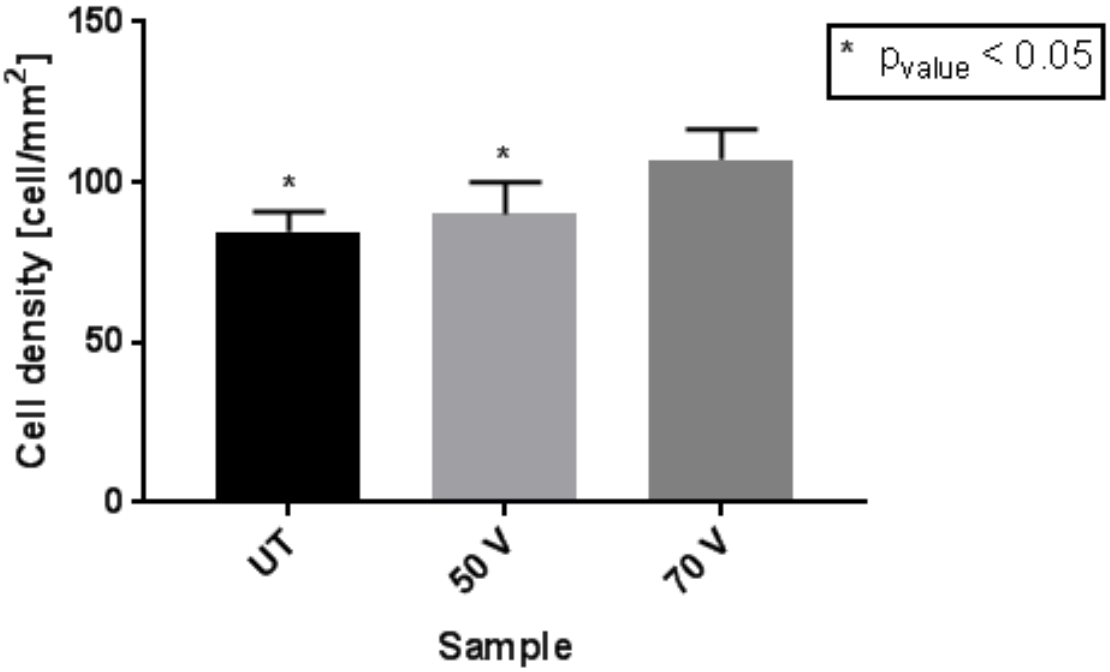

Figure 3.32: Cell densities at 65 hours of incubation on untreated titanium disk (UT), sample treated at 50 V (50) and disk anodised at 70 V (70).

For each sample, the number of cells obviously increased increasing the incubation time and the amounts of cells in each time point were statistically bigger than in previous point. Moreover, in contrast with literature [10, 11], from these data came out that after 65 hours of culture (Fig. 3.32), the number of cells is almost the same on the untreated sample and the disk treated at 50 V, while this number is higher for sample with bigger nanotubes (i.e. 70 V), suggesting that on this nanostructure cells found a more comfortable substrate and proliferated more fastly.

3.2.3.2.2 Phalloidin staining

Considering the phalloidin staining of cells cultured on titanium disks with or without nanotubes, could be observed that after 24 hours, cells cultured on the untreated sample showed filopodia structures and are more polygonal shaped than the ones seeded on treated material on which all cells exhibited the rounded form, which is typical of the first phases of substrate adhesion.
Furthermore, leaving cells more time on the substrates, could be noticed from picture 3.33 that cells seeded on the nanotubular structure had now a polygonal flattened shape as well and interactions between adjacent osteoblasts could be observed. However,

seemed that on anodized samples, particularly the one treated at 70 V, many cells maintained a shape that is reminiscent of the preliminary rounded form.

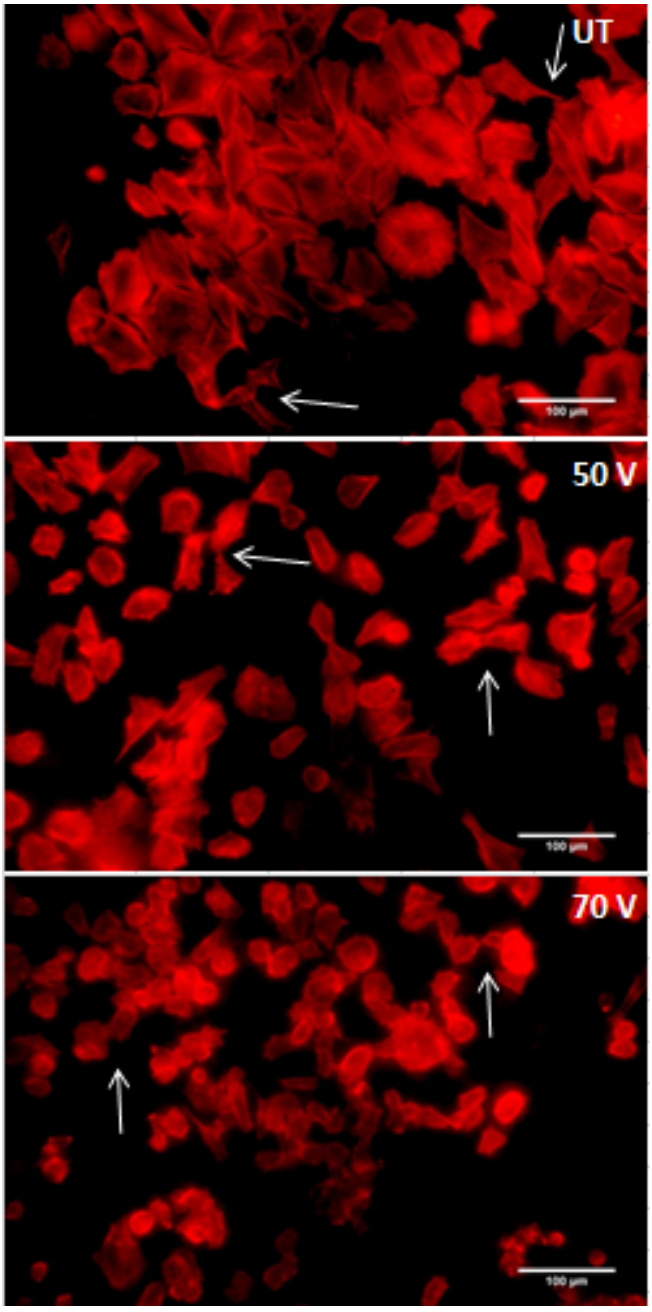

Figure 3.33: Phalloidin stainings of cells cultured for 65 hours on untreated titanium disk (UT), sample anodised at 50 V (50 V) and at 70 V (70 V). The arrows indicates some interactions between adjacent cells.

3.2.3.2.3 Alamar blue viability test

The results of the Alamar blue viability test performed on samples functionalized with nanotube are represented in table 3.4.

Sample	Viability [%]
TC	100 ± 2.8
UT	114.4 ± 4.6
50	111.8 ± 11.1
70	109.2 ± 8.4

Table 3.4: Results of Alamar blue test performed on the tissue culture plate (TC), untreated titanium (UT) and sample anodized at 50 and 70 V.

Each sample show a viability higher than the tissue culture plate, but there are no differences between the untreated sample and the ones with nanotubes. This could be due to the fact that cells reached confluence in 3 days of culture and then wasn't possible to detect differences in the proliferation between the samples cause they all were covered by cells.

3.2.3.3 Titanium disks with soy isoflavones extracts

3.2.3.3.1 Cells count

In this section will be compared results concerning cell count on different samples coated or not with gel 1 as described in section 3.2.1.

The genistein loading on samples should have the effect to inhibit cell proliferation because it interact with the estrogen receptor β blocking the proliferation cycle by inhibiting the topoisomerase II enzyme [13]. In figure 3.34, indeed, could be seen that on both the anodized samples, after 65 hours of culture, the number of cells is significantly lower on the coated disks. Particularly, this trend is more evident on sample treated at 70 V and this should be due to the fact that, as emerged from the release experiment (Sec. 3.2.1), this disk had been loaded with an higher quantity of soy isoflavones extracts.

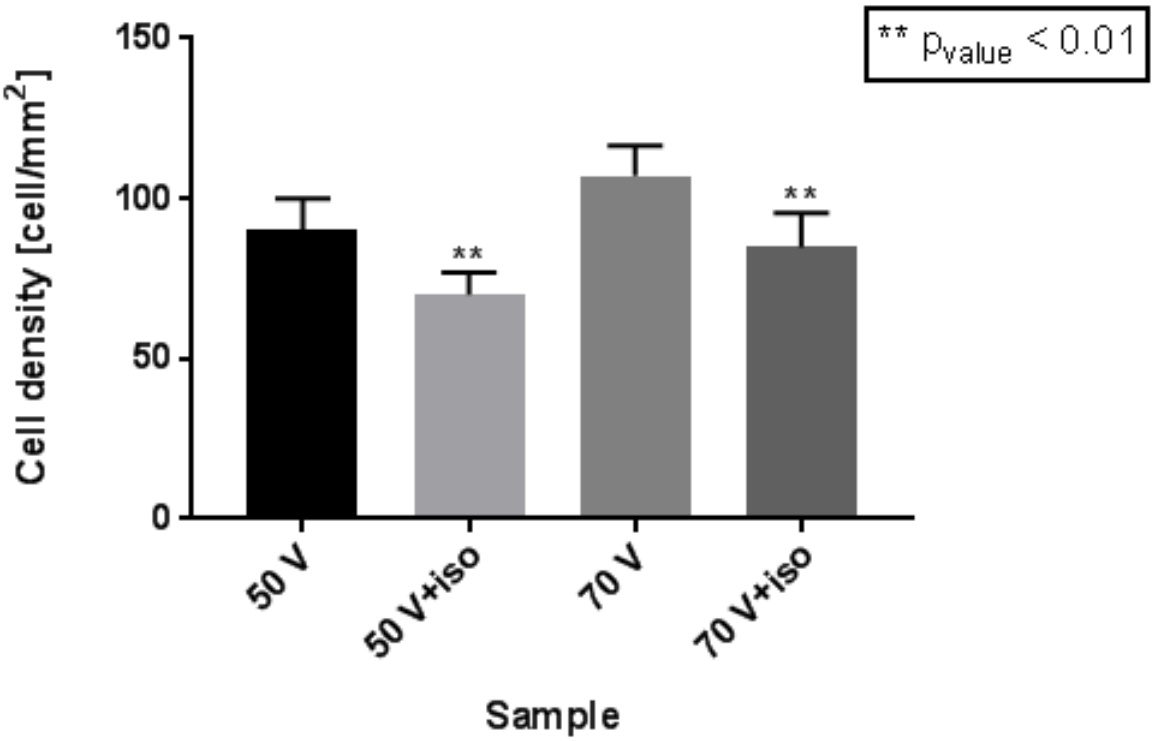

Figure 3.34: Trend of number of cells, in dependence of the incubation time, on sample anodized at 50 and 70 volt with (50 V and 70 V) or without coating of soy isoflavones extracts (50 V+iso and 70 V + iso).

3.2.3.3.2 Phalloidin staining

Cells cultured on the coated samples were observed and results are showed in figure 3.35. Unfortunately, the positions of untreated samples in the multiwell plates cultured for 48 and 65 hours were found infected and then wasn't possible to observe this kind of sample in those two time points.

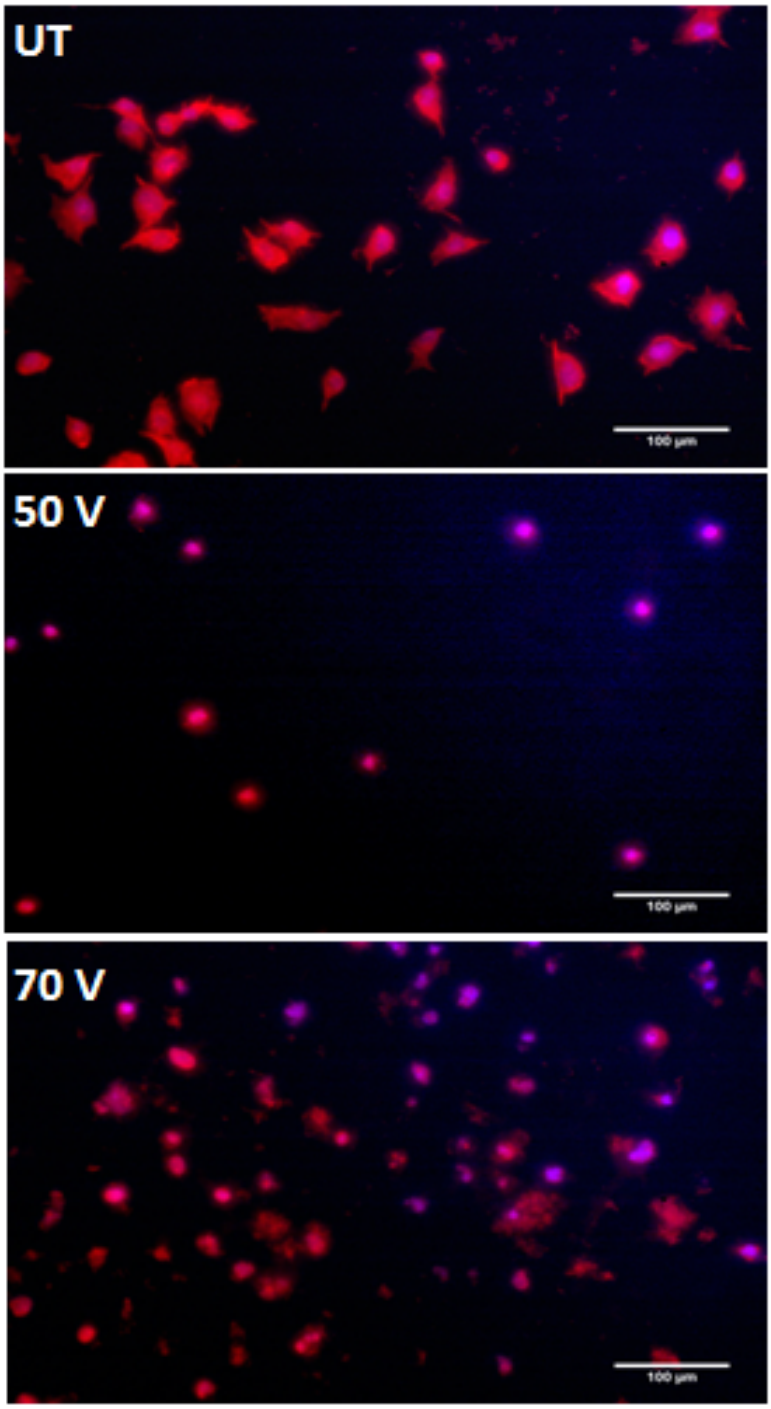

Figure 3.35: Phalloidin staining of cells cultured for 24 hours on samples coated with a soy isoflavones extracts-based solution. 'UT' stays for untreated titanium disk, '50 V' is for sample anodized at 50 V and '70 V' for the one treated at 70 V.

Considering samples cultured for 24 hours, could be easily said that cells on the untreated disk were bigger than on the other samples and, most of all, they already had

a more flattened shape and cytoskeleton extensions.

Then in figure 3.36 could be observed that, culturing cells for more than 24 hours, they really increased their dimensions and tended to migrate toward other cells.

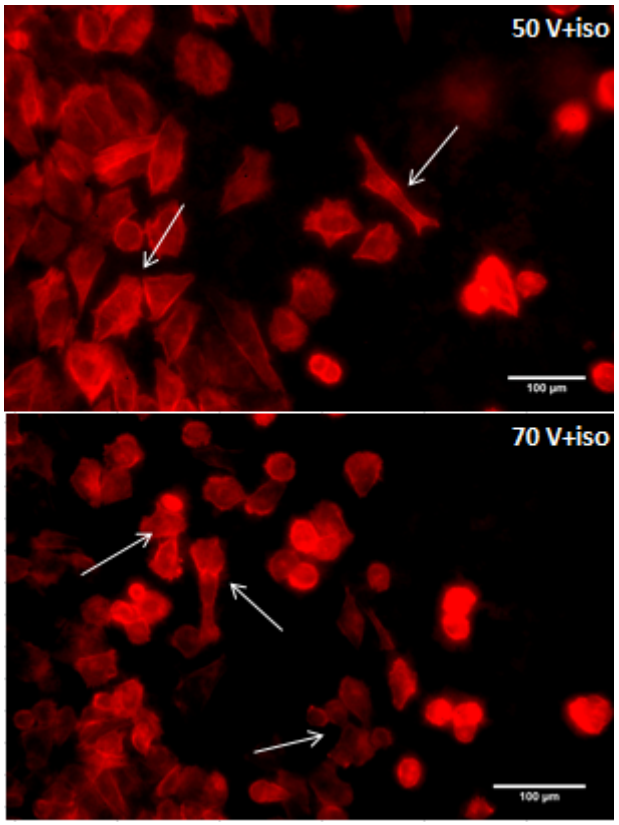

Figure 3.36: Phalloidin staining of cells cultured for 65 hours on titanium disk anodized at 50 and 70 V and coated with a soy isoflavones extracts-based solution (respectively 50 V + iso and 70 V+iso). The arrows indicates some interactions between adiacent cells.

Superficially these samples appeared almost equal to the cells seeded on the uncoated disks, even if Saos-2 seemed to be more flattened and polygonal shaped, particularly on the 50 V disk than on the one with biggest nanotubes.
Subsequently, a SEM analysis of samples was performed to better define the effect of soy isoflavones extracts on Saos-2 cell line.

3.2.3.4 SEM analysis

After watching seeded cells through the previous stainings, SEM analysis was performed to evaluate if Saos-2 cell line covered all the available surface and if they adhered on nanotubolar structures.

In picture 3.37 are represented the SEM images of samples with or without nanotubes.

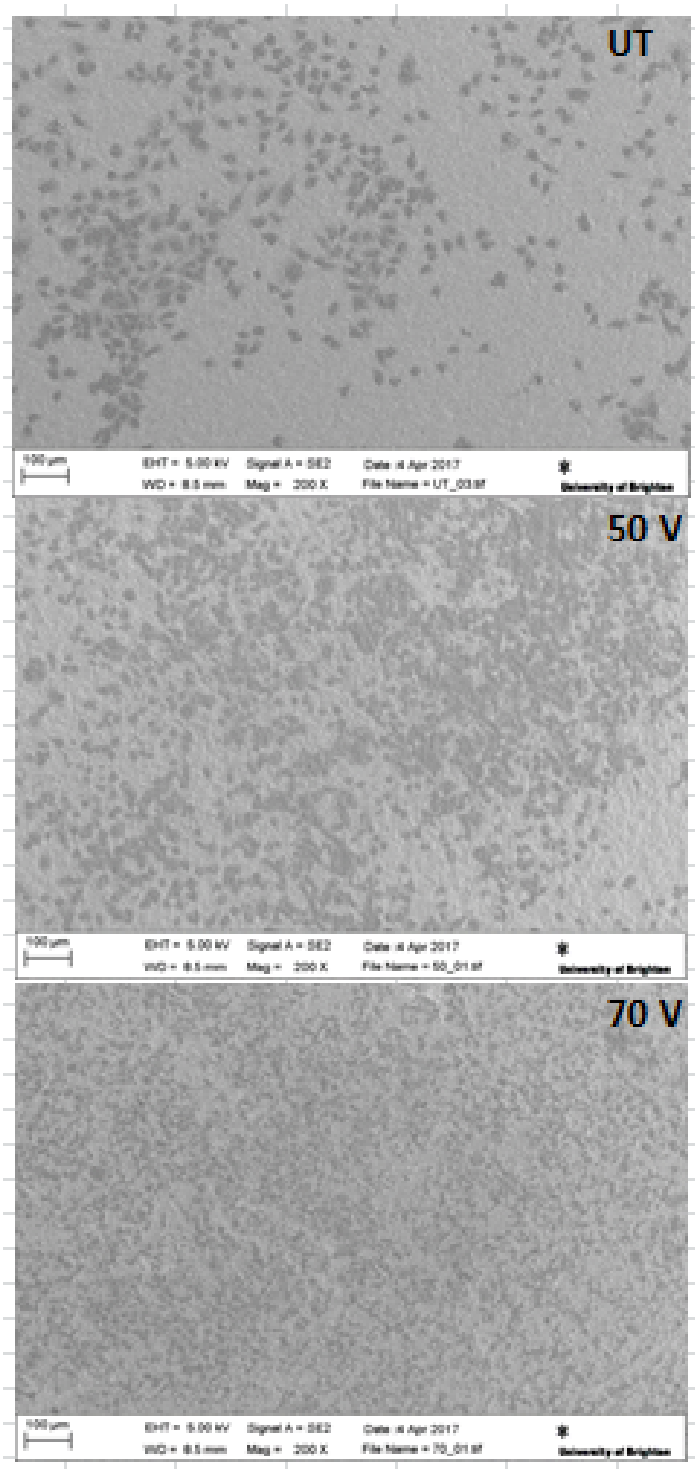

Figure 3.37: SEM analysis of cells cultured for 65 hours on untreated (UT) and anodized titanium disks (50 V and 70 V).

Could be seen that after 65 hours Saos-2 are homogeneously distributed on all the available substrates and did not form clusters on the surfaces.
Moreover, from this pictures seemed that cells cultured on anodised samples were less flattened but really more numerous than the ones on untreated titanium. Moreover, they seemed to be less isolated on sample anodized at 50 V.

Considering then the anodised samples coated with soy isoflavones extracts, SEM results are reported in figure 3.38.

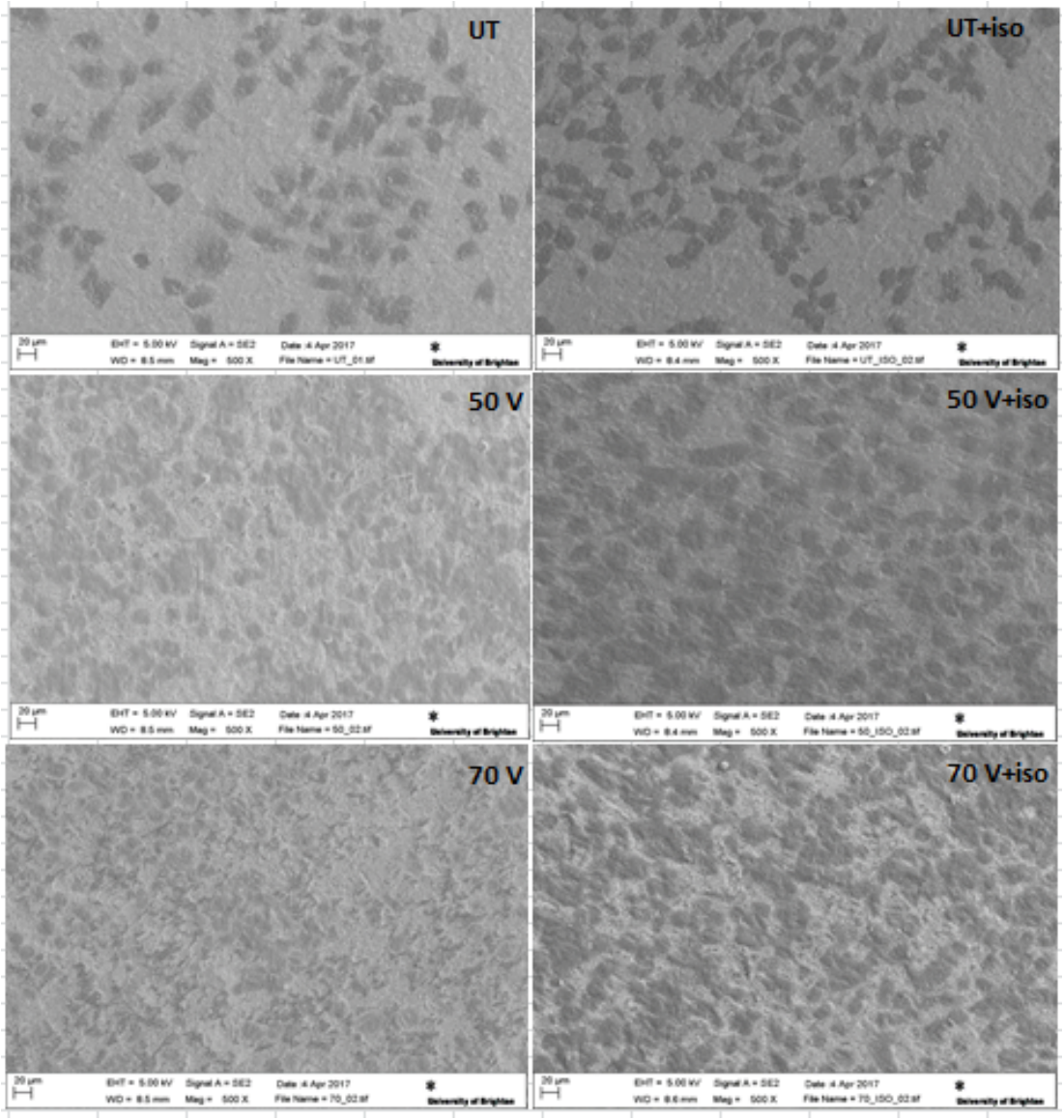

Figure 3.38: SEM analysis of cells cultured for 65 hours on untreated ('UT') and anodized titanium disks uncoated ('50 V' and '70 V') and coated with soy isoflavones extracts (UT+iso, 50 V+iso and 70 V+iso).

Despite of the inhibition of cells proliferation made by genistein, Saos-2 uniformly covered the entire sample area, especially on the nanotubular samples. Moreover, could be observed the positive effect that this molecule has on osteoblasts [13] behaviour: cells possess a polygonal shape and they're really more flattened than on samples with just nanotubes. Moreover, in presence of isoflavones Saos-2 seemed to be less isolated and to interact more between each other.

Chapter 4

Conclusions and further developments

Titanium dioxide nanotubes (TiO_2 NTs) fabrication is one of the most promising surfat the nano scale for enhancing implant to tissue interactions for dental and orthopaedic implants.
TiO_2 NTs could be obtained through an electrochemical anodization treatment in a fluoride containing electrolyte and their geometry could be tuned by varying the treatment parameters [28].
Moreover, TiO2 NTs could carry bioactive molecules and can be used as a local drug delivery system [18].
The first aim of this project was to optimize the anodization parameters to provide a regular and homogeneous nanotube array with a thickness about ten micrometers and two different diameter size..
The second aim of this study was to investigate the possibility to coat the nanotube coating with biomolecules, and in particular with a soybean-based biomaterial. The effect of the two different diameter size on biomolecule uptake was also evaluated.

Concerning the nanotube manufacturing, the best anodization process was found applying potentiostatic conditions, and the size of the nanotube diameter can be varied by varying the applied potential. Other electrochemical parameters were also identified, investigated and optimized. The initial potential application, the solution composition and concentration, treatment time and process temperature were all important parameters. The anodization in an ethilenglycol-based electrolyte, produced nanotubes with homogeneous distribution, smooth walls and bigger dimensions than using aqueous-based electrolytes. As a drawback, using such organic electrolyte led to the formation of highly disordered oxide layer covering the nanotubular structure. The solution to this problem was obtained by pretreating the titanium surface to obtain a highly polished

titanium surface and by post-treating the nantube covered titanium samples by a proper gentle cleaning procedure. The pre- and post-treatment procedure had to be tuned to each anodization conditions (choice of applied potential).

The treatment time variation influenced the nanotube length, that increased for longer treatment times. A proper treatment time was selected to obtain a fixed length of 10-12 micrometers.

The increase of the applied potential led to higher diameters. Our data showed that such increase of diameter did not affect the nanutobe wall thickness, that remained quite constant changing the voltage.

Based on those results, is possible to produce specimens with reproducible dimensionally different nanotubes diameters applying different potential values.

From contact angle measurements, we observed that hydrophilicity on nanotube coated surfaces, decreasing increasing the diameter size. This may suggest a proper role in the surface protein interaction and adsorption, cell adhesion, proliferation and osteoblastic differentiation, perhaps making TiO2 NTs a potentially promising substrate to improve tissue integration of orthopaedic and dental implants.

Untreated titanium and two different nanotube diameter coated titanium were also coated by a soy isoflavones extracts gel, known to provide positive anabolic effect on bone metabolism, inhibiting bone loss in the tissue culture system.

The isoflavones release trend of TiO_2 NTs presented an initially high release rate and then a nearly constant release that could be maintained over a long period of time. Moreover, the anodized samples showed an uptake and release isoflavones amount higher than the untreated disk. Increasing the nanotube diameter will provide higher biomolecule uptake and release. This confirmed that TiO_2 NTs could be used as local drug delivery system to support the implant to tissue interactions post surgery.

The biological characterization of uncoated and coated samples were performed with osteosarcoma cell line and showed that cells proliferation is enhanced by nanotubes, and it increases on larger nanotubes. Moreover, TiO2 NTs were found to stimulate cell interactions, that showed a polygonal shape and appeared more flattened on samples with smaller nanotubes.

Surpraising, soy isoflavones extract was found to inhibit cells proliferation but showed some potential positive effect evidenced by cell morphology probably related to anabolic effect that isoflavones and genestein may have on osteoblasts.

Concerning future developments, it would be useful to evaluate the relationship between anodization treatment time and voltage especially considering the removal of the oxide covering the nanotubes that occasionally was observed in the first experiments.

This understanding could give the opportunity to produce opened nanotubular structures with smaller and different diameters.

Further and deeper studies also on the biological side, combined with finer analytical and characterization methods, may also provide better understanding of the interactions of such innovative surface modification in the nanoscale that we obtained in this exploratory study.

Appendix A

Graphics data

In this appendix are reported the numerical data used to draw graphics contained in the section 'Results'.

Sample	**L [μm]**
1_60_4	24.8 $\pm$ 2.3
1_60_6	17.8 $\pm$ 0.4
1_60_8	21.7 $\pm$ 1.3

Table A.1: Trend of nanotubes lenghts in dependence of time for samples coming from sheet 1, treated in solution 2, at 60 V and for three different times (Tab. 2.5; 1_60_4, 1_60_6 and 1_60_8). Rapresented in figure 3.9.

Sample	**L [μm]**
1_60_6	17.9 $\pm$ 0.4
2_60_6	8.9 $\pm$ 0.4
3_60_6	9.4 $\pm$ 0.6

Table A.2: Lenght values of samples treated at 60 V for 6 hours, coming from different sheet (1_60_6, 2_60_6 and 3_60_6).

Sample	D_{in}	D_{out}
1_60_6	102.6 ± 9.3	213.3 ± 6.2
2_60_6	141.6 ± 8.9	207.9 ± 9.9
3_60_6	97.7 ± 9.8	213.6 ± 7.9

Table A.3: Diameters values of samples treated at 60 V for 6 hours, coming from different sheet (1_60_6, 2_60_6 and 3_60_6).

Sample	L [μm]
60_6	8.9 ± 0.4
60_4	3.6 ± 0.2
60_2	6.2 ± 0.7
60_1	5.8 ± 0.4

Table A.4: Trend of nanotubes lengths in dependence of time for samples coming from sheet 2, treated in solution 2, at 60 V and for four different times (Tab. 2.5; 60_6, 60_4, 60_2, 60_1). Represented in figure 3.13.

Sample	D_{in}	D_{out}
60_6	141.6 ± 8.9	207.9 ± 9.9
60_2	137.5 ± 6.8	211.7 ± 6.7

Table A.5: Diameters values in dependence of time for samples coming from sheet 2, treated in solution 2, at 60 V and for three different times (Tab. 2.5; 60_6, 60_4, 60_2). Represented in figure 3.14.

Sample	L [μm]
30_2	3.2 ± 0.3
40_2	3.4 ± 0.2
50_2	5.0 ± 0.2
60_2	6.2 ± 0.7

Table A.6: Nanotubes lengths trend in dependence of the applied voltage for samples coming from sheet 2, anodised for 2 hours at 30, 40, 50, 60 and 70 V (Tab. 2.5; 30_2, 40_2, 50_2, 60_2 and 70_2. Represented in figure 3.17.

Sample	D_{in}	D_{out}
20_2	41.2 ± 6.8	109.0 ± 6.3
30_2	64.8 ± 8.9	136.5 ± 7.1
40_2	87.4 ± 6.9	171.2 ± 6.3
50_2	122.0 ± 6.7	198.1 ± 6.6
60_2	137.5 ± 6.8	211.7 ± 6.9
70_2	149.4 ± 6.1	234.4 ± 6.8

Table A.7: Diameters sizes in dependence of the applied voltage for samples coming from sheet 2, anodised for 2 hours at 20, 30, 40, 50, 60 and 70 V (Tab. 2.5; 20_2, 30_2, 40_2, 50_2, 60_2 and 70_2. Represented in figure 3.18.

Voltage [V]	Sample	D_{in} [nm]	D_{out} [nm]
50	Single	118.05 ± 8.47	188.75 ± 8.85
	Multisample	111.26 ± 7.64	192.74 ± 8.01
	Total	114.65 ± 8.02	190.75 ± 8.44
70	Single	154.28 ± 7.93	229.15 ± 9.17
	Multisample	150.00 ± 10.83	236.59 ± 16.83
	Total	151.92 ± 9.61	233.25 ± 13.88

Table A.8: Diameters sizes of samples treated in solution 2 at for two hours at 50 and 70 V. Some samples were anodized singularly and the others were anodized simultaneously using a multisample holder.

Appendix B

Measurement uncertainties

In this appendix are reported euqations used to calculate measurement uncertainties. Concerning N indipendent measurements of the same experimental quantity X_j, the following variables could be calculated:

- mean value:

$$x_j = M_x = \frac{1}{N}\sum_{k=1}^{N} x_{j,k} \tag{B.1}$$

- variance:

$$\sigma_{x_j}{}^2 = \frac{1}{N-1}\sum_{k=1}^{N} x_{j,k} - M_x{}^2 \tag{B.2}$$

- standard deviation:

$$\sigma_{x_j} = SD(X) = \sqrt{\sigma_{x_j}{}^2} \tag{B.3}$$

The standard deviation rapresents the uncertainty value $u(x_j)$ associated with x_j.

Considering then physical quantities obtained by the composition of other measures, the following expression were used:

- if y = A + B - C

$$u(y) = \sqrt{u(A)^2 + u(B)^2 + u(C)^2} \tag{B.4}$$

- if y = $\frac{ABC}{D}$

$$u(y) = |y| * \sqrt{\frac{u(A)^2}{|A|^2} + \frac{u(B)^2}{|B|^2} + \frac{u(C)^2}{|C|^2} + \frac{u(D)^2}{|D|^2}} \tag{B.5}$$

Bibliography

[1] Brunette et al. *Titanium in medicine: material science, surface science, engineering, biological responses and medical applications*. Springer Science & Business Media, 2012.

[2] Le Guehennec et al. "Surface treatments of titanium dental implants for rapid osseointegration". In: *Dental materials* 23.7 (2007), pp. 844–854.

[3] Sul et al. "Oxidized implants and their influence on the bone response". In: *Journal of Materials Science: Materials in Medicine* 12.10-12 (2001), pp. 1025–1031.

[4] Sul et al. "Resonance frequency and removal torque analysis of implants with turned and anodized surface oxides". In: *Clinical oral implants research* 13.3 (2002), pp. 252–259.

[5] Paulose et al. "Anodic growth of highly ordered TiO2 nanotube arrays to 134 μm in length". In: *The Journal of Physical Chemistry B* 110.33 (2006), pp. 16179–16184.

[6] Macak et al. "Smooth anodic TiO2 nanotubes". In: *Angewandte Chemie International Edition* 44.45 (2005), pp. 7463–7465.

[7] Paulose et al. "TiO2 nanotube arrays of 1000 μm length by anodization of titanium foil: phenol red diffusion". In: *The Journal of Physical Chemistry C* 111.41 (2007), pp. 14992–14997.

[8] Yahia et al. "Effect of anodizing potential on the formation and EIS characteristics of TiO2 nanotube arrays". In: *Journal of The Electrochemical Society* 159.4 (2012), K83–K92.

[9] Gulati et al. "Titania nanotubes for local drug delivery from implant surfaces". In: *Electrochemically Engineered Nanoporous Materials*. Springer, 2015, pp. 307–355.

[10] Hao et al. “Effect of nanotube diameters on bioactivity of a multifunctional titanium alloy”. In: *Applied Surface Science* 268 (2013), pp. 44–51.

[11] Park et al. “TiO_2 nanotube surfaces: 15 nm—an optimal length scale of surface topography for cell adhesion and differentiation”. In: *Small* 5.6 (2009), pp. 666–671.

[12] Indira et al. “A review on TiO2 nanotubes: influence of anodization parameters, formation mechanism, properties, corrosion behavior, and biomedical applications”. In: *Journal of Bio-and Tribo-Corrosion* 1.4 (2015), p. 28.

[13] Santin and Luigi Ambrosio. “Soybean-based biomaterials: preparation, properties and tissue regeneration potential”. In: *Expert review of medical devices* 5.3 (2008), pp. 349–358.

[14] Christopher Morris et al. “The soybean isoflavone genistein induces differentiation of MG63 human osteosarcoma osteoblasts”. In: *The Journal of nutrition* 136.5 (2006), pp. 1166–1170.

[15] Santin et al. “A new class of bioactive and biodegradable soybean-based bone fillers”. In: *Biomacromolecules* 8.9 (2007), pp. 2706–2711.

[16] Middleton, Chithan Kandaswami, and Theoharis C Theoharides. “The effects of plant flavonoids on mammalian cells: implications for inflammation, heart disease, and cancer”. In: *Pharmacological reviews* 52.4 (2000), pp. 673–751.

[17] Kim, Andrei Ghicov, and Patrik Schmuki. “TiO_2 nanotube arrays: elimination of disordered top layers (“nanograss”) for improved photoconversion efficiency in dye-sensitized solar cells”. In: *Electrochemistry Communications* 10.12 (2008), pp. 1835–1838.

[18] Signoretto et al. “Effect of textural properties on the drug delivery behaviour of nanoporous TiO 2 matrices”. In: *Microporous and mesoporous Materials* 139.1 (2011), pp. 189–196.

[19] Lekholm et al. “Survival of the Brånemark implant in partially edentulous jaws: a 10-year prospective multicenter study”. In: *International Journal of Oral and Maxillofacial Implants* 14.5 (1999), pp. 639–645.

[20] Adell et al. “Long-term follow-up study of osseointegrated implants in the treatment of totally edentulous jaws”. In: *Int J Oral Maxillofac Implants* 5.4 (1990), pp. 347–359.

[21] Fugazzotto. “Success and failure rates of osseointegrated implants in function in regenerated bone for 72 to 133 months.” In: *International Journal of Oral & Maxillofacial Implants* 20.1 (2005).

[22] Ellen. “Microbial colonization of the peri-implant environment and its relevance to long-term success of osseointegrated implants.” In: *International Journal of Prosthodontics* 11.5 (1998).

[23] Esposito et al. “Biological factors contributing to failures of osseointegrated oral implants,(II). Etiopathogenesis”. In: *European journal of oral sciences* 106.3 (1998), pp. 721–764.

[24] Stach and Sean S Kohles. “A meta-analysis examining the clinical survivability of machined-surfaced and osseotite implants in poor-quality bone”. In: *Implant Dentistry* 12.1 (2003), pp. 87–96.

[25] El Askary, Roland M Meffert, and Terrence Griffin. “Why do dental implants fail? Part I.” In: *Implant dentistry* 8.2 (1999), pp. 173–185.

[26] Misch. *Dental implant prosthetics*. Elsevier Health Sciences, 2014.

[27] Sennerby and Johan Roos. “Surgical determinants of clinical success of osseointegrated oral implants: a review of the literature.” In: *International Journal of Prosthodontics* 11.5 (1998).

[28] Zwilling et al. “Structure and physicochemistry of anodic oxide films on titanium and TA6V alloy”. In: *Surface and Interface Analysis* 27.7 (1999), pp. 629–637.

[29] Ghicov et al. “Titanium oxide nanotubes prepared in phosphate electrolytes”. In: *Electrochemistry Communications* 7.5 (2005), pp. 505–509.

[30] Pozio et al. “Titanium nanotubes stimulate osteoblast differentiation of stem cells from pulp and adipose tissue”. In: *Dental research journal* 9.Suppl 2 (2012), S169.

[31] Narendrakumar et al. “Adherence of oral streptococci to nanostructured titanium surfaces”. In: *Dental Materials* 31.12 (2015), pp. 1460–1468.

[32] Leyens and Manfred Peters. *Titanium and titanium alloys*. Wiley Online Library, 2003.

[33] Boyer. “An overview on the use of titanium in the aerospace industry”. In: *Materials Science and Engineering: A* 213.1 (1996), pp. 103–114.

[34] Schutz and Watkins. “Recent developments in titanium alloy application in the energy industry”. In: *Materials Science and Engineering: A* 243.1 (1998), pp. 305–315.

[35] Guodong and Wang Guisheng. “Development of titanium and its industry”. In: *Chinese Journal of Rare Metals* 33.6 (2009), p. 903.

[36] Berger et al. “The electrochemistry of nanostructured titanium dioxide electrodes”. In: *ChemPhysChem* 13.12 (2012), pp. 2824–2875.

[37] Nickels. “3D printing the world’s first metal bicycle frame”. In: *Metal Powder Report* 69.2 (2014), pp. 38–40.

[38] Elias et al. “Biomedical applications of titanium and its alloys”. In: *Jom* 60.3 (2008), pp. 46–49.

[39] Rack and JI Qazi. “Titanium alloys for biomedical applications”. In: *Materials Science and Engineering: C* 26.8 (2006), pp. 1269–1277.

[40] Esposito et al. “Immunohistochemistry of soft tissues surrounding late failures of Brånemark implants”. In: *Clinical oral implants research* 8.5 (1997), pp. 352–366.

[41] Brocard et al. “A multicenter report on 1,022 consecutively placed ITI implants: a 7-year longitudinal study.” In: *International Journal of Oral & Maxillofacial Implants* 15.5 (2000).

[42] Lemons. “Biomaterials, biomechanics, tissue healing, and immediate-function dental implants”. In: *Journal of Oral Implantology* 30.5 (2004), pp. 318–324.

[43] Buser et al. “Influence of surface characteristics on bone integration of titanium implants. A histomorphometric study in miniature pigs”. In: *Journal of biomedical materials research* 25.7 (1991), pp. 889–902.

[44] Urban et al. “Dissemination of wear particles to the liver, spleen, and abdominal lymph nodes of patients with hip or knee replacement”. In: *J Bone Joint Surg Am* 82.4 (2000), pp. 457–457.

[45] Browne and Gregson. “Effect of mechanical surface pretreatment on metal ion release”. In: *Biomaterials* 21.4 (2000), pp. 385–392.

[46] Roccuzzo et al. “Early loading of sandblasted and acid-etched (SLA) implants: a prospective split-mouth comparative study”. In: *Clinical oral implants research* 12.6 (2001), pp. 572–578.

[47] Ong, David Carnes, and Kazuhisa Bessho. “Evaluation of titanium plasma-sprayed and plasma-sprayed hydroxyapatite implants in vivo”. In: *Biomaterials* 25.19 (2004), pp. 4601–4606.

[48] Aparicio et al. “Corrosion behaviour of commercially pure titanium shot blasted with different materials and sizes of shot particles for dental implant applications”. In: *Biomaterials* 24.2 (2003), pp. 263–273.

[49] Gotfredson et al. “Anchorage of TiO2-blasted, HA-coated, and machined implants: An experimental study with rabbits”. In: *Journal of Biomedical Materials Research Part A* 29.10 (1995), pp. 1223–1231.

[50] Ivanoff et al. “Histologic evaluation of the bone integration of TiO2 blasted and turned titanium microimplants in humans”. In: *Clinical oral implants research* 12.2 (2001), pp. 128–134.

[51] Gotfredsen and Ulf Karlsson. “A prospective 5-year study of fixed partial prostheses supported by implants with machined and TiO2-blasted surface”. In: *Journal of Prosthodontics* 10.1 (2001), pp. 2–7.

[52] Steenberghe et al. “A prospective split-mouth comparative study of two screw-shaped -tapping pure titanium implant systems”. In: *Clinical oral implants research* 11.3 (2000), pp. 202–209.

[53] Wennerberg et al. “A histomorghometric study of screw-shaped and removal torque titanium implants with three different surface topographies”. In: *Clinical oral implants research* 6.1 (1995), pp. 24–30.

[54] Arthur Novaes Jr et al. “Histomorphometric analysis of the bone-implant contact obtained with 4 different implant surface treatments placed side by side in the dog mandible.” In: *International Journal of Oral & Maxillofacial Implants* 17.3 (2002).

[55] Piattelli et al. “Bone response to machined and resorbable blast material titanium implants: an experimental study in rabbits”. In: *Journal of Oral Implantology* 28.1 (2002), pp. 2–8.

[56] Mueller et al. “Evaluation of the interface between bone and titanium surfaces being blasted by aluminium oxide or bioceramic particles”. In: *Clinical Oral Implants Research* 14.3 (2003), pp. 349–356.

[57] Massaro et al. “Comparative investigation of the surface properties of commercial titanium dental implants. Part I: chemical composition”. In: *Journal of Materials Science: Materials in Medicine* 13.6 (2002), pp. 535–548.

[58] Novaes et al. “Influence of implant microstructure on the osseointegration of immediate implants placed in periodontally infected sites”. In: *Clinical Oral Implants Research* 15.1 (2004), pp. 34–43.

[59] Cooper et al. “Fluoride modification effects on osteoblast behavior and bone formation at TiO 2 grit-blasted cp titanium endosseous implants”. In: *Biomaterials* 27.6 (2006), pp. 926–936.

[60] Ellingsen et al. “Improved retention and bone-to-implant contact with fluoride-modified titanium implants.” In: *International Journal of Oral & Maxillofacial Implants* 19.5 (2004).

[61] Ellingsen. “Pre-treatment of titanium implants with fluoride improves their retention in bone”. In: *Journal of Materials Science: Materials in Medicine* 6.12 (1995), pp. 749–753.

[62] Yokoyama et al. “Fracture mechanisms of retrieved titanium screw thread in dental implant”. In: *Biomaterials* 23.12 (2002), pp. 2459–2465.

[63] Sul et al. “Optimum Surface Properties of Oxidized Implants for Reinforcement of Osseointeg ration: Surface Chemistry, Oxide Thickness, Porosity, Roughness, and Crystal Structure.” In: *International Journal of Oral & Maxillofacial Implants* 20.3 (2005).

[64] Schupbach et al. “The Human Bone–Oxidized Titanium Implant Interface: A Light Microscopic, Scanning Electron Microscopic, Back-Scatter Scanning Electron Microscopic, and Energy-Dispersive X-Ray Study of Clinically Retrieved Dental Implants”. In: *Clinical implant dentistry and related research* 7.s1 (2005).

[65] Keller, Hunter, and Robinson. “Structural features of oxide coatings on aluminum”. In: *Journal of the Electrochemical Society* 100.9 (1953), pp. 411–419.

[66] Masuda and Kenji Fukuda. “Ordered metal nanohole arrays made by a two-step replication of honeycomb structures of anodic alumina”. In: *science* 268.5216 (1995), p. 1466.

[67] Matsui, Kazuyuki Nishio, and Hideki Masuda. “Highly ordered anodic porous alumina by imprinting using Ni molds prepared from ordered array of polystyrene particles”. In: *Japanese journal of applied physics* 44.10R (2005), p. 7726.

[68] Kelly. “The influence of fluoride ions on the passive dissolution of titanium”. In: *Electrochimica Acta* 24.12 (1979), pp. 1273–1282.

[69] Roy, Steffen Berger, and Patrik Schmuki. "TiO2 nanotubes: synthesis and applications". In: *Angewandte Chemie International Edition* 50.13 (2011), pp. 2904–2939.

[70] Macak, K Sirotna, and P Schmuki. "Self-organized porous titanium oxide prepared in Na_2SO_4/NaF electrolytes". In: *Electrochimica Acta* 50.18 (2005), pp. 3679–3684.

[71] Macak, Hiroaki Tsuchiya, and Patrik Schmuki. "High-aspect-ratio TiO2 nanotubes by anodization of titanium". In: *Angewandte Chemie International Edition* 44.14 (2005), pp. 2100–2102.

[72] Macak, Sergiu P Albu, and Patrik Schmuki. "Towards ideal hexagonal self-ordering of TiO2 nanotubes". In: *physica status solidi (RRL)-Rapid Research Letters* 1.5 (2007), pp. 181–183.

[73] Paramasivam et al. "Electrochemical synthesis of self-organized TiO 2 nanotubular structures using an ionic liquid (BMIM-BF 4)". In: *Electrochimica Acta* 54.2 (2008), pp. 643–648.

[74] Tsuchiya et al. "Self-organized TiO 2 nanotubes prepared in ammonium fluoride containing acetic acid electrolytes". In: *Electrochemistry communications* 7.6 (2005), pp. 576–580.

[75] Zhang, Md Faruk Hossain, and Takakazu Takahashi. "Photoelectrochemical water splitting on highly smooth and ordered TiO 2 nanotube arrays for hydrogen generation". In: *International journal of hydrogen energy* 35.16 (2010), pp. 8528–8535.

[76] Habazaki et al. "Fast migration of fluoride ions in growing anodic titanium oxide". In: *Electrochemistry Communications* 9.5 (2007), pp. 1222–1227.

[77] Albu et al. "Self-organized TiO2 Nanotube Arrays: Critical Effects on Morphology and Growth". In: *Israel Journal of Chemistry* 50.4 (2010), pp. 453–467.

[78] Yasuda and Patrik Schmuki. "Control of morphology and composition of self-organized zirconium titanate nanotubes formed in (NH 4) 2 SO 4/NH 4 F electrolytes". In: *Electrochimica Acta* 52.12 (2007), pp. 4053–4061.

[79] Kim et al. "Gravity assisted growth of self-organized anodic oxide nanotubes on titanium". In: *Electrochemistry Communications* 10.7 (2008), pp. 1082–1086.

[80] Macak et al. "Mechanistic aspects and growth of large diameter self-organized TiO 2 nanotubes". In: *Journal of Electroanalytical Chemistry* 621.2 (2008), pp. 254–266.

[81] Albu et al. "Formation of Double-Walled TiO2 Nanotubes and Robust Anatase Membranes". In: *Advanced Materials* 20.21 (2008), pp. 4135–4139.

[82] Beranek, H Hildebrand, and P Schmuki. "Self-organized porous titanium oxide prepared in H_2SO_4/HF electrolytes". In: *Electrochemical and solid-state letters* 6.3 (2003), B12–B14.

[83] Macak et al. "Influence of different fluoride containing electrolytes on the formation of self-organized titania nanotubes by Ti anodization". In: *Journal of Electroceramics* 16.1 (2006), pp. 29–34.

[84] Shankar et al. "Highly-ordered TiO_2 nanotube arrays up to 220 μm in length: use in water photoelectrolysis and dye-sensitized solar cells". In: *Nanotechnology* 18.6 (2007), p. 065707.

[85] Prakasam et al. "A new benchmark for TiO_2 nanotube array growth by anodization". In: *The Journal of Physical Chemistry C* 111.20 (2007), pp. 7235–7241.

[86] Li et al. "Anodization fabrication of highly ordered TiO_2 nanotubes". In: *The Journal of Physical Chemistry C* 113.29 (2009), pp. 12759–12765.

[87] Raja, T Gandhi, and Manoranjan Misra. "Effect of water content of ethylene glycol as electrolyte for synthesis of ordered titania nanotubes". In: *Electrochemistry communications* 9.5 (2007), pp. 1069–1076.

[88] Lee et al. "Effect of electrolyte conductivity on the formation of a nanotubular TiO2 photoanode for a dye-sensitized solar cell". In: *Journal of the Korean Physical Society* 54.3 (2009), pp. 1027–1031.

[89] David et al. "A comparative study on the morphological features of highly ordered titania nanotube arrays prepared via galvanostatic and potentiostatic modes". In: *Current Applied Physics* 14.6 (2014), pp. 868–875.

[90] Taveira et al. "Voltage oscillations and morphology during the galvanostatic formation of self-organized TiO2 nanotubes". In: *Journal of The Electrochemical Society* 153.4 (2006), B137–B143.

[91] Yoriya et al. "Fabrication of vertically oriented TiO_2 nanotube arrays using dimethyl sulfoxide electrolytes". In: *The Journal of Physical Chemistry C* 111.37 (2007), pp. 13770–13776.

[92] LV Taveira et al. "Initiation and growth of self-organized TiO2 nanotubes anodically formed in NH4F/(NH4) 2SO4 electrolytes". In: *Journal of the Electrochemical Society* 152.10 (2005), B405–B410.

[93] Cai et al. "The effect of electrolyte composition on the fabrication of self-organized titanium oxide nanotube arrays by anodic oxidation". In: *Journal of materials research* 20.01 (2005), pp. 230–236.

[94] Wang and Zhiqun Lin. "Anodic formation of ordered TiO_2 nanotube arrays: effects of electrolyte temperature and anodization potential". In: *The Journal of Physical Chemistry C* 113.10 (2009), pp. 4026–4030.

[95] Macak and Patrik Schmuki. "Anodic growth of self-organized anodic TiO_2 nanotubes in viscous electrolytes". In: *Electrochimica Acta* 52.3 (2006), pp. 1258–1264.

[96] Varghese et al. "Hydrogen sensing using titania nanotubes". In: *Sensors and Actuators B: Chemical* 93.1 (2003), pp. 338–344.

[97] Mor et al. "A review on highly ordered, vertically oriented TiO_2 nanotube arrays: fabrication, material properties, and solar energy applications". In: *Solar Energy Materials and Solar Cells* 90.14 (2006), pp. 2011–2075.

[98] Paulose et al. "Visible light photoelectrochemical and water-photoelectrolysis properties of titania nanotube arrays". In: *Journal of photochemistry and photobiology A: Chemistry* 178.1 (2006), pp. 8–15.

[99] Kulkarni. *Synthesis and applications of titania nanotubes: Drug delivery and ionomer composites*. ProQuest, 2008.

[100] Losic et al. "Titania nanotube arrays for local drug delivery: recent advances and perspectives". In: *Expert opinion on drug delivery* 12.1 (2015), pp. 103–127.

[101] Popat et al. "Influence of engineered titania nanotubular surfaces on bone cells". In: *Biomaterials* 28.21 (2007), pp. 3188–3197.

[102] Bjursten et al. "Titanium dioxide nanotubes enhance bone bonding in vivo". In: *Journal of Biomedical Materials Research Part A* 92.3 (2010), pp. 1218–1224.

[103] Brammer et al. “Improved bone-forming functionality on diameter-controlled TiO 2 nanotube surface”. In: *Acta biomaterialia* 5.8 (2009), pp. 3215–3223.

[104] Qureshi et al. “Antimicrobial biocompatible bioscaffolds for orthopaedic implants”. In: *Journal of tissue engineering and regenerative medicine* 8.5 (2014), pp. 386–395.

[105] Buchholz et al. “Management of deep infection of total hip replacement”. In: *Bone & Joint Journal* 63.3 (1981), pp. 342–353.

[106] Wu and David W Grainger. “Drug/device combinations for local drug therapies and infection prophylaxis”. In: *Biomaterials* 27.11 (2006), pp. 2450–2467.

[107] Newman et al. “Effects of enamel matrix derivative on Porphyromonas gingivalis”. In: *Journal of periodontology* 74.8 (2003), pp. 1191–1195.

[108] Gultepe et al. “Sustained Drug Release from Non-Eroding Nanoporous Templates”. In: *Small* 6.2 (2010), pp. 213–216.

[109] Peng et al. “Long-term small molecule and protein elution from TiO_2 nanotubes”. In: *Nano letters* 9.5 (2009), pp. 1932–1936.

[110] Yao and Thomas J Webster. “Prolonged antibiotic delivery from anodized nanotubular titanium using a co-precipitation drug loading method”. In: *Journal of Biomedical Materials Research Part B: Applied Biomaterials* 91.2 (2009), pp. 587–595.

[111] Popat et al. “Decreased Staphylococcus epidermis adhesion and increased osteoblast functionality on antibiotic-loaded titania nanotubes”. In: *Biomaterials* 28.32 (2007), pp. 4880–4888.

[112] Zhang et al. “Daunorubicin-TiO_2 nanocomposites as a “smart” pH-responsive drug delivery system”. In: *International journal of nanomedicine* 7 (2012), p. 235.

[113] Paunesku et al. “Biology of TiO_2-oligonucleotide nanocomposites”. In: *Nature materials* 2.5 (2003), pp. 343–346.

[114] Aw, Karan Gulati, Dusan Losic, et al. “Controlling drug release from titania nanotube arrays using polymer nanocarriers and biopolymer coating”. In: *Journal of Biomaterials and Nanobiotechnology* 2.05 (2011), p. 477.

[115] Zhang et al. “Deltasoy—an internet-based soybean database for official variety trials”. In: *Agronomy Journal* 94.5 (2002), pp. 1163–1171.

[116] Pandjaitan et al. "Evaluation of genistin and genistein contents in soybean varieties and soy protein concentrate prepared with 3 basic methods". In: *Journal of food science* 65.3 (2000), pp. 399–402.

[117] Luthria, Ronita Biswas, and Savithiry Natarajan. "Comparison of extraction solvents and techniques used for the assay of isoflavones from soybean". In: *Food Chemistry* 105.1 (2007), pp. 325–333.

[118] Liu et al. "Evidence for involvement of tyrosine phosphorylation in taxol-induced apoptosis in a human ovarian tumor cell line". In: *Biochemical pharmacology* 48.6 (1994), pp. 1265–1272.

[119] Spinozzi et al. "The natural tyrosine kinase inhibitor genistein produces cell cycle arrest and apoptosis in Jurkat T-leukemia cells". In: *Leukemia research* 18.6 (1994), pp. 431–439.

[120] Yamaguchi and YH Gao. "Anabolic effect of genistein on bone metabolism in the femoral-metaphyseal tissues of elderly rats is inhibited by the anti-estrogen tamoxifen". In: *Research in Experimental Medicine* 197.2 (1997), pp. 101–107.

[121] Blair et al. "Variable effects of tyrosine kinase inhibitors on avian osteoclastic activity and reduction of bone loss in ovariectomized rats". In: *Journal of cellular biochemistry* 61.4 (1996), pp. 629–637.

[122] Arjmandi et al. "Dietary soybean protein prevents bone loss in an ovariectomized rat model of osteoporosis". In: *The Journal of Nutrition* 126.1 (1996), p. 161.

[123] Santin, Luigi Nicolais, and Luigi Ambrosio. *Soybean-based thermoplastic as biomaterials*. US Patent App. 10/343,555. Aug. 2001.

[124] Yang et al. "Thickness-conversion ratio from titanium to TiO 2 nanotube fabricated by anodization method". In: *Materials Letters* 62.4 (2008), pp. 775–779.

[125] Chang et al. "Nanomechanical properties of array TiO 2 nanotubes". In: *Microporous and Mesoporous Materials* 145.1 (2011), pp. 87–92.

[126] Kilinc, E Sennik, and ZZ Ozturk. "Fabrication of TiO_2 nanotubes by anodization of Ti thin films for VOC sensing". In: *Thin Solid Films* 520.3 (2011), pp. 953–958.

[127] Jaroenworaluck et al. "Macro, micro and nanostructure of TiO_2 anodised films prepared in a fluorine-containing electrolyte". In: *Journal of Materials Science* 42.16 (2007), pp. 6729–6734.

[128] Chang et al. "Nanomechanical properties of array TiO 2 nanotubes". In: *Microporous and Mesoporous Materials* 145.1 (2011), pp. 87–92.

[129] Morris et al. "The soybean isoflavone genistein induces differentiation of MG63 human osteosarcoma osteoblasts". In: *The Journal of nutrition* 136.5 (2006), pp. 1166–1170.

[130] Sugimoto and M Yamaguchi. "Anabolic effect of genistein in osteoblastic MC3T3-E1 cells." In: *International journal of molecular medicine* 5.5 (2000), pp. 515–535.

[131] Yamaguchi and Emi Sugimoto. "Stimulatory effect of genistein and daidzein on protein synthesis in osteoblastic MC3T3-E1 cells: activation of aminoacyl-tRNA synthetase". In: *Molecular and cellular biochemistry* 214.1 (2000), pp. 97–102.

[132] Meikle et al. "Synthesis and characterization of soybean-based hydrogels with an intrinsic activity on cell differentiation". In: *Tissue Engineering Part A* 18.17-18 (2012), pp. 1932–1939.

[133] Uckun et al. "Cytotoxic activity of epidermal growth factor-genistein against breast cancer cells." In: *Clinical Cancer Research* 4.4 (1998), pp. 901–912.

[134] Zhang et al. "Natural isoflavones regulate the quadruplex–duplex competition in human telomeric DNA". In: *Nucleic acids research* 37.8 (2009), pp. 2471–2482.

[135] Rodan et al. "Characterization of a human osteosarcoma cell line (Saos-2) with osteoblastic properties". In: *Cancer research* 47.18 (1987), pp. 4961–4966.

[136] Czekanska et al. "In search of an osteoblast cell model for in vitro research". In: *Eur Cell Mater* 24.4 (2012), pp. 1–17.

[137] Ramaglia et al. "Sandblasted-acid-etched titanium surface influences in vitro the biologicalbehavior of SaOS-2 human osteoblast-like cells". In: *Dental materials journal* 30.2 (2011), pp. 183–192.

[138] Filova et al. "The diameter of nanotubes formed on Ti-6Al-4V alloy controls the adhesion and differentiation of Saos-2 cells". In: *International journal of nanomedicine* 10 (2015), p. 7145.

[139] Balaur et al. "Wetting behaviour of layers of TiO 2 nanotubes with different diameters". In: *Journal of Materials Chemistry* 15.42 (2005), pp. 4488–4491.

[140] Jyoti, Shikha Saxena, and Archana Sharma. “Phytoestrogen “Genistein”: Its Extraction and Isolation from Soybean Seeds”. In: *International Journal of Pharmacognosy and Phytochemical Research* 7.6 (2015), pp. 1121–1126.

[141] Kudou et al. “Malonyl isoflavone glycosides in soybean seeds (Glycine max Merrill)”. In: *Agricultural and Biological Chemistry* 55.9 (1991), pp. 2227–2233.

[142] Lin et al. “Inhibited bacterial biofilm formation and improved osteogenic activity on gentamicin-loaded titania nanotubes with various diameters”. In: *International journal of nanomedicine* 9 (2014), p. 1215.

[143] Tan et al. “Review of titania nanotubes: fabrication and cellular response”. In: *Ceramics International* 38.6 (2012), pp. 4421–4435.

[144] Dale et al. “Electrochemical growth of titanium oxide nanotubes: the effect of surface roughness and applied potential”. In: *Journal of nanoscience and nanotechnology* 9.7 (2009), pp. 4215–4219.

[145] Minagar et al. “Cell response of anodized nanotubes on titanium and titanium alloys”. In: *Journal of biomedical materials research Part A* 101.9 (2013), pp. 2726–2739.